POLITECNICO DI MILANO
DEPARTMENT OF ENERGY
DOCTORAL PROGRAMME IN ELECTRICAL ENGINEERING

APPLICATION OF THEORY OF POSSIBILITY AND RANDOM-FUZZY VARIABLES (RFVS) IN KALMAN FILTER AND BAYES THEOREM FOR INDUSTRIAL CONFORMITY ANALYSIS

Doctoral Dissertation of:
Harsha Vardhana Jetti

Supervisor:
Prof. Simona Salicone

Tutor:
Prof. Alessandro Ferrero

The Chair of the Doctoral Program:
Prof. Marco Mussetta

2018 – 34 Cycle

Acknowledgment

The importance of a good team and colleagues can never be underestimated in any work environment. And this is even more true when it comes to a PhD.

So I feel fortunate to say that I have enjoyed every moment of my PhD here in Politecnico Di Milano.

Firstly, I would like to express my deepest gratitude to my PhD supervisor, Prof. Simona Salicone, for her valuable and helpful guidance throughout the duration. Then, I would like to thank my tutor, Prof. Alessandro Ferrero, for his help during the research and his expert suggestions which made my research that much more easy.

Finally, I extend my thanks to my family, all my friends and colleagues that have made my journey so far a memorable one.

Harsha

Abstract

Measurement has always fascinated humans. With growing need for measurement, there has been a growing need for mathematical theories to express our knowledge about the measurement. The theory of error was the first theory that attempted to quantify the certainty about the measurement. More recently, the theory of uncertainty has been proposed and is widely accepted and is currently in use. As the name says, the theory of uncertainty quantifies the uncertainty or the amount of doubt we have about the measurement. The mathematical theory that has been adapted to represent has long been the theory of probability. But, with growing complexity of scenarios and thereby the data in the scenarios, the theory of probability is no more adequate to deal with all classes of data. The theory of possibility and more specifically, Random-fuzzy variables form an interesting choice to represent uncertainty since RFVs can represent both systematic and random contributions to uncertainty in a mathematically accurate way.

There has been a lot of research corresponding to the application of the theory of possibility and RFVs in different fields. But, so far, there has not been much research in Kalman filter especially using RFVs. Similarly, there hasn't been much research about the use of RFVs in an industrial setting especially in the Bayes' theorem during a conformity analysis. This is what my thesis focuses on. This thesis presents an overview of the existing concepts in metrology and kalman filters. Then, a new definition for a Kalman filter using RFVs is provided. Then the defined Kalman filter has been applied in a few case studies. Then, another slightly modified version of the RFV based Kalman filter has been proposed which allows to partially compensate for the systematic error. Finally, an overview of the conformity analysis has been presented along with an overview of the use of Bayes' theorem in metrology and for conformity assessment. Finally, the drawbacks of using the Bayes' theorem blindly are given along with a modified version of the Bayes' theorem such that it uses the RFVs is given along with a simulation based as well as experimental validation of the proposed idea.

Summary

Measurement has long been the focus of mankind. Ever since the beginning of civilization, the first measurements started as soon as the humans started to keep track of time. Along with the advancement in society, the role of measurements kept getting bigger and bigger. And along with the advancement in technology, the requirement for more accuracy in measurements kept growing. Soon the act of measurement became much more than simply assigning a numerical value on a quantity.

Soon, we started to question the correctness of the measurements being made. So, how do we know if the value we assigned to a particular quantity is right? Soon there were numerous theories that tried to tackle this question.

The first development towards the modern era of metrology is the theory of error which was primarily because of the efforts of K F Gauss. The concept of the theory of error is very simple. It assumed and rightly so that there was a true value for every quantity that we measure. So, the theory of error tried to represent the measurements with respect to the true value of the measurand. This had an inherent problem though, how do we find the true value? It is impossible to do it because every instrument on earth has at least the tiniest bit of error. So, soon it was discovered that the theory of error had lots of drawbacks and hence it was not suitable to represent our knowledge about the measurand.

The next popular theory that has been widely adapted after the theory of error is the theory of uncertainty which is currently in use. According to this theory, the true value can never be found but it can be given with a reasonable certainty if the true value is close to the measured value or not. Now the question is what mathematical theory is good to represent and formulate the theory of uncertainty.

Since the theory of probability has long been in existence, it has been adapted as the dominant theory to represent uncertainty. But, probability inherently has problems such as the inability to be able to represent some classes of data in a logically and mathematically accurate manner.

Comparatively recently, in the final decades of the 20th century, there have been other theories like the theory of evidence, theory of possibility, fuzzy set theory etc which tried to tackle the problems that probability did not have the tools to tackle.

One such attempt is the declaration of random-fuzzy variables (RFVs) based on the

fuzzy set theory and the theory of possibility which are essentially a special form of the more general type 2 fuzzy variables. RFVs are a great option to represent uncertainty since they can represent both the systematic and the random contributions to uncertainty together and in an easier way.

There has been a lot of research highlighting the advantages of RFVs and theory of possibility in lots of different areas of application. But, there has not been much research in the area of RFV based Kalman filtering. Also, there has not been much research about the use of RFVs in Bayes theorem especially during an industrial conformity analysis. These applications form the focus of my research. This thesis can be broken down into two major areas. The first is the Kalman filter domain. The second is the Bayes theorem for conformity analysis.

A graphical abstract is shown in fig. 1.

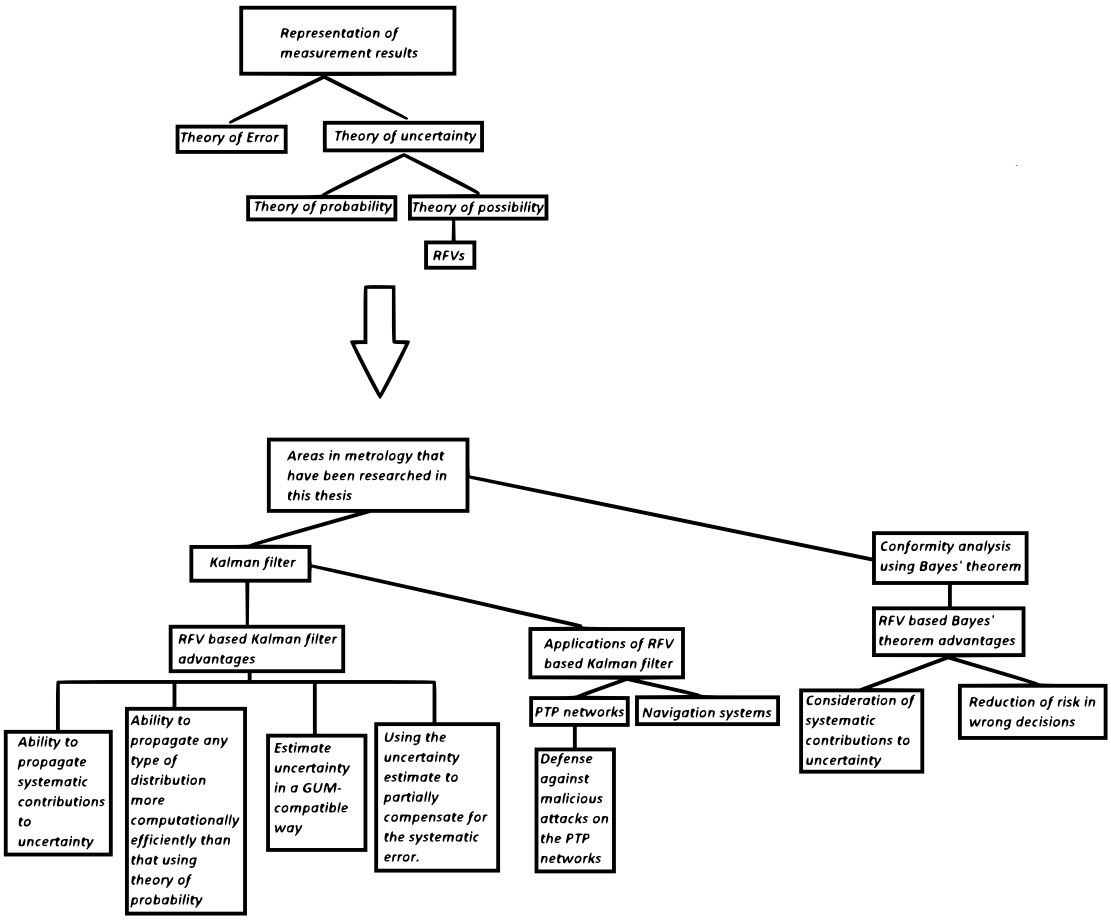

Figure 1: *A graphical abstract of the thesis.*

The thesis is organized as follows.

Chapter 1 provides an overview of metrology in general, the different theories that try to represent our knowledge about the measurand. Then it introduces the Guide to uncertainty evaluation in measurements (GUM) which is the international standard that provides all the guidelines required to evaluate the uncertainty related to a particular measurement. The guidelines given in the guide have also been quickly introduced.

Chapter 2 provides an overview of the more general theory of evidence and then

moves on to say how the theory of probability and the theory of possibility are both special cases of the theory of evidence.

Chapter 3 provides and overview of the set theory and the RFVs, how they can be constructed and how they can be combined with each other.

Chapter 4 provides an introduction to the concepts of Kalman filter and then some examples have been provided to show that the probability based KF are not the best choice.

Chapter 5 provides an overview of the existing possibilistic KF and its drawbacks. Finally, a new definition to the possibilistic Kalman filter has been provided.

Chapter 6 provides an overview of the PTP protocol and the application of the possibilistic KF that has been defined in 5 has been shown using it in PTP networks.

Chapter 7 provides a defense strategy against the malicious attacks on PTP networks using the Kalman filter.

Chapter 8 provides a sightly modified definition to the possibilistic KF defined in chapter 5 such that systematic error in the state predictions is at least partially compensated for.

Chapter 9 provides a brief overview of the concepts of metrology and conformity analysis and discusses the role of Bayes' theorem in metrology. Then it demonstrates how the blind use of Bayes' theorem can be problematic along with some simulations to prove the point.

Chapter 10 provides a modification to the Bayes' theorem in probability based on the Random-fuzzy variables and the effectiveness has been proved with simulated and experimental data.

Contents

CHAPTER 1

Uncertainty and mathematical theories to process uncertainty

The practice of measurement can be traced back to the oldest human civilizations. For example, if the measurement of time is considered, it dates back to since the beginning of civilization when people had to keep track of time. Measurement is essentially the process of assigning a numerical value to a physical quantity, also called measurand. However, during the process of measurement, how can the numerical value be associated to the quantity? This is where reference units and standards come in. So, any measurement can be expressed as a multiple of the reference unit for the particular quantity.

Then the next question arises. How can the correctness of the measurement be determined? No matter how carefully the measurement has been performed, there is always an error. Even when the same quantity is measured multiple times using the same instrument, the result of the measurement is generally not the same. There could be various sources of deviations in the measurement of the particular quantity. They can be something human such as an error during the observation of the value on the instrument or an error in the measurement process.

So, to deal with these deviations in the values, various mathematical theories have been proposed. One such theory is the Theory of error that has been proposed by Karl Freidrich Gauss.

1.1 Theory of error

According to the theory of error, it is assumed that any physical quantity has a *true value* and any measurement of the said quantity is compared with the true value. The true value is assumed to be the value that the most accurate instrument would have

produced.

After guessing the true value, different errors in the measurement can be defined as follows:

- $Absolute\,error = X_{meas} - X_{true}$
- $Relative\,error = \frac{X_{meas} - X_{true}}{X_{true}}$
- $Percentage\,error = \frac{X_{meas} - X_{true}}{X_{true}}.100$

Where X_{meas} is the result of the measurement of quantity X and X_{true} is the true value of X.

Errors are then divided into two categories: Systematic errors and Random errors.

1.1.1 Random Errors

Random errors are errors that are due to unpredictable and unknown changes in the environmental conditions or in the measuring instruments. Like the name suggests, these are completely random in nature and cannot be predicted. So, they cannot be compensated for either. They occur with different magnitudes and signs every time the measurement is performed. But, since they are random in nature, if the same measurement is repeated under the same conditions infinite times, the mean value of the error in all those measurements becomes zero. In other words, if the same measurement is repeated infinite times, the average of all measurements is the true value of the measurand. This means that, even if a random error can not be compensated for, if we have enough measurements, it can be averaged to a very small value.

When N measurements are taken of a given measurand, the mean value and the variance are defined as given in (1.1). It should be noted that these are only the experimental mean and variance and they are not equal to the mean and variance of the random errors.

$$\begin{aligned} \overline{X} &= \frac{1}{N}\sum_{i=1}^{N} X_{meas_i} \\ \sigma_X^2 &= \frac{1}{N-1}\sum_{i=1}^{N}(X_{meas_i} - \overline{X})^2 \end{aligned} \tag{1.1}$$

where $\overline{X}$ is the mean value of all the N measurements and σ_X^2 represents the variance which is also a measure of the dispersion of the measurements around the mean value.

In mathematical terms, any measurement can be expressed in terms of the true value of the measurand and the error in measurement as in (1.2)

$$X_{meas_i} = X_{true} + \epsilon_i \tag{1.2}$$

where X_{meas_i} is the $i-th$ measurement of the measurand and ϵ_i is the error in the $i-th$ measurement.

If it is supposed that the error in the measurement is purely random, when N measurements are taken and the mean value of all of them is computed as given in (1.3), then,

$$\begin{aligned}\overline{X} &= \frac{1}{N}\sum_{i=1}^{N} X_{meas_i} \\ \overline{X} &= \frac{1}{N}\sum_{i=1}^{N}(X_{true} + \epsilon_i) \\ \overline{X} &= X_{true} + \frac{1}{N}\sum_{i=1}^{N}\epsilon_i\end{aligned} \tag{1.3}$$

Since the error in the measurement is purely random, it belongs to an unbiased probability distribution. So, this means that, if infinite values are drawn from the corresponding probability distribution, their mean value would be zero.

This means that in (1.3), if N tends to infinity, the mean value of the error given by $\frac{1}{N}\sum_{i=1}^{N}\epsilon_i$ tends to zero. So, the mean value of the measurements $\overline{X}$ tends to X_{true} as given in (1.4).

$$\begin{aligned}\lim_{N\to\infty}\overline{X} &= X_{true} + \lim_{N\to\infty}\frac{1}{N}\sum_{i=1}^{N}\epsilon_i \\ \lim_{N\to\infty}\frac{1}{N}\sum_{i=1}^{N}\epsilon_i &= 0 \\ X_{true} &= \lim_{N\to\infty}\overline{X}\end{aligned} \tag{1.4}$$

So, in practice, the mean value of the N measurements can be taken to be the best estimate of the true value of the measurand. Calculating the average of the measurements also helps in reducing the random error as the variance of the mean is N times lower than the variance associated with a single measurement.

1.1.2 Systematic Errors

Systematic errors, on the other hand, do not change and are constant provided that the measurement conditions and parameters have not changed. So, if the measurement of the same quantity is repeated with the same instrument, measurement process and environment, the systematic error is always of the same magnitude with the same sign.

This means that, ideally, the systematic errors, unlike random errors, can be completely compensated and corrected for in a measurement, as long as they are correctly and fully identified.

However, in a practical scenario, as explained earlier, no instrument can be one hundred percent accurate. So, it is not really possible that the systematic error can be exactly identified and thereby can never be fully compensated for. So, in most cases, the effect of the systematic error contribution can only be reduced and not fully compensated for.

1.2 Discussion

As can be seen from the discussion till now, there is an inherent problem in the theory of error. The entire theory of error depends on the knowledge of the true value of the measurand. But, if every measurement no matter how accurate the instrument suffers from an error, the true value of a measurand can never be found. So, to express our knowledge about the measurement, the theory of error is not sufficient anymore. To tackle this problem, the theory of uncertainty has been proposed whose overview has been presented in the next section.

1.3 Theory of uncertainty

The theory of uncertainty in measuement has been proposed towards the end of the twentieth century as a result of the discussion inside a committee, the "working group on the statement of Uncertainties" appointed by the International Bureau of Weights and Measures (BIPM). This is based on the modern probability which has been developed primarily due to the efforts by mathematician Kolmogorov who refined and redefined probability through his axioms. It still represents the knowledge about the measurement but in a different way from the theory of error.

Uncertainty as the word suggests means incomplete knowledge about something. So, this means that one is not sure about something. The theory of uncertainty as well, says that one is not sure about the measurement result. There is only a reasonable estimation one can make from the measurement result and no one can know the true value of the quantity being measured.

Uncertainty in metrology has in fact been clearly explained in the document Guide to expression of Uncertainty in Measurement (GUM) published by the Joint committee for Guides in Metrology (JCGM) starting from the recommendation INC-1 issued in 1980 by the "working group on the statement of uncertainties" and approved by the BIPM in 1981. It has been defined that " *the word "uncertainty" means doubt, and thus in its broadest sense "uncertainty of measurement" means doubt about the validity of the result of a measurement.* It has also been defined in the same document that uncertainty is also *a parameter, associated with the result of a measurement, that characterizes the dispersion of the values that could reasonably be attributed to the measurand* [27]".

So, in metrology, uncertainty refers to the doubt associated to the measurement result but also refers to the parameter that measures the amount of that doubt. This has been clarified even in the GUM that, "*because of the lack of different words for this general concept of uncertainty and the specific quantities that provide quantitative measures of the concept of uncertainty, it is necessary to use the word "uncertainty" in these two different senses*" [27].

When there is a measurement, it is also important to know how accurate the measurement is or how sure one is of the measurement result. Otherwise, a measurement just becomes a random guess or a random value attached to a quantity. In other words, the measurement uncertainty associated to the measurement result needs to be evaluated and specified. The same has been mentioned even in the GUM: "*When reporting the result of a measurement of a physical quantity, it is obligatory that who use it can assess its reliability. Without such an indication, measurement results cannot be compared, either among themselves or with reference values given in a specification or*

standard. It is therefore necessary that there may be a reality implemented, easily understood, and generally accepted procedure for characterizing the quality of a result of a measurement, i.e., for evaluating and expressing its uncertainty" [27].

Now that it has been established that the uncertainty associated to the measurement result needs to be evaluated, the next question is as to how it needs to be evaluated. Should one use whatever method feels right for them? Definitely not. There needs to be a universal framework to evaluate the uncertainty. Otherwise, just like any unit of measure, it can not be corroborated with or used with other evaluations of the unit or a standard. The same has been explained in GUM: "*Just as the nearly universal use of the International System of Units (SI) has brought coherence to all scientific and technological measurements, a worldwide consensus on the evaluation and expression of uncertainty in measurement would permit the significance of a vast spectrum of measurement results in science, engineering, commerce, industry, and regulation to be readily understood and properly interpreted. In this era of the global marketplace, it is imperative that the method for evaluating and expressing uncertainty be uniform throughout the world so that measurements performed in different countries can be easily compared*" [27].

There are multiple approaches that are available and proposed to evaluate uncertainty. Currently, the most widely accepted mathematical theory used to evaluate measurement uncertainty is the theory of probability.

1.4 Theory of probability

Classic probability has been defined by Jacob Bernoulli in early eighteenth century as follows: *the probability of an event is the ratio of the number of equally likely cases that favor it to the total number of equally likely cases possible under the circumstances.*

From this, two rules have been proposed for probability by De Moivre.

- The addition theorem or theorem of total probability which states that if A and B are two mutually exclusive events, probability of A or B happening is simply the sum of the individual probabilities of A and B.

  $P(A \cup B) = P(A) + P(B)$

  if A and B are two mutually exclusive events

- The theory of compound probability or multiplication theorem which states that for any two events A and B, probability of both A and B happening is the the probability of A multiplied by the conditional probability of B happening if A has already happened.

  $P(A \cap B) = P(A) * P(B|A)$

  where $P(B|A)$ is the probability of event B given that A has already happened.

Probability is basically the chance of a particular event happening. In other words, probability is also a measure of the ignorance of a particular event. This is because, theoretically speaking, any phenomenon that observes the laws of classical mechanics can be mathematically modeled and if we know the value of all parameters involved and all initial states with one hundred percent accuracy, the outcome of the phenomenon would be known with complete certainty. So, that would mean that nothing in the

universe is random and everything is perfectly deterministic in nature. But, there is a basic problem with this. Is there such a thing as one hundred percent accuracy? At least, in the human world, it hasn't been possible to achieve it so far. So, there is always a certain amount of imprecision with respect to any and all observations. This is one of the reasons probability comes into play so that useful predictions can be made about something with a good degree of certainty.

Probability can be defined in two important ways.

- Probability is the relative frequency of an event happening with respect to the universal set of events.
- Probability is the degree of belief that an event would occur given the states of the environment regardless of any random process.

1.4.1 Frequentist approach to probability

According to the frequentist approach, probability is determined through repetitions of the experiment. So, theoretically, the probability of an event is the relative frequency of the particular event after infinite repetitions of the same experiment. For example, if an unbiased die is rolled, the probability of rolling a three is not $\frac{1}{6}$ because there are six equally likely faces. Rather, if the rolling is performed infinite times, the relative frequency of rolling a three approaches $\frac{1}{6}$. As can be seen very easily, the inherent problem with this approach is the infinite repetitions. It is practically impossible to perform an infinite number of trials. So, instead, guidelines have been provided on using a frequentist approach based on hypothesis testing.

A statistical hypothesis is a statement that can be tested by observing the corresponding phenomenon modeled by a set of random variables. The hypothesis can be accepted or rejected based on the observed data according to a threshold probability which is called significance level. But again, there is an intrinsic problem. Who decides the significance level? Who decides how much error is tolerable in which scenario?

1.4.2 Bayesian approach to probability

In the subjective approach, probability is subjective which means that probability is a degree of belief of an individual who is assessing the state of the phenomenon being observed.

Bayesian approach to probability is a case of subjective probability in which the prior probability of an event is updated to a posterior probability when new evidence is presented.

Again, the inherent problem in bayesian approach is the degree of belief. Who decides the accuracy of the degree of belief assigned to a particular event? What happens if the prior probability of an event is not accurately known? In other words, how can ignorance about an event be properly represented?

Despite this, the theory of probability has been widely established and long since been in existence. It is, in fact, able to deal with most practical scenarios. Due to this, probability has been proposed as the mathematical tool to handle uncertainty. In particular, the modern interpretation of probability proposed by Kolmogorov is used as the basis for handling measurement uncertainty.

1.5 Fundamentals of probability

Let us assume that there is a discrete universal set of all possible outcomes represent by U. For every event e that belongs to U, let's assume that a probability can be assigned to the particular event is $p(e)$, then $p(e)$ should satisfy the following properties.

$$\begin{aligned} &0 \geq p(e) \leq 1 \; for \; all \; e \; \epsilon \; U \\ &\sum_{e \, \epsilon \, U} p(e) = 1 \end{aligned} \tag{1.5}$$

Going by the addition rule of probability, if there are a set of mutually exclusive events represented by A, then the probability of the set A is given by

$$p(A) = \sum_{e \, \epsilon \, A} p(e) \tag{1.6}$$

The above rules apply when the sets of events are discrete. But, if the event space is continuous, $p(e)$ is called the probability density function.

If a random variable X is considered, starting from a cumulative probability $C(i) = P(X \leq i)$ which is the probability that X is less than or equal to i, then, the relation between the cumulative probability and probability density function is given by,

$$\begin{aligned} C(i) &= \int_{-\infty}^{i} p(i) \, di \\ p(i) &= \frac{dC(i)}{di} \end{aligned} \tag{1.7}$$

The probability density function should be such that the cumulative probability over the universal set should be 1.

$$\int_{i \, \epsilon \, U} p(i) = 1 = P(X \, \epsilon \, U) \tag{1.8}$$

Consequentially, the probability of the random variable X being in a set A which is a subset of U, is

$$P(X \, \epsilon \, A) = \int_{i \, \epsilon \, A} p(i) \tag{1.9}$$

The Kolmogorov axioms of probability are as follows:

$$\begin{aligned} &P(X \, \epsilon \, U) = 1 \\ &P(A) \geq 0, \; for \; all \; A \subseteq U \\ &P(A_1 \cup A_2 \ldots A_n) = \sum_{i=1}^{n} P(A_i) \text{if } A_1, A_2, \ldots, A_n \text{ are all disjoint sets} \end{aligned} \tag{1.10}$$

1.6 Measurement uncertainty representation using probability

1.6.1 GUM guidelines for measurement uncertainty

The guide to the expression of uncertainty in measurement or GUM is regarded as the international reference standard for the evaluation and expression of uncertainty in measurements. As explained earlier, measurement uncertainty refers to the parameter that quantifies the dispersion of values that could be attributed to the measurand in a reasonable way [27].

In particular, standard uncertainty refers to measurement uncertainty associated to the result of a measurement expressed as a standard deviation.

According to the GUM, the possible methods to evaluate standard uncertainty can be classified into two Type A and Type B methods depending on how it has been evaluated.

1.6.2 Type A Method:

The method to evaluate standard uncertainty from a statistical analysis of a series of observations of the measurand is called a Type A method of evaluation of standard uncertainty.

When N independent measurements $(x_1, x_2, \ldots, x_N)$ of a measurand X are taken, the best estimate of the expected value of the measurand is given by the arithmetic mean of the N values as in (1.11)

$$\overline{X} = \frac{1}{N}\sum_{i=1}^{N} x_i \tag{1.11}$$

Since the N independent observations differ because of the random effects in the measurement, the experimental variance is given as in (1.12)

$$\sigma_X^2 = \frac{1}{N-1}\sum_{i=1}^{N}(x_i - \overline{X})^2 \tag{1.12}$$

The variance of the quantity X is calculated according to (1.13)

$$u_X^2 = \frac{\sigma_X^2}{N} \tag{1.13}$$

The standard uncertainty of X is the positive square root of the variance in (1.13). An inherent requirement for Type A evaluation of uncertainty is that the number of observations N should be large enough to prove a reliable estimate of the expectation and uncertainty of the measurand X.

1.6.3 Type B Method:

In most scenarios, a Type A evaluation of uncertainty is impractical, mainly for time and cost reasons. Hence, the measurement uncertainty in the cases where there are not enough independent observations is evaluated based on all available information on the variability of the measurand. A Type B evaluation of uncertainty can be made based on [27].

- Already available measurement data about the measurand.
- Experience with or general knowledge of the behavior and properties of relevant materials and instruments.
- Specifications provided by the manufacturer.
- Data that have been provided during calibration or other certificates that are available of the instrument.
- Reference data that have been taken from handbooks and the uncertainty that is associated to them.

1.6.4 Expanded Uncertainty:

After obtaining the standard uncertainty in either of the two ways of evaluation, usually, the expanded uncertainty is computed. Expanded uncertainty is defined as a multiple of the standard uncertainty which provides the interval in which a specified percentage (usually a high percentage) of values lie that can be reasonably attributed to the measurand.

Expanded uncertainty is calculated from the standard uncertainty as given in (1.14)

$$U(X) = k \cdot u_X \tag{1.14}$$

where k is called the coverage factor. The value of k determines how much percentage of the values reasonably attributed to the measurand lie in the expanded uncertainty interval.

The probability distribution function associated to the measurand should be known to define the expanded uncertainty.

1.6.5 Combined uncertainty:

In most cases, the measurand is not directly measured but evaluated based on the measurements of other input quantities. The set of mathematical equations representing the relation between the input quantities and the measurand is called the measurement model.

Assuming that the measurand is represented by Y and if there are N input quantities represented by $X_1, X_2, \ldots, X_N$,

$$Y = f(X_1, X_2, \ldots, X_N) \tag{1.15}$$

where Y, X_i are random variables of the respective quantities.

It is possible that the input quantities $X_1, X_2, \ldots, X_N$ are themselves not measured directly but may be based on the measurement of other quantities. Also, individually, they are subject to all kinds of uncertainty contributions including systematic contributions and the necessary corrections for the systematic errors.

The function f that relates the input quantities to the output quantity Y, may be either mathematically modeled or modeled experimentally using data. If the mathematically modeled function f does not represent the data accurately, it must be modified by adding other input quantities.

After the function is defined, the mean value of the output quantity Y may be obtained by either (1.16) or (1.17)

$$\begin{aligned} \overline{Y} &= f(\overline{X_1}, \overline{X_2}, \ldots, \overline{X_N}) \\ \overline{X_i} &= \frac{1}{N}\sum_{k=1}^{N} X_{i,k} \end{aligned} \tag{1.16}$$

$$\overline{Y} = \frac{1}{N}\sum_{k=1}^{N} f(X_{1,k}, X_{2,k}, \ldots, X_{N,k}) \tag{1.17}$$

Both the equations are the same if the function is linear. In the case of a non linear function, (1.17) offers a more accurate result.

To evaluate the total uncertainty in measurand Y, the individual standard uncertainties of X_i need to be evaluated. The uncertainties in the input quantities X_i can be evaluated using either of the Type A or Type B evaluation methods. Then, the total uncertainty in the measurand Y is calculated by combining the standard uncertainties of all the input quantities using the Law of propagation of the standard uncertainties.

The law of propagation of the standard uncertainties (LPU) is given by (1.18) if all the input quantities are independent of each other and by (1.19) if there are correlated quantities,

$$u_c^2(y) = \sum_{k=1}^{N} (\frac{\partial f}{\partial X_k})^2 u^2(X_k) \tag{1.18}$$

$$u_c^2(Y) = \sum_{k=1}^{N} (\frac{\partial f}{\partial X_k})^2 u^2(X_k) + 2\sum_{k=1}^{N}\sum_{i=1, i\neq k}^{N} \frac{\partial f}{\partial X_k} \cdot \frac{\partial f}{\partial X_i} cov(X_k, Xi) \tag{1.19}$$

where $u_c^2(Y)$ is the combined standard uncertainty of Y. The mathematical derivation of (1.18) and (1.19) can be found in the GUM [27].

This formula is based on the first order Taylor series expansion and hence, in a strict sense, is only for linear functions. But, in most practical scenarios, it is still good enough.

In most industrial scenarios, a coverage interval or expanded uncertainty needs to be provided using the standard uncertainty of the quantity. The combined expanded uncertainty of Y can be obtained by using (1.14) after calculating the combined standard uncertainty as stated above in (1.18) or (1.19).

As mentioned earlier, strictly speaking, this is only possible if the distribution of the quantity is known. But, in cases where it is unknown, the central limit theorem is used.

1.6.6 Central limit theorem:

Let $X_1, X_2, \ldots, X_N$ be independent random variables. Assume that both the expected value μ and the standard deviation σ exist and are finite.

Then the sum of the random variables given by $S_N = X_1 + X_2 + \ldots + X_N$ has an expected value $N\mu$ and a variance of $N\sigma^2$.

Moreover, as N approaches ∞, the distribution of S_N approaches a normal distribution with mean $n\mu$ and a variance of $N\sigma^2$.

To apply the central limit theorem, the following assumptions should be satisfied:

- The random variables $X_1, X_2, \ldots, X_N$ are all independent of each other and none of them dominate the others. So, this means that all of them should have similar variances.
- N is large and ideally reaches infinity.
- The combination of the random variables should be linear.

1.6.7 Discussion

The central limit theorem is a very useful result in metrology. Let us assume that we obtain N measurement results. If the value of N is large enough, it can be assumed with a reasonable certainty that the expected value of the measurand has a normal distribution with mean μ_x and variance σ_x^2 exploiting the central limit theorem.

Hence, the combined standard uncertainty of the measurand can be evaluated from the LPU and the expanded uncertainty can be obtained by assuming a normal distribution using the central limit theorem.

So far, the GUM guidelines seemed good enough to be used to characterize uncertainty.

But, from the third assumption of the central limit theorem, in a strict sense, the central limit theorem can only be used if the function f, which expresses the measurand in terms of the input quantities must be linear and the number of random variables N tends to infinity. There are a lot of cases when these conditions are not satisfied. So, in those cases, the central limit theorem can not be applied. Hence, the probability distribution of the measurand can not be determined. In these cases, the combined standard uncertainty can still be evaluated using the LPU. But, a expanded uncertainty can not be calculated since the probability distribution is not known and hence the coverage probabilities are unknown.

JCGM 101 or Supplement 1 to the "guide to the expression of uncertainty in measurement" - Propagation of distributions using a Monte Carlo method [28] provides the guidelines to be applied in these situations.

1.7 Supplement to the GUM

According to the supplement [28], uncertainty is evaluated in three steps : *formulation, propagation and summarizing*.

- Formulation is done in four steps as given below:
  - The output quantity or the measurand Y should be defined.
  - The input quantities $(X_1, X_2, \ldots, X_N)$ on which Y depends should be determined.
  - The relationship between the measurand and the input quantities should be modeled.

  - Assign a probability distribution function to the input quantities based on the available knowledge about them. If any of the quantities are not independent of each other, a join probability distribution function needs to be assigned to them.

- Propagation: Obtain the distribution for the measurand Y by propagating the distributions of the input quantities $X_1, X_2, \ldots, X_N$ through the model. Propagation is done using monte carlo method (MCM) in cases where the approaches discussed in Section 1.6.1 can not be applied.

- Summarizing is done in three steps:

  - The expectation of Y is obtained from the probability distribution of Y.
  - The standard deviation of Y is calculated from it's distribution and is taken as the standard uncertainty of Y.
  - The coverage interval for a specific coverage probability is also calculated from the distribution of Y.

1.7.1 Monte Carlo Method

According to the guidelines given in [28], MCM is applied in the following steps:

- Select the number M of Monte Carlo trials to be made.
- Generate M vectors, by sampling from the assigned PDFs, as realizations of the (set of N) input quantities $X_1, X_2, \ldots, X_N$.
- For each such vector, form the corresponding model value of Y, yielding M model values.
- Sort these M model values into strictly increasing order, using the sorted model values to provide the distribution of Y.
- Use the distribution to form an estimate of the mean and standard uncertainty of Y.
- Use the distribution to form an appropriate coverage interval for Y for a specified coverage probability p.

There are also certain conditions that need to be satisfied when using the MCM as specified in [27]:

- The function f relating the input quantities and the measurand Y is continuous with respect to the input quantities in the neighborhood of the best estimates of the input quantities.
- the distribution function for Y is continuous and strictly increasing.
- the probability distribution function (pdf) for Y is
  - continuous over the interval for which this pdf is strictly positive.
  - unimodal, and

  - strictly increasing(or zero) to the left of the mode and strictly decreasing to the right of the mode.

- the mean and variance of Y exist
- a sufficiently large value of M is used.

Especially the last condition that a sufficiently large value of M needs to be used is a serious computational limitation. Another huge limitation of the MCM is that convergence is not always assured.

1.8 Discussion

So far, the theory of probability still seems suitable enough for handling uncertainty. But, there are still a few situations where probability does not have the tools to deal with them. For example, there can be a systematic error in the measurement. According to the GUM, all systematic errors are assumed to have been identified and corrected for. When this is strictly followed, probability is still good to represent uncertainty even if there is a residual bias due to the uncertainty of the compensation, it can be expressed as a random variable since the uncertainty of compensation results from the random measurement error while evaluating the systematic error there by making it random in nature.

But, this condition is not always satisfied. There could be cases where the systematic error is not known and hence cannot be compensated for. But, an estimate of the interval of its existence may be known. In this situation, probability distributions can not represent the systematic error in a mathematically correct way. This may result in an underestimation of uncertainty.

Another case would be where the data is so sparse that a standard probability distribution can not be attributed to the data. In these cases, probability fails to offer an appropriate solution to represent our knowledge or ignorance about the data. So a different theory is necessary where all such situations can be dealt with.

This is where the more general theory of evidence and the theory of possibility offer a better solution as explained in the next chapter.

CHAPTER 2

Theory of evidence.

2.1 Introduction

As discussed in chapter 1, the concept of uncertainty was the first attempt to quantify our knowledge or ignorance about a certain event. Probability, on the other hand, is great to express our knowledge about a certain random event but does not have the required tools to represent total ignorance as has been demonstrated in [47, 48, 50]. Total ignorance is the lack of any evidence or, in other words, data to support any belief about a certain event. Hence, a more suitable theory is needed to represent uncertainty in a more accurate way. One such theory is the theory of evidence.

The theory of evidence [50] was proposed by Glenn Shafer in 1970 starting from the research by Arthur P Dempster in which he introduces the notion of upper and lower probabilities [6].

According to the theory of evidence, the chance of an event is represented by belief functions rather than assigning traditional probability distributions. Even in the theory of evidence, the degree of belief is still assigned a value between 0 and 1 like in probability. But, the rules that govern the combination of these degrees of belief are less restricted than those in the theory of probability. This characteristic makes them a great choice to represent missing data or ignorance about data. Belief functions assign probability values to sets of events instead of individual events.

In the theory of probability, there is a lot of emphasis on how to evaluate the probability or, in other words, how to assign a numerical value to the chance of a particular event. Instead, as has been said by Shafer in his original book [50]: *whenever I write "degree of support" that a given evidence provides for a proposition or of the "degree of belief" that an individual accords to the proposition, I picture in my mind an act of judgment. I do not pretend that there exists an objective relation between given evidence and a given proposition that determines a precise numerical degree of support.*

Nor do I pretend that an actual human being's state of mind with respect to a proposition can ever be described by a precise real number called his degree of belief. Rather, I merely suppose that an individual can make a judgment, he can announce a number that represents the degree to which he judges that the evidence to support a given propositions and, hence, the degree of belief he wishes to accord the proposition. So, the theory of evidence, instead of focusing on how the degree of beliefs are calculated, concentrates instead on the rules of combination of the degrees of belief.

The next section gives some basic definitions in the theory of evidence and the rules of combinations for belief functions.

2.2 Basic definitions in the theory of evidence

According to Dempster, if a hypothesis is assigned a particular degree of belief, it means that any other hypothesis that is implied by the said hypothesis also carries the same degree of belief. In other words, if a degree of belief is assigned to one subset of a particular set, it means that the same degree of belief is assigned to all of its subsets.

So, let there be a function m, called the basic probability assignment function be defined for the power set of A as follows:

$$m : P(A) \rightarrow [0, 1] \tag{2.1}$$

and m satisfies the following conditions:

$$m(\emptyset) = 0 \tag{2.2}$$

$$\sum_{B \in P(A)} m(B) = 1 \tag{2.3}$$

Eq. 2.2 means that the belief assigned to a null set is zero and (2.3) means that the total belief is 1.

The degree of belief assigned to each subset B is called the basic probability number and it is the degree of belief assigned to the subset B and it strictly refers to the entire set and does not say anything about any of the subsets or elements of the set B.

Any subset B is called a focal element of the set A if $m(B) > 0$

The belief function of a set A can be defined as follows:

$$Bel(A) = \sum_{B|B \subseteq A} m(B) \tag{2.4}$$

as long as it satisfies the following properties:

$$\begin{aligned} Bel(\emptyset) &= 0 \\ Bel(A) &= 1 \end{aligned} \tag{2.5}$$

$$Bel(B_1 \cup B_2 \ldots \cup B_n) \geq \sum_i Bel(B_i) - \sum_{i<j} Bel(B_i \cap B_j) + \ldots + -1^{(n+1)} Bel(B_1 \cap B_2 \ldots \cap B_n) \tag{2.6}$$

Where $B_1, B_2, \ldots, B_n$ are all subusets of A.
From (2.6), it can be determined that

$$Bel(A) + Bel(\overline{A}) \leq 1 \tag{2.7}$$

When the rules given in (2.6) and (2.7) correspond to just the equality, the belief functions are called Bayesian belief functions.

The degree of doubt for set A can be defined as

$$Dou(A) = Bel(\overline{A}) \tag{2.8}$$

The plausibility of A on the other hand can be defined as:

$$Pl(A) = 1 - Dou(A) = 1 - Bel(\overline{A}) \tag{2.9}$$

It can also be defined in terms of the basic probability assignment function m as follows:

$$Pl(A) = \sum_{B|B\cap A\neq\emptyset} m(B) \tag{2.10}$$

This basically means that the belief function of A is a lower limit of the probability assigned to the set A and the plausibility of A is the upper limit of the probability that is assigned to A.

From (2.7) and (2.9), it can be derived that

$$\begin{aligned} &Bel(A) + Bel(\overline{A}) \leq 1 \\ &1 - Pl(A) + 1 - Pl(\overline{A}) \leq 1 \\ &Pl(A) + Pl(\overline{A}) \geq 1 \end{aligned} \tag{2.11}$$

2.3 Particular cases of the theory of evidence

2.3.1 The theory of probability

Section 2.2 gives some basic definitions of the various functions in theory of evidence. Bayesian belief functions have been mentioned as well.

It has been also mentioned that belief functions are the lower limit for probability assigned to a particular set. So, what happens if there are more limitations that are applied to the definitions of belief functions?

It is known that if there are two sets A and B, the probability function for the two sets is supposed to satisfy the below condition,

$$Pro(A \cup B) = Pro(A) + Pro(B) - Pro(A \cap B) \tag{2.12}$$

whereas a belief function is supposed to satisfy the below rule,

$$Bel(A \cup B) \geq Bel(A) + Bel(B) - Bel(A \cap B) \tag{2.13}$$

It has been mentioned earlier that the belief functions are degrees of beliefs assigned to a particular set A and they do not say anything about the degrees of belief assigned to the elements of the set or to any of its subsets.

The basic probability assignment function m has also been defined for the sets in the power set of A. But what if the focal elements of the set A are all singletons?

Then the belief function simply corresponds to the probability function of A.

According to (2.4), if all the focal elements are singletons, the belief function becomes,

$$Bel(A) = \sum_{B|B \subseteq A} m(B) = \sum_{x \in A} m(x) \tag{2.14}$$

In the same way, the plausibility function defined in 2.10 becomes,

$$Pl(A) = \sum_{B|B \cap A \neq \emptyset} m(B) = \sum_{x \in A} m(x) \tag{2.15}$$

In other words, the belief and plausibility of A are equal. So, it follows that

$$\begin{aligned} &Bel(A) = Pl(A) \\ &Bel(A) = 1 - Bel(\overline{A}) \\ &Bel(A) + Bel(\tilde{(}A)) = 1 \end{aligned} \tag{2.16}$$

The above rule is similar to the rules for probability.

Also as explained earlier, belief function is the lower limit of probability and the plausibility is the upper limit of probability. So, if the belief and plausibility are equal, it means that it is simply the probability.

This means that the belief functions are nothing but probability functions if the focal elements are all singletons.

2.3.2 The theory of possibility

The theory of possibility is another particular case of the theory of evidence. The theory of possibility considers the belief functions when the focal elements are all nested. This means that all the focal elements can be arranged in such a way that every focal element is contained in the following one.

Nested focal elements are also called as consonants [48]. A belief function whose focal elements are nested is said to be a consonant.

If the focal elements in a universal sets are all consonants, then theory of evidence corresponds to a particular case called the theory of possibility.

When the focal elements are consonants, the belief and plausibility functions satisfy the following conditions [48]:

$$\begin{aligned} Bel(A \cap B) &= min[Bel(A), Bel(B)] \\ Pl(A \cup B) &= max[Pl(A), Pl(B)] \end{aligned} \tag{2.17}$$

When a belief and plausibility function satisfy the corresponding rules given in (2.17), they are called the necessity function and the possibility function respectively [48]. Hence, the equations become,

$$\begin{aligned} Nec(A \cap B) &= min[Nec(A), Nec(B)] \\ Pos(A \cup B) &= max[Pos(A), Pos(B)] \end{aligned} \tag{2.18}$$

The possibility distribution function

In the theory of possibility, one of the important property is that a frame of discernment (the universal set containing all the hypothesis considered) can be completely determined using the plausibilities assigned to the singletons of the frame of discernment [48]. So, if X represents the frame of discernment and that a single element x in the set X is considered, if a possibility function Pos is defined on X, then the possibility distribution function r can be derived.

$$r : X \rightarrow [0, 1] \tag{2.19}$$

such that:

$$r(x) = Pos(x) \quad \forall x \in X. \tag{2.20}$$

In turn, every possibility function on the power set of X $(P(X))$ can be determined from the possibility distribution function of X.

For any discrete set A, the possibility of A can be given by,

$$Pos(A) = \max_{x \in A} r(x). \tag{2.21}$$

If the set A is continuous, the possibility is in turn given by,

$$Pos(A) = \sup_{x \in A} r(x). \tag{2.22}$$

Representing information in theory of possibility

If we consider the case where there is a discrete possibility distribution of length n as given below:

$$r(x) = [r(x_1), r(x_2), \ldots, r(x_n)]. \tag{2.23}$$

The smallest possibility distribution would correspond to the case where the possibility assigned to just one of the elements in the possibility distribution is 1 and the rest are all 0. This means that we are absolutely sure that the element to which the possibility of 1 is assigned, will occur. So, this represents the case of perfect evidence or no uncertainty.

The largest possibility distribution, on the other hand, would correspond to the case where we are completely ignorant and hence we do not have any evidence for any of the elements. In this case, the possibilities assigned to all the elements would be 1.

When a continuous set is considered, total ignorance is represented by a *Uniform possibility distribution*. This is as shown in the fig. 2.1

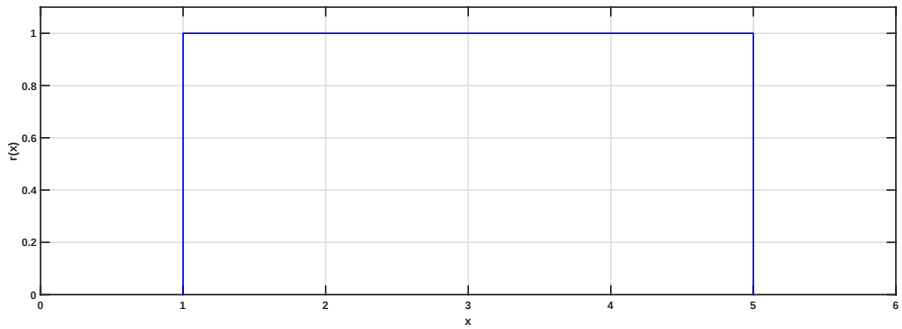

Figure 2.1: *Uniform possibility distribution representing total ignorance.*

Similarly, depending on the evidence on the different hypothesis, other possibility distributions could be modeled.

Probability-Possibility Transformation

In particular, possibility distributions can also be modeled from probability distributions using probability-possibility (p-p) transformations [8,15,16,36,48]. A probability-possibility transformation can be done starting from the definition of the possibility being the upper probability measure. So, a specific p-p transformation is valid if, there is a probability distribution function p_x such that, when it is transformed into possibility, it results in a possibility distribution (PD) r_X such that,

$$\begin{aligned} &Pos(X \in E) \geq P(X \in E), \forall \, \mathrm{E} \\ &\sup r_X(x) \geq \int_{x \in E} p_X(x)\, dx, \forall \, \mathrm{E} \end{aligned} \tag{2.24}$$

When the above equations are satisfied, the PD is said to dominate the probability distribution function (pdf).

The confidence interval denoted by p and the necessity measure of a set E are defined by,

$$\begin{aligned} &p = P(X \in E) \\ &Nec(X \in E) = 1 - Pos(X \in \overline{E}) \end{aligned} \tag{2.25}$$

So, this would mean that, $Nec(X \in E) \leq p$.

Let the set X^* be taken as the set built by having a confidence interval of p around a value x. If different such sets are obtained when the confidence level p is changed keeping x constant, all the obtained sets are actually nested confidence intervals. This is because, as the confidence the level p increases, the obtained set with the increased confidence level would contain the set obtained with the previous confidence level. So, a PD can, in fact, be modeled by obtaining the nested sets using different confidence intervals of a probability distribution around its mode.

But, an infinite number of PDs can be modeled starting from a pdf such that the PDs dominate the pdf. So, an infinite number of p-p transformations can be made starting from a single pdf. This family of infinite PDs is given by:

$$r_X(x) \geq \sup_{X^*|x \in X^*} (1 - P(X \in X^*)) \tag{2.26}$$

So, a possible way to choose a specific p-p transformation would be to choose a transformation such that most of the information of the original pdf is retained. This is called maximum specificity principle. According to this, the smallest PD out of all the dominating PDs represented by (2.26) must be chosen as a suitable p-p transform. So, for a certain confidence level p, the confidence interval I_x should have a minimum length. Such intervals can be obtained by building them around the mode of the pdf. Hence, a maximally specific PD can be given by:

$$r_X(x) = 1 - P(X \in I_x) \tag{2.27}$$

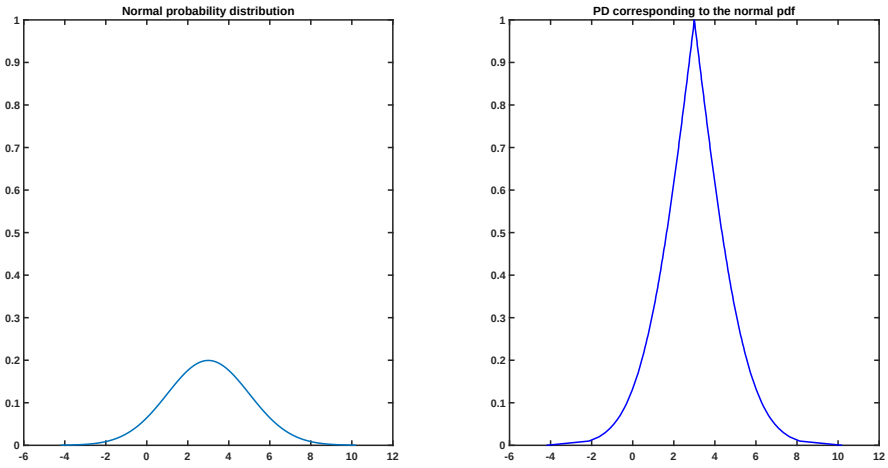

Figure 2.2: *Normal probability distribution and the corresponding possibility distribution.*

A few examples of different possibility distributions and the corresponding probability distributions obtained from a maximally specific p-p transformation can be seen in Fig. 2.2, 2.3 and 2.4

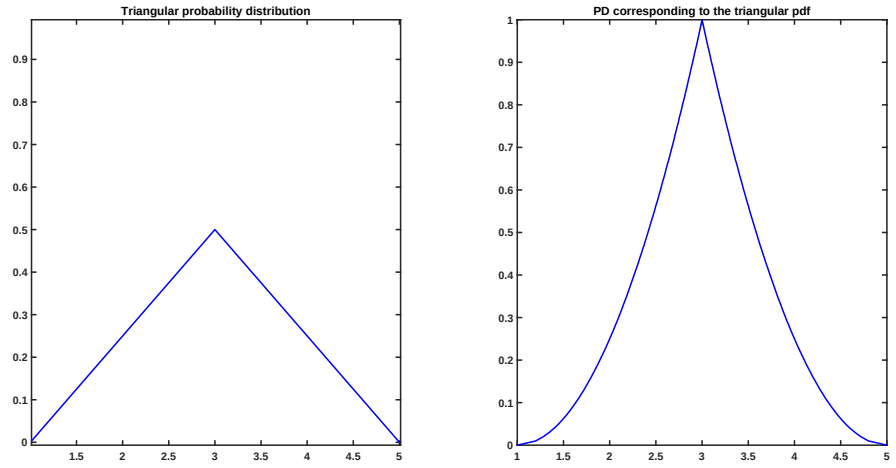

Figure 2.3: *Triangular probability distribution and the corresponding possibility distribution.*

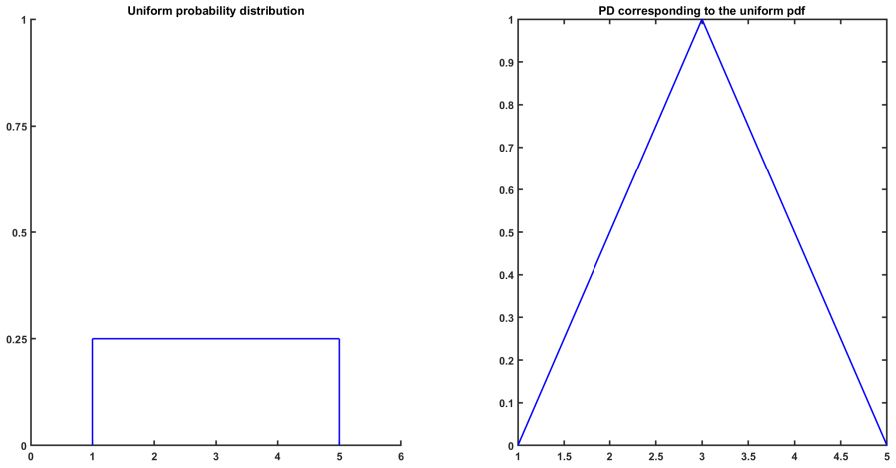

Figure 2.4: *Uniform probability distribution and the corresponding possibility distribution.*

Combination of possibility distributions

The aggregation operation of possibility distributions (PDs) is made using triangular norms or t-norms [2, 3, 32–34, 48]. An aggregation operation is when different possibility distributions are combined to form a single possibility distribution. In other words, they can be used to define the joint possibility distributions and to make algebraic operations for different PDs.

There are various t-norms, for example, a min t-norm, Frank t-norm, Dombi t-norm etc. that have been defined and they should be used depending on how the PDs should be combined [47].

The definitions of a few fundamental t-norms are as given below [47, 48]:

$$T_{min}(a, b) = min(a, b) \tag{2.28}$$

$$T_{prod}(a,b) = a \cdot b \tag{2.29}$$

$$T_L(a,b) = maxa + b - 1, 0 \tag{2.30}$$

$$T_D(a,b) = \begin{cases} b \text{ if } a = 1 \\ a \text{ if } b = 1 \\ 0 \text{ Otherwise} \end{cases} \tag{2.31}$$

Where T_{min} is the min t-norm, T_{prod} is the prod t-norm, T_L is the Lukasiewicz's t-norm, T_D is the drastic t-norm.

Using the fundamental t-norms, Frank t-norm can be defined as given below:

$$T_\gamma^F(a,b) = \begin{cases} T_{min}(a,b) & \text{if } \gamma = 0 \\ T_{prod}(a,b) & \text{if } \gamma = 1 \\ T_L(a,b) & \text{if } \gamma = +\infty \\ 1 - \log_\gamma(1 + \frac{(\gamma^a - 1)\cdot(\gamma^b - 1)}{\gamma - 1}) & \text{otherwise} \end{cases} \tag{2.32}$$

Frank t-norm has only one parameter λ that determines how the combination is done on the PDs. There are also t-norms with multiple parameters which offer a greater degree of freedom.

The generalized Dombi operator (Dombi t-norm) is one such t-norm with two parameters and is defined as follows [7, 47, 48]:

$$T_{\gamma_1,\gamma_2}^{GDO}(r) = \frac{1}{1 + (\frac{1}{\gamma_1}(\prod_{i=1}^{N}(1 + \gamma_1(\frac{1-r_i}{r_i})^{\gamma_2}) - 1))^{\frac{1}{\gamma_2}}} \tag{2.33}$$

The case where two triangular PDs have been added using a min t-norm and a Frank t-norm with $\gamma = 0.7$ has been shown in fig. 2.5.

2.4 Conclusion

In this chapter, the theory of evidence has been briefly recalled and the basic definitions in the theory of evidence have been given. Then, it has been shown how the theory of probability and the theory of possibility are specific cases of the theory of evidence. The definitions for possibility distributions and the rules of combination have been introduced. In the next chapter, a brief introduction will be given about fuzzy variables and then Random-fuzzy variables and an explanation will be given about how they can represent uncertainty. Finally, the construction and combination of RFVs will be introduced.

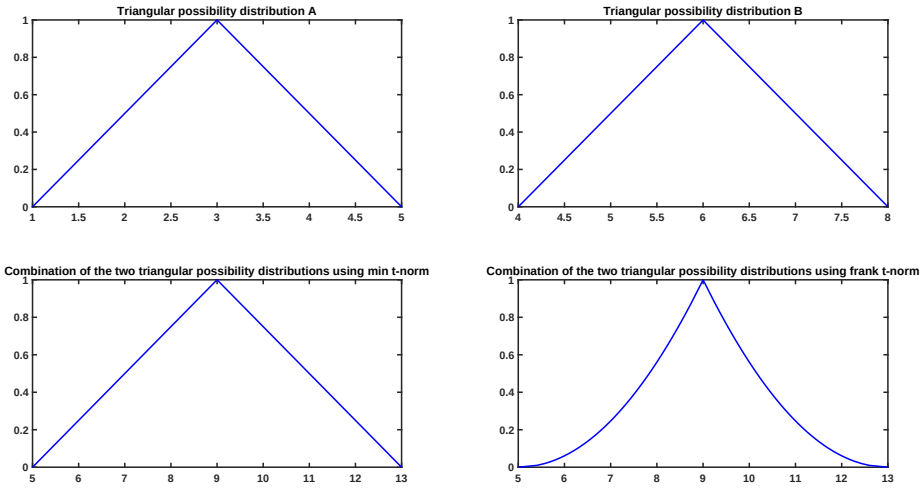

Figure 2.5: *Sum of two triangular possibility distribution using min t-norm and the Frank t-norm.*

CHAPTER 3

Random fuzzy variables and their construction.

In chapter 1, the concepts of measurement, the theory of probability have been recalled. It has also been mentioned earlier that the theory of probability does not have the required tools to represent ignorance or missing data. For this purpose, in chapter 2, the theory of evidence and the theory of possibility have been introduced. These are two of the theories that can represent ignorance about a particular event in a better way than the theory of probability. But they have not yet been applied to the case of metrology to represent our knowledge about a measurement result.

For this purpose, in this chapter, the concepts about the construction and the mathematics of Random-Fuzzy Variables (RFVs) that have been framed within the theory of possibility have been recalled. RFVs are a specific case of Fuzzy variables. So, before moving on to the concepts of RFVs, it is important to recall information about fuzzy variables and fuzzy set theory.

The Fuzzy set theory is framed within the theory of possibility. It has been introduced in 1965. It finds application in most of the fields in the modern world like artifical intelligence, robotics, machine learning, control theory etc. The first publications of fuzzy set theory have been made by Zadeh and Goguen.

In Zadeh's own words: "The notion of a fuzzy set provides a convenient point of departure for the construction of a conceptual framework which parallels in many respects the framework used in the case of ordinary sets, but is more general than the latter and, potentially, may prove to have a much wider scope of applicability, particularly in the fields of pattern classification and information processing. Essentially, such a framework provides a natural way of dealing with problems in which the source of imprecision is the absence of sharply defined criteria of class membership rather than the presence of random variables." [54].

Some basic definitions of fuzzy set theory are given in the next section.

3.1 Fuzzy set theory

3.1.1 Basic definitions

If X is a collection of objects, denoted generically by x, then a fuzzy set A in X is a set of ordered pairs:

$$A = (x, \mu_A(x))|x \in X \tag{3.1}$$

where $\mu_A(x)$ is called the membership function which maps X to the membership space M which defines the degree of support that the element x belongs to X. Its range is the subset of non negative real numbers whose supremum is finite. When $sup\,\mu_A(x))$ = 1, then the fuzzy set is a normalized fuzzy set. So, in a normalized fuzzy set, the membership space M extends from 0 to 1.

A crisp set on the other hand is deterministic in nature. So, the an element either belong to a crisp set or they do not. There is no fuzziness about it.

The support of a fuzzy set A, denoted with $S(A)$, is the crisp set given by:

$$S(A) = x \in X|\mu_A(x) > 0 \tag{3.2}$$

The $\alpha-$ level set or the $\alpha-$ cut of a fuzzy set A, denoted by A_α, is the crisp set given by:

$$A_\alpha = x \in X|\mu_A(x) \geq \alpha \tag{3.3}$$

When the above condition is strictly greater and not equal to α, it is called a strong $\alpha-$ cut.

A set is called a convex set if every element in between two elements in a set is also in the set. One of the important properties of fuzzy sets is that they are convex.

A fuzzy set A is convex if all of its $\alpha-$cuts are convex.

3.1.2 Rules of operation for fuzzy sets

Zadeh defined the following rules of operation on fuzzy sets [54]:

- Intersection: The membership function of the intersection of two fuzzy sets A and B is defined as
$$\mu_{A\cap B}(x) = min(\mu_A(x), \mu_B(x)) \tag{3.4}$$
- Union: The membership function of the union of two fuzzy sets A and B is defined as
$$\mu_{A\cup B}(x) = max(\mu_A(x), \mu_B(x)) \tag{3.5}$$
- Complement: The membership function of the complement of a fuzzy set A is defined as
$$\mu_{\overline{A}}(x) = 1 - \mu_A(x) \tag{3.6}$$

3.1.3 Fuzzy numbers

Fuzzy numbers or fuzzy variables form an important part of the fuzzy set theory.

A fuzzy number M is a convex, normalized fuzzy set of the real line $\mathbb{R}$ such that:

- it exists exactly one $x_0 \in \mathbb{R}$ such that $\mu_M(x_0) = 1$. x_0 is called the mean value of M;
- $\mu_M(x)$ is piecewise continuous.

The fuzzy numbers that are defined as above are called Type 1 fuzzy numbers.
An alternate definition for a fuzzy number is as follows [35]:
A fuzzy number is a fuzzy set A on $\mathbb{R}$, which satisfies at least the following properties:

- A is a normal fuzzy set;
- $\alpha-$cut A_α is a closed interval for every $\alpha \in (0, 1]$.
- the support of A is bounded.

An example of $\alpha-$cut is shown in Fig. 3.1.

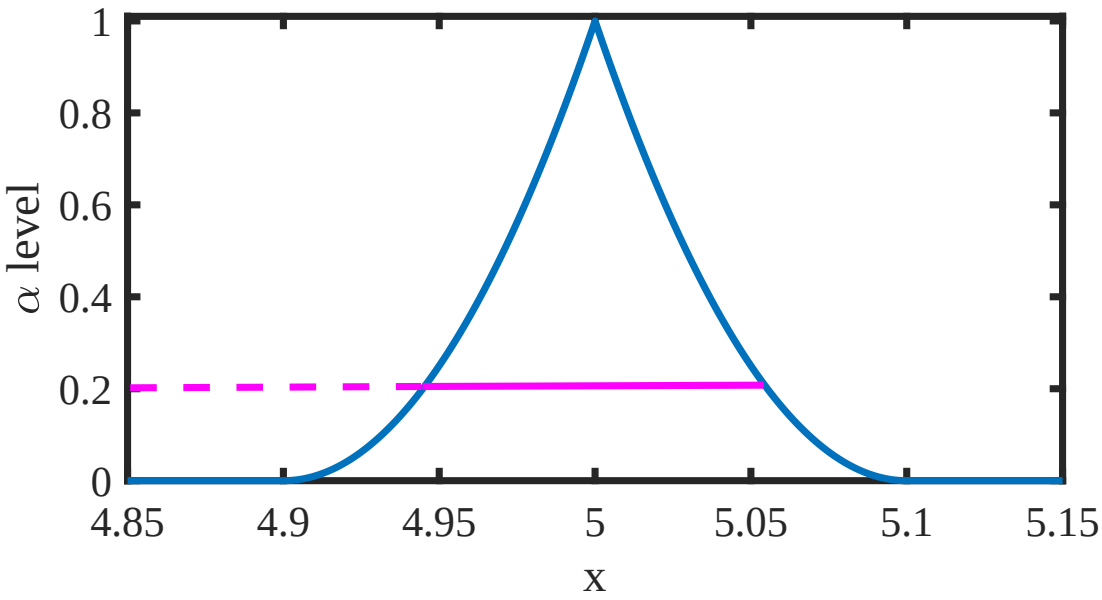

Figure 3.1: *Example of a fuzzy number of type 1 and its $\alpha-$cut at $\alpha-$level 0.2*

The $\alpha-$cuts of a fuzzy number of type 1 are closed intervals in $\mathbb{R}$: $A_\alpha = [a_1^\alpha, a_2^\alpha]$
If m is any integer greater than 1, a type m fuzzy set can be defined as a fuzzy set whose membership value are themselves a type $m-1$ fuzzy sets in [0,1]. So, starting from this, we can say that a type 2 fuzzy number or a type 2 fuzzy variable are fuzzy sets whose membership values are in turn type 1 fuzzy sets in [0,1].
According to the authors in [31], $\alpha-$cuts of type 1 are intervals of confidence of type 1. This means that they are closed intervals in $\mathbb{R}$ and within these intervals, there is the possibility of finding possible values of an uncertain result.
The $\alpha-$cuts of type 2 are also by definition closed intervals in $\mathbb{R}$ but they contain a second closed interval inside the original interval. Hence type 2 $\alpha-$cuts can be represented as:

$$A_\alpha = [a_1^\alpha, a_2^\alpha, a_3^\alpha, a_4^\alpha] \tag{3.7}$$

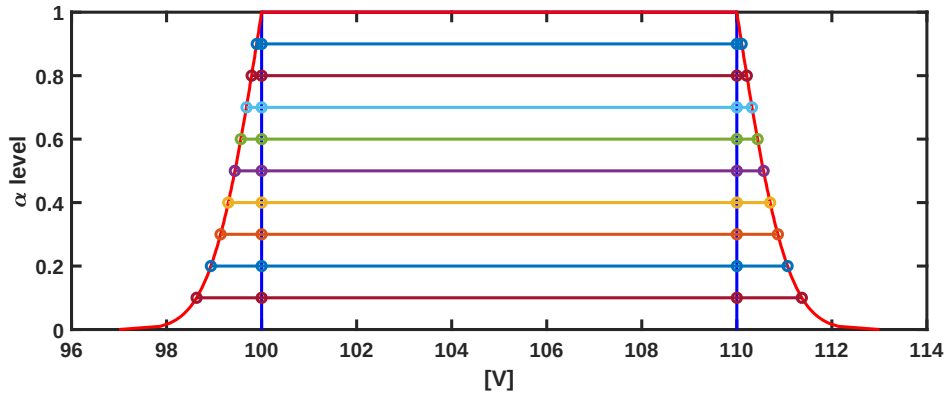

Figure 3.2: *Example of a fuzzy number of type 2 and its $\alpha-$cuts*

A type 2 fuzzy variable and its alpha cuts can be seen in Fig. 3.2

Just like the type 1 fuzzy variables, type 2 fuzzy variables can also be defined in terms of a set of type 2 confidence intervals as given in (3.7). They have to obey the following set of rules:

- $a_1^\alpha \leq a_2^\alpha \leq a_3^\alpha \leq a_4^\alpha$.
- the sequence of intervals of confidence of type 1 $[a_1^\alpha, a_4^\alpha]$ generates a membership function that is normal and convex.
- The sequence of intervals of confidence of tupe 1 $[a_2^\alpha, a_3^\alpha]$ generates a membership function that is convex.
- $\forall\alpha$ and $\alpha\prime \in [0,1]$:

$$\alpha\prime > \alpha \Rightarrow \begin{cases} [a_1^{\alpha\prime}, a_3^{\alpha\prime}] \subset [a_1^\alpha, a_3^\alpha] \\ [a_2^{\alpha\prime}, a_4^{\alpha\prime}] \subset [a_2^\alpha, a_4^\alpha] \end{cases} \quad \text{for } a_2^{\alpha\prime} \leq a_3^{\alpha\prime} \tag{3.8}$$

- If the maximum of the membership function generated by the sequence of confidence intervals $[a_2^\alpha, a_3^\alpha]$ is found at level α_m, then:

$$[a_2^{\alpha_m}, a_3^{\alpha_m}] \subseteq [a_1^{\alpha=1}, a_4^{\alpha=1}] \tag{3.9}$$

If the above rules are made stricter as given below:

- $a_1^\alpha \leq a_2^\alpha \leq a_3^\alpha \leq a_4^\alpha$.
- the sequence of intervals of confidence of type 1 $[a_1^\alpha, a_4^\alpha]$ generates a membership function that is normal and convex.

- The sequence of intervals of confidence of tupe 1 $[a_2^\alpha, a_3^\alpha]$ generates a membership function that is normal and convex.
- $\forall\alpha$ and $\alpha\prime \in [0,1]$:

$$\alpha\prime > \alpha \Rightarrow \begin{cases} [a_1^{\alpha\prime}, a_3^{\alpha\prime}] \subset [a_1^\alpha, a_3^\alpha] \\ [a_2^{\alpha\prime}, a_4^{\alpha\prime}] \subset [a_2^\alpha, a_4^\alpha] \end{cases} \tag{3.10}$$

- If the maximum of the membership function generated by the sequence of confidence intervals $[a_2^\alpha, a_3^\alpha]$ is found at level $\alpha = 1$, then:

$$[a_2^{\alpha=1}, a_3^{\alpha=1}] \equiv [a_1^{\alpha=1}, a_4^{\alpha=1}] \tag{3.11}$$

The last rule states that the internal and the external intervals always should coincide when $\alpha = 1$.

Then a subclass of the more general type 2 fuzzy variables is obtained, which are called Random-Fuzzy variables (RFVs) [47].

3.1.4 Relation between the fuzzy set theory and the theory of evidence

If there is a fuzzy variable X and if the $\alpha-$cuts X_α are considered, it can be seen that for different values of α the $\alpha-$cuts of a fuzzy variable can be ordered in a nested structure. The $\alpha-$cuts have a non zero probability assigned to them (because the $\alpha-$cut is a set that represents a confidence interval). So, $\alpha-$cuts are also focal elements of the fuzzy variable X.

In chapter 2, it has been demonstrated how the theory of possibility deals with belief functions when the focal elements are all nested and how a possibility distribution function can be defined for a set whose focal elements are all nested. Hence, because the $\alpha-$cuts are all the focal elements of the universal set X or in this case the fuzzy variable X and are also nested sets, they satisfy all requirements of the theory of possibility. So, basic probability mass can be assigned to the $\alpha-$cuts which in turn enables us to define the necessity function, the plausibility function and finally a possibility distribution function.

So, in terms of $\alpha-$cuts:

$$Nec(X_{\alpha_i}) = \sum_{X_\alpha | X_\alpha \subseteq X_{\alpha_i}} m(X_\alpha) = \sum_{\alpha=\alpha_i}^{1} m(X_\alpha) \tag{3.12}$$

$$Pos(X_{\alpha_i}) = \sum_{X_\alpha | X_\alpha \cap X_{\alpha_i} \neq} m(X_\alpha) = \sum_{\alpha=0}^{1} m(X_\alpha) \tag{3.13}$$

As explained before, another way to define a fuzzy variable is using its membership function. The membership function in fact assigns a numerical value between 0 and 1 which says to what extent the element belongs to the fuzzy set. So, this is equivalent to a degree of belief being assigned to the element x.

Hence, it can be said that the membership function of a fuzzy variable is nothing but the possibility distribution function in the possibility theory.

Extending the logic, it can be proved that the value α at each $\alpha-$cut is nothing but the value assigned to the possibility distribution at the extreme points of the particular $\alpha-$cut, as given below.

$$r_i = r(x_i) = \alpha_i \tag{3.14}$$

It can also be proved that the necessity function at an $\alpha-$cut is given by the following equation:

$$Nec(X_\alpha) = 1 - \alpha \tag{3.15}$$

So, the confidence level of an interval can be simply given by 1-α.

3.2 Random-Fuzzy Variables

Although Random-fuzzy variables have already been mentioned in Sect. 3.1.3, a more exhaustive definition of RFVs can be given in the two following ways one according to the possibility distribution and the other according to the $\alpha-$cuts [47, 48]:

- A random-fuzzy variable (RFV) is a type 2-fuzzy variable such that:
  - An internal and an eternal membership functions can be identified.
  - Both the internal and the external membership functions are normal and convex, that is, they are PDs.
  - A unitary possibility value is associated, by the two PDs, to the same interval.

  The internal and external PDs are named, respectively, r^{int} and r^{ext}.
- A random-fuzzy variable is a type 2-fuzzy variable defined by a set of nested intervals of confidence of type 2 $A_\alpha = [a_1^\alpha, a_2^\alpha, a_3^\alpha, a_4^\alpha]$, with $\alpha \in [0, 1]$ such that:

$$[a_2^{\alpha=1}, a_3^{\alpha=1}] \equiv [a_1^{\alpha=1}, a_4^{\alpha=1}] \tag{3.16}$$

3.2.1 Construction of an RFV

As has already been stated in the definition, there are two membership functions in an RFV: an internal membership function and an external membership function both of which are PDs.

The internal membership function r^{int}

The internal membership function or internal PD, denoted by r^{int}, is the PD that takes into consideration the systematic contributions to uncertainty in the measurement. So, the internal PD can be built on the available knowledge about the possible systematic contributions to uncertainty.

As has been stated in chapter 2, a uniform PD is the largest possibility distribution function over a given interval. And it has been explained that a uniform PD represents total ignorance about the situation.

In practice, in most cases in measurement, total ignorance is the most common occurrence with respect to the systematic contributions to uncertainty. We can only guess that it falls in a certain interval of values but absolutely have no idea which one of those values is the true value. This perfectly represents the scenario of total ignorance.

Hence, in such cases, the internal membership function is simply taken to be a uniform (rectangular) PD.

Of course, in case we have other information available about the dispersion of the systematic values and a pdf can be assigned to it, we can build the PD starting from the available information and applying the maximally specific probability-possibility transform, as explained in Sec. 2.3.2.

The random membership function r^{ran}

The random PD, denoted by r^{ran} takes into account the random contributions to uncertainty in the measurement. This PD can be built based on the metrological information that we have on the measurand, which is given in terms of a pdf.

Therefore, r^{ran} can be built starting from the given pdf by applying the maximally specific p-p transformation.

An example of a random PD built from a triangular pdf can be seen in the fig. 3.3,

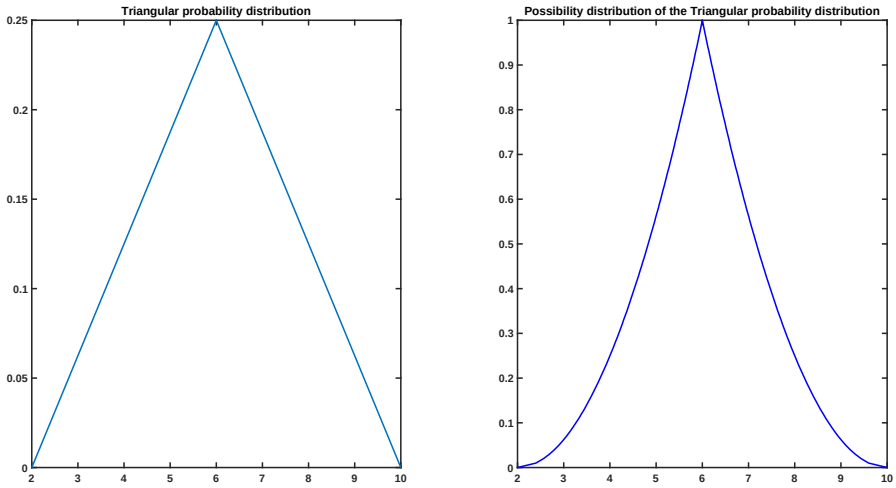

Figure 3.3: *Triangular pdf and the corresponding PD, obtained by applying the maximally specific p-p transform.*

The external membership function r^{ext} and the RFV

As soon as the two PDs, the internal PD and the random PD, are both available, the external membership function (external PD) and the RFV can be built.

The external PD can be derived using the following equation:

$$r_X^{ext}(x) = \sup_{x\prime} T_m[r_X^{ran}(x - x\prime + x^*), r_X^{int}(x\prime)] \tag{3.17}$$

where x^* is the mode of $r_X^{ran}(x)$ and T_m is the min t-norm as explained in chapter 2 in sec. 2.3.2.

It is also possible to construct the RFV from the internal PD and the random PD if we consider their $\alpha-$cuts.

Let us consider the $\alpha-$ cuts at the same α level for both the random and the internal

PDs. Let the corresponding $\alpha-$cuts be $[a_L^\alpha, a_R^\alpha]$ and $[b_L^\alpha, b_R^\alpha]$ respectively. An $\alpha-$ cut is nothing but a closed interval. So, the interval can be broken down to two separate intervals around its mode $x*$ given by $[a_L^\alpha, x^*]$ and $[x^*, a_R^\alpha]$. Then the $\alpha-$cut of the RFV $[x_a^\alpha, x_b^\alpha, x_c^\alpha, x_d^\alpha]$ can be obtained as follows:

$$\begin{aligned} x_a^\alpha &= b_L^\alpha - (x^* - a_L^\alpha) \\ x_b^\alpha &= b_L^\alpha \\ x_c^\alpha &= b_R^\alpha \\ x_d^\alpha &= b_R^\alpha + (a_R^\alpha - x^*) \end{aligned} \tag{3.18}$$

An example of construction of an RFV starting from a random and an internal PD is shown in Fig. 3.4

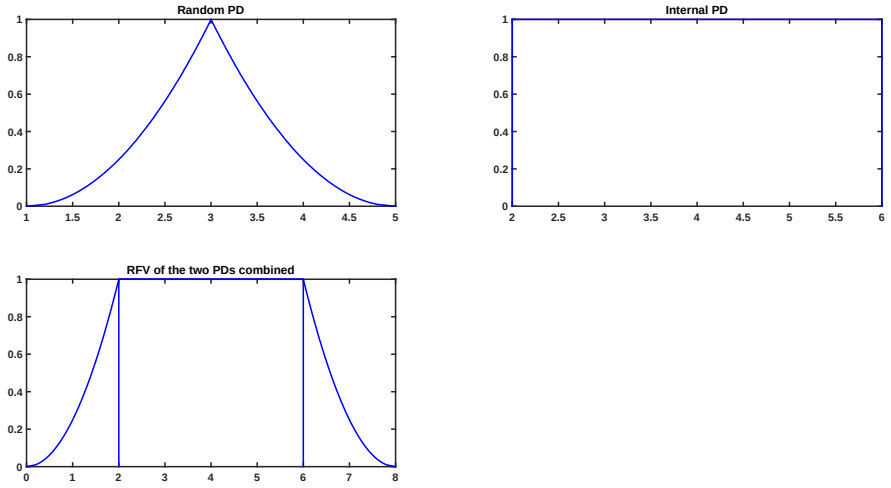

Figure 3.4: *RFV obtained from the random and internal PDs.*

So, by evaluating the $\alpha-$cut of the RFV for every α, the final RFV is obtained. Once the RFV is built, it is capable of representing the effects of both random and systematic contributions to uncertainty very effectively.

3.2.2 Combination of RFVs

As has been established earlier, a fuzzy variable can be expressed both in terms of its possibility distribution and in terms of its $\alpha-$cuts. The Zadeh extension principle can be used to combine the fuzzy variables if they are expressed as possibility distributions.

On the other hand, when the fuzzy variable is expressed in terms of its $\alpha-$cuts, the Nguyen's theorem could be used to combine the fuzzy variables.

The theorem can be stated as follows: Given two fuzzy variables X and Y expressed in terms of their $\alpha-$cuts, X_α and Y_α respectively, the $\alpha-$cut of the result Z which is a function of X and Y can be given by,

$$
\begin{aligned}
Z_\alpha &= [f(X,Y)]_\alpha = \bigcup_{T(\epsilon,\eta)\geq\alpha} f(X_\epsilon, Y_\eta) \quad \alpha \in (0,1] \\
Z_{\alpha=0} &= [f(X,Y)]_{\alpha=0}
\end{aligned}
\tag{3.19}
$$

where $T(\epsilon, \eta)$ is the t-norm that has been applied.

The t-norms are applied depending on how the two fuzzy variables are combining with each other.

When the two quantities are interacting and combining with each other in a systematic way, then the min t-norm is applied to combine the two corresponding fuzzy variables. This is the reason that even for the obtaining the external membership function of an RFV, we use the min t-norm to join the random and internal PDs.

On the other hand, when a Frank or a Dombi t-norm is applied, there is a certain level of compensation that is observed. So, it is almost as if the two PDs are somehow slightly compensating each other. This happens only when the two quantities are interacting with each other in a random way. So, when two variables are combining with each other in a random manner as do the random contributions to uncertainty or when there are multiple systematic contributions to uncertainty that combine in a random way, the t-norms other than the min t-norm are used.

It should be noted however that the combination of two PDs using a Frank or Dombi t-norm is only an approximation, although a very close approximation, of the reference PD which is obtained by applying the probability-possibility transformation to the resultant pdf obtained from the combination of the two corresponding pdfs in probability [47, 48]. Also, since the t-norms have parameters that dictate the resultant PD, it is important that a suitable value of the parameters are used to approximate the combination as closely as possible. It has also been demonstrated in [47, 48] that the Dombi t-norm is more accurate than the Frank t-norm when there are a large number of contributions to uncertainty that combine in a random way. So, when there are large number of random contributions to uncertainty that need to be combined, it is recommended to use the Dombi t-norm.

Fig. 3.5 shows the sum of two PDs corresponding to normal probability distributions with a min t-norm, a Frank t-norm and a Dombi t-norm as explained in sec. 2.3.2. The values of the parameter for Frank t-norm is $\gamma = 0.7$ and the parameters for the Dombi t-norm are $\gamma_1 = 1.1$ and $\gamma_2 = 1.7$

Since RFVs are constructed from an internal and a random membership function both of which are PDs, to combine two RFVs A and B to get a resultant RFV C, it should be done according to the following steps:

- Break A and B into their corresponding internal membership functions A^{int}, B^{int} and the corresponding random membership functions A^{ran}, B^{ran} respectively.
- Combine the respective internal PDs using a t-norm depending on how they are interacting with each other (if it is in a random way or a systematic way) as explained earlier to obtain the internal membership function of C (C^{int}).
- Combine the random PDs, to get the random membership function of C (C^{ran}), using a t-norm such as a Frank t-norm or a Dombi t-norm since random contributions to uncertainty can not interact with each other in a systematic way.

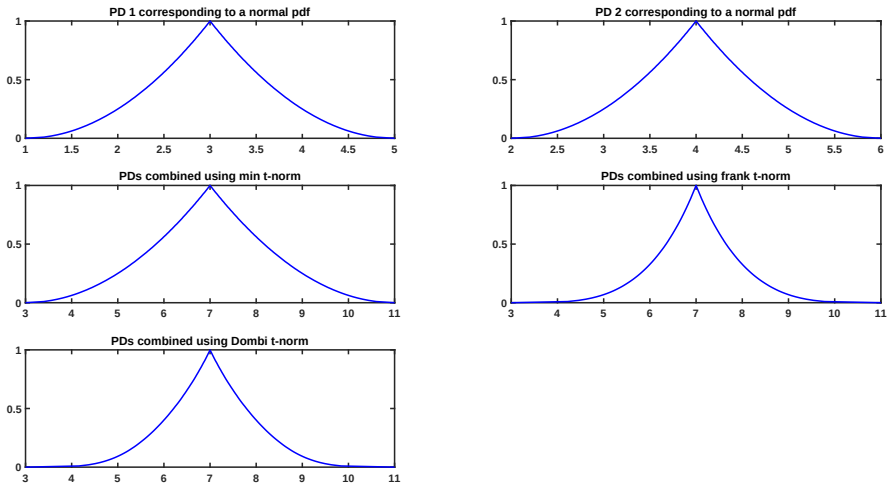

Figure 3.5: *Different t-norms applied to the same two PDs.*

- Construct the RFV C using the internal membership function (C^{int}) and the random membership function (C^{ran}) obtained in the previous steps.

3.2.3 RFVs in metrology

As has been established in the first chapter, there are various drawbacks to the theory of probability. Firstly, it can not represent all kinds of data (sparse data or ignorance) accurately. So, there is the need of a different theory which is more flexible and allows us to work with any form of data in a logically sound manner.

So, we found a more general theory which is the theory of evidence. This is a more general theory in which the theory of probability and the theory of possibility have been found to be special cases. Then we found that the theory of possibility forms a better option for representing uncertainty since it can represent also ignorance about the measurand in a mathematically accurate way. So, the systematic contributions to uncertainty can be represented in a mathematically accurate way.

Another advantage is that if the probability distribution function is actually available for the measurand, it can be transformed into a PD using the probability-possibility transforms. The rules of combination for possibility functions are also more flexible and not so rigid like in the theory of probability. This makes the use of the theory of possibility very appealing for representing measurement uncertainty. In turn, this makes the fuzzy variables as a good alternative to represent uncertainty because they are also represented by PDs.

As it has been explained earlier, the $\alpha-$cut ($[\alpha_1, \alpha_2]$) of a type 1 fuzzy variable is a closed set which represents a confidence interval with confidence $1-\alpha$. So, it is perfectly sufficient if a single confidence interval is needed which corresponds to just the random contributions to uncertainty or just the systematic contributions to uncertainty or the overall interval corresponding to the combined uncertainty of both the systematic and random contributions to uncertainty.

But, the $\alpha-$cut ($[\alpha_1, \alpha_2, \alpha_3, \alpha_4]$) has two nested sets in it. The $\alpha-$cut $[\alpha_1, \alpha_4]$ gives

the confidence interval of the external membership function and hence it represents the confidence interval corresponding to the combined uncertainty of both the systematic and random contributions to uncertainty. And the $\alpha-$cut $[\alpha_2, \alpha_3]$ gives the confidence interval of the internal membership function and hence it represents the confidence interval corresponding to just the systematic contributions to uncertainty.

This makes the use of RFVs which are also type 2 fuzzy variables a perfect choice to represent uncertainty in metrology. The advantages of RFVs are:

- Both Random and systematic contributions to uncertainty can be represented together and are well recognized.
- The combinations are done using closed-form formulae. So, the mathematics is easier compared to the probabilistic mathematics especially when dealing with pdfs other than the normal pdf.

The next few chapters focus on the applications and the use of RFVs in different scenarios.

CHAPTER 4

The Kalman filter.

4.1 Introduction

The Kalman filter (KF) is a well-known algorithm for predicting the state variables of a system [11]. It is a recursive discrete data filtering technique. It has been named after Rudolf E. Kalman. In the current times, it has become one of the most common data fusion algorithms in use. This is because of the low computational requirements to implement the filter, recursive property, representation of the linear system estimator assuming gaussian noise which is actually one of the reason for the easy computations and hence it is easy to be implemented in real time.

Kalman filter, in a way, is an extension of Gauss's least squares method to estimate the unknown parameters of a model which estimates the parameters by minimizing the mean square error in the model. Earlier, most of the systems were static and the measurements therefore remained constant with respect to time. Currently, though, systems are more dynamic in nature and the measurements are made at regular time intervals. Hence, Kalman filter becomes a very suitable algorithm to estimate the parameters using the real time measurements.

Some important aspects of the Kalman filter are:

- It is a type of recursive filter.
- It is a discrete filter which means that it processes samples taken at regular time intervals and not continuous signals.
- It predicts the future state of the system based on the current measurements and then the prediction is adjusted based on the next obtained measurement.
- In a strict sense, it considers gaussian noise as the only "disturbing" effect on the

input quantities. In practice though, this is often not the case when experimental data are collected.

The classical Kalman filter applies, in a strict sense, only to linear systems. But, in current times, lot of problems are non linear in nature. So, there have been variations to the original algorithm that have been proposed like the extended Kalman filter.

4.2 Kalman filter

Kalman filter differs from a regular filter in the sense that it requires a mathematical model of the system whose states are to be predicted. In other words, the process needs to be defined by a set of mathematical equations which define how the system state evolves depending on the previous system state and the control variables of the system.

Let us assume a process which is modeled by the mathematical equations given by:

$$\begin{aligned} x(k) &= Ax(k-1) + Bu(k-1) + w(k-1) \\ y(k)^{estimated} &= Hx(k) \end{aligned} \tag{4.1}$$

where:

$$x(k) = \begin{bmatrix} x_1(k) \\ x_2(k) \\ \vdots \\ x_n(k) \end{bmatrix}; \tag{4.2}$$

$$u(k) = \begin{bmatrix} u_1(k) \\ u_2(k) \\ \vdots \\ u_n(k) \end{bmatrix}; \tag{4.3}$$

$$y(k)^{estimated} = \begin{bmatrix} y_1(k)^{estimated} \\ y_2(k)^{estimated} \\ \vdots \\ y_n(k)^{estimated} \end{bmatrix}; \tag{4.4}$$

$$w(k) = \begin{bmatrix} w_1(k) \\ w_2(k) \\ \vdots \\ w_n(k) \end{bmatrix} \tag{4.5}$$

In the above equations, $x(k)$ is the vector of the system states, $u(k)$ is the vector of the system control variables, $y(k)^{estimated}$ is the output quantity vector and $w(k)$ is the

vector of the noise in the process. A is called the state-transition matrix, H is called the transformation matrix and B is the control-input matrix.

Using the variances of each element in the noise vector $w(k)$, a matrix represented by Q called the noise covariance matrix can be formulated as given in (4.6). As the name suggests Q is the matrix that represents the variances of each element and any possible covariances between the different elements of the noise in case they are correlated. In most cases, the process is homoscedastic. This means that the variance of the process remains constant over time. So, noise in the process $w(k)$ is a random variable drawn from a probability distribution that remains constant over time. Hence the variance of each element in the noise vector remains constant over time.

$$Q(k) = \begin{bmatrix} Var(w_1(k)) & Cov(w_1(k), w_2(k)) \dots Cov(w_1(k), w_n(k)) \\ Cov(w_2(k), w_1(k)) & Var(w_2(k)) \dots Cov(w_2(k), w_n(k)) \\ \vdots\vdots & \dots\vdots \\ Cov(w_n(k), w_1(k)) & Cov(w_n(k), w_2(k)) \dots Var(w_n(k)) \end{bmatrix} \tag{4.6}$$

The function of the Kalman filter is to use this mathematical model and produce a prediction of the next state of the system. But, if this was all there is to it, it would not be robust and would be highly sensitive to the inaccuracies in the model and the noise. Instead, the Kalman filter also takes into account the measurements that are made in every iteration to tune the predictions and adjust them according to the measurements made.

The measurement model can be represented by:

$$y(k) = y(k)^{estimated} + r(k) \tag{4.7}$$

where:

$$y(k)^{estimated} = \begin{bmatrix} y_1(k)^{estimated} \\ y_2(k)^{estimated} \\ \vdots \\ y_n(k)^{estimated} \end{bmatrix} \tag{4.8}$$

$$y(k) = \begin{bmatrix} y_1(k) \\ y_2(k) \\ \vdots \\ y_n(k) \end{bmatrix} \tag{4.9}$$

$$r(k) = \begin{bmatrix} r_1(k) \\ r_2(k) \\ \vdots \\ r_n(k) \end{bmatrix} \tag{4.10}$$

In the above equations, $y(k)$ is the measurement vector and $r(k)$ is the vector of the noise in the measurement and $y(k)^{estimated}$ is again the output quantity vector.

So, the function of the Kalman filter is to provide an estimate of $x(k)$ at an instant k given the previous system states $x(k-1)$ and the measurement vector, $z(k)$. This is done in two steps.

The first stage is called the prediction stage. This is basically using the mathematical model and the previous adjusted state estimate to provide the initial prediction of the state vector as given by (4.11)

$$\begin{aligned} x^a(k) &= Ax^f(k-1) + Bu^f(k-1) \\ p^a(k) &= Ap^f(k-1)A^T + Q \end{aligned} \tag{4.11}$$

$x^a(k)$ is the predicted estimate of the system state prior to using the measured values to adjust the estimate at instant k. $x^f(k-1)$ is the corrected estimate of the system state after using the measured values at instant $k-1$. $p(k)$ is the estimated state covariance matrix at instant k. Similar super scripts a and f are used for the control variable vector u and the state covariance matrix p to denote the predicted estimate and the corrected estimate respectively. Q is the noise covariance matrix and is usually constant.

It can be seen that the estimated state covariance matrix at instant k increases from the updated state covariance matrix at instant $k-1$ as Q is added to it every iteration. This would make sense since the uncertainty associated to the prediction is in fact higher since it has not been corrected yet using the measurements.

From (4.1), the error vector at instant k, $e(k)$, in the predicted states using the measured values is given by (4.12),

$$\begin{aligned} e(k) &= y(k) - y(k)^{estimated} \\ y(k)^{estimated} &= Hx(k) \\ e(k) &= y(k) - Hx(k) \end{aligned} \tag{4.12}$$

The second step is to correct the predicted estimate of the state variables using the error, a weighted ratio of the noise covariance matrix $c(k)$ and $r(k)$ called the Kalman gain $K(k)$ at instant k, the measurement noise vector as given in (4.13).

$$\begin{aligned} e(k) &= y(k) - Hx^a(k) \\ K(k) &= \frac{p^a(k)H^T}{(R + Hp^a(k)H^T)} \\ x^f(k) &= x^a(k) + K(k)e(k) \\ p^f(k) &= (I - KH)p^a(k) \end{aligned} \tag{4.13}$$

The Kalman gain $K(k)$ is calculated in such a way that the variance of the error $e(k)$ is minimized.

R is the noise covariance matrix of the measurements and is usually constant because of the homoscedasticity of the measurement process. Since the variance of the measurements remains constant over time as the measurement process remains unchanged, the noise covariance matrix of the measurements also remains unchanged

over time. It can again be seen that the updated state covariance matrix is smaller than the predicted state covariance matrix and this makes sense as well since the uncertainty associated to the updated states would be lower since the correction has been applied based on the measurements.

For an easy comprehension, the above classical KF algorithm has been shown in Fig. 4.1.

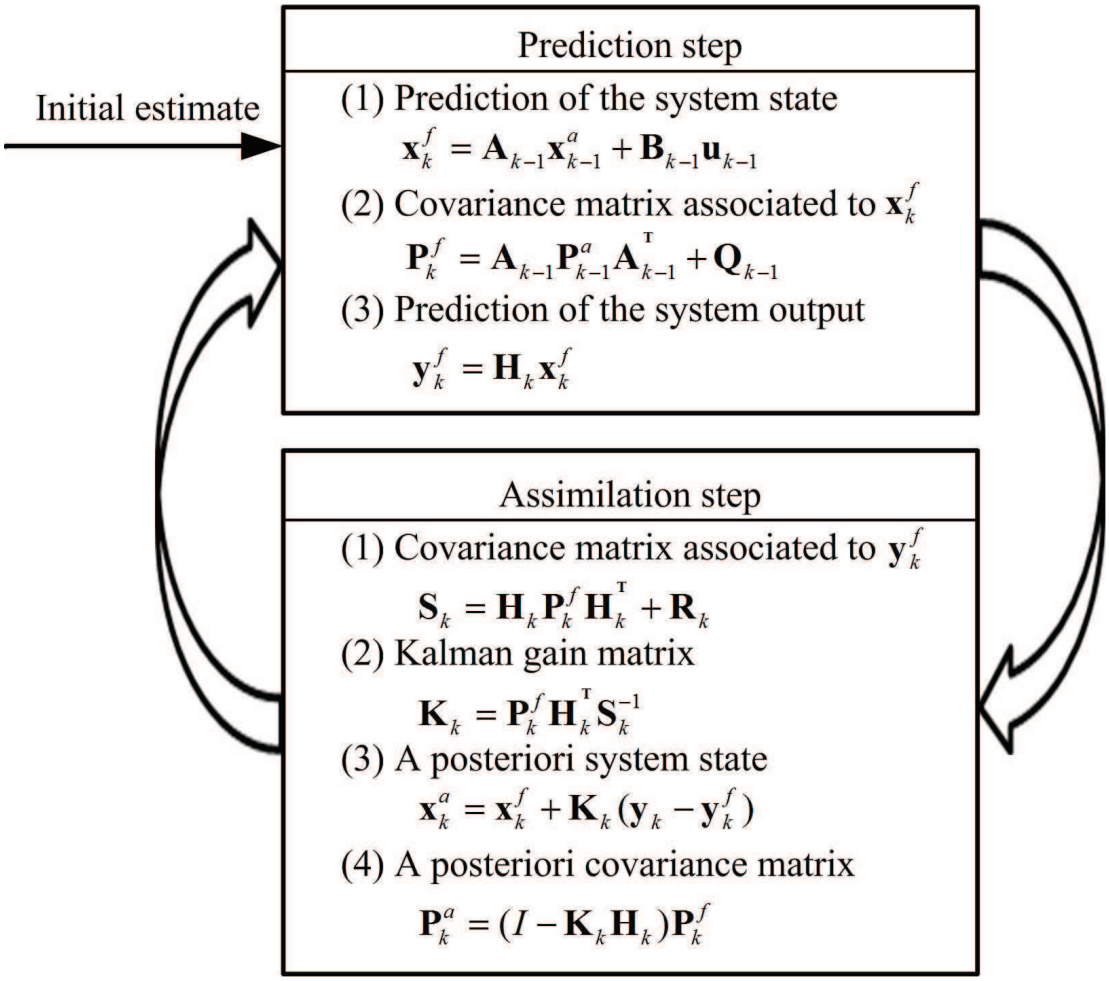

Figure 4.1: *Prediction and assimilation steps alternation in the classical Kalman filter.*

4.3 Example: Velocity and acceleration of a vehicle

A simple example is considered, in which a vehicle is moving at a velocity $v_{\mathrm{ref}}(t)$, according to the impressed acceleration $a_{\mathrm{ref}}(t)$, as shown in Fig. 4.2.

The classical Kalman filter described in Sect. 4.2 is used to estimate velocity and acceleration of the vehicle.

Eq. (4.14) shows the state equations of the model:

- v_k and a_k are velocity and acceleration of the vehicle at time k;
- w_k^v and w_k^a are the standard deviation of the noise in velocity and acceleration respectively at time k;

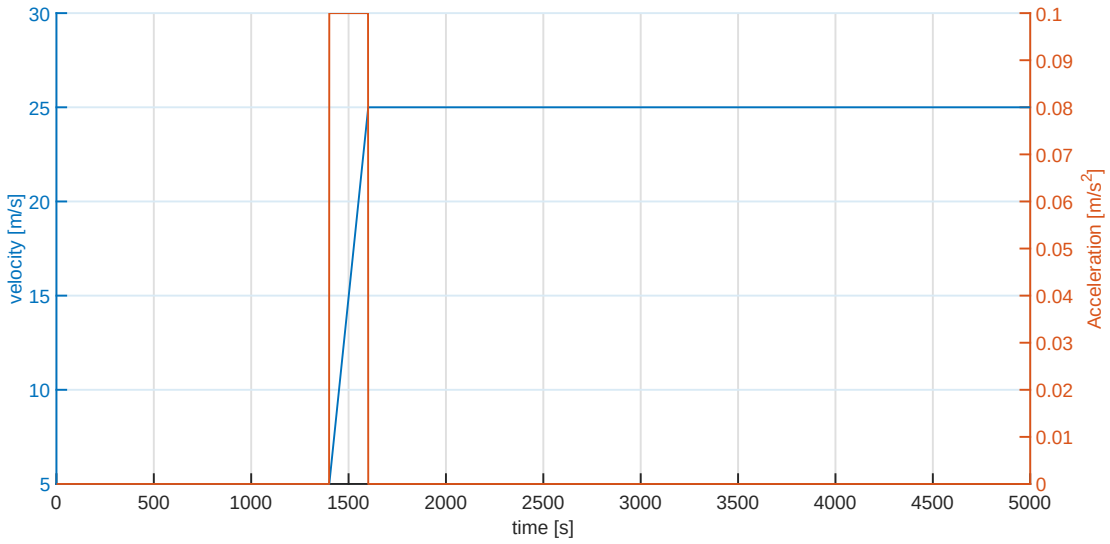

Figure 4.2: *Reference values of velocity (blue line) and acceleration (red line) over time.*

- τ is the time period within two successive measurements

$$\begin{aligned} v_k &= v_{k-1} + \tau \cdot a_{k-1} + w_k^v \\ a_k &= a_{k-1} + w_k^a \end{aligned} \tag{4.14}$$

τ has been assumed to be constant and equal to 1 s.

For the considered example, the state vector is $\mathbf{x}_k = \begin{bmatrix} v_k \\ a_k \end{bmatrix}$; the *state-transition matrix*, denoted with **A** in (4.11), is constant $\mathbf{A} = \begin{bmatrix} 1 & \tau \\ 0 & 1 \end{bmatrix}$; the *control-input matrix*, denoted with **B** in (4.11) is zero; the *transformation matrix*, denoted with **H** in (4.13), is: $\mathbf{H} = \begin{bmatrix} 1 & 0 \\ 0 & 1 \end{bmatrix}$ and the measurement vector is: $\mathbf{y}_k = \begin{bmatrix} v_{mk} \\ a_{mk} \end{bmatrix}$.

As shown in (4.11) and (4.13), two matrices have to be defined: the covariance matrix $\mathbf{Q}_k$, which considers the process noise, and the covariance matrix $\mathbf{R}_k$, which considers the measurement noise, that is the uncertainty associated to the measured values. Therefore, it is: $\mathbf{Q}_k = \begin{bmatrix} w_{k\,v}^2 & 0 \\ 0 & w_{k\,a}^2 \end{bmatrix}$ and $\mathbf{R}_k = \begin{bmatrix} u_{k\,v}^2 & 0 \\ 0 & u_{k\,a}^2 \end{bmatrix}$, where $u_{k\,v}$ is the standard uncertainty associated to the measured values of velocity and $u_{k\,a}$ is the standard uncertainty associated to the measured values of acceleration.

The following assumptions are done, as far as the initial values of the state variables and their associated uncertainty values are considered.

- It is supposed that $\mathbf{Q}_k$ and $\mathbf{R}_k$ do not vary with k, i. e. $\mathbf{Q}_k = \mathbf{Q} = \begin{bmatrix} w_v^2 & 0 \\ 0 & w_a^2 \end{bmatrix}$ and $\mathbf{R}_k = \mathbf{R} = \begin{bmatrix} u_v^2 & 0 \\ 0 & u_a^2 \end{bmatrix}$.
- The initial velocity of the vehicle is assumed to be a normal distribution with mean equal to the first measured value of velocity (v_{m1}) and standard deviation

0.003 m/s. Therefore: $v_0 = v_{m1}$ m/s and $w_v = 0.003$ m/s. This last value has been chosen by considering the accuracy of a GPS, which is quite accurate compared to the speedometer of the vehicle, and it is directly retrieved from the official GPS website [1].

- The initial acceleration is assumed to be a normal distribution centered at the first measured value of acceleration (a_{m1}) obtained from the accelerometer, with a standard deviation of $0.0005\ m/s^2$, due to some kind of noise either due to the circuit or due to the driver applying force on the accelerator. Therefore: $a_0 = a_{m1}$ m/s^2 and $w_a = 0.0005$ m/s^2.

On the other side, at every step k, as far as measurements are concerned, the uncertainty contributions affecting the measured values must be also considered. It has been assumed that the measured values are affected by both random and systematic uncertainty contributions. In particular, as far as the velocity is concerned, typical accuracy values have been assumed for the on-board sensor, which are generally one or two orders of magnitude less accurate than a GPS-based speedometer:

- The random contribution is supposed to be normally distributed, with a standard deviation $u^v_{\text{ran}} = 0.16$ m/s.
- All systematic errors have been assumed to have been compensated for.

Similarly, also for the acceleration, it is supposed that no systematic contributions affect the measurement procedure, while a typical random contribution is considered which is supposed to be normally distributed, with a standard deviation $u^a_{\text{ran}} = 0.005$m/s^2 that is one order of magnitude less accurate than the model.

The classical Kalman filter, as explained in Sect. 4.2 is applied, where, according to the above assumptions, at $k = 0$ it is:

- $\mathbf{x}^a_0 = \begin{bmatrix} v_{m1} \\ a_{m1} \end{bmatrix}$;
- $\mathbf{P}^a_0 = \mathbf{Q}$.

The results can be seen in Fig. 4.3 and 4.4 respectively for velocity and acceleration. The blue lines in the respective figures represent the difference between the predicted states (velocity and acceleration) and the actual states. The red lines represent the uncertainty estimates for the velocity and acceleration in the respective figures.

It can be seen that the Kalman filter is clearly able to predict the states perfectly inside the uncertainty limits.

But what happens when the ideal conditions required for a Kalman filter are not satisfied. For example, what if there is an uncompensated systematic error in the measurements? Of course, the theory of the Kalman filter prevents using it when the measurement values have a systematic error. So, the following example is simply aimed at demonstrating the error in the estimation of the uncertainty associated to the states by the classical KF in the case of an incorrect application of the Kalman filter, in violation of the theoretical assumptions behind it.

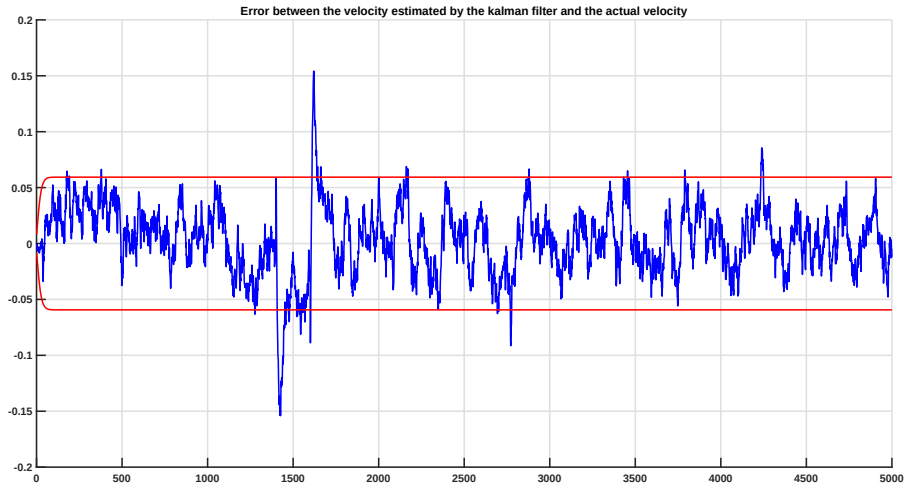

Figure 4.3: *Difference in the reference and predicted velocity values (blue line) provided by the classical Kalman filter, together with the predicted uncertainty interval (red lines).*

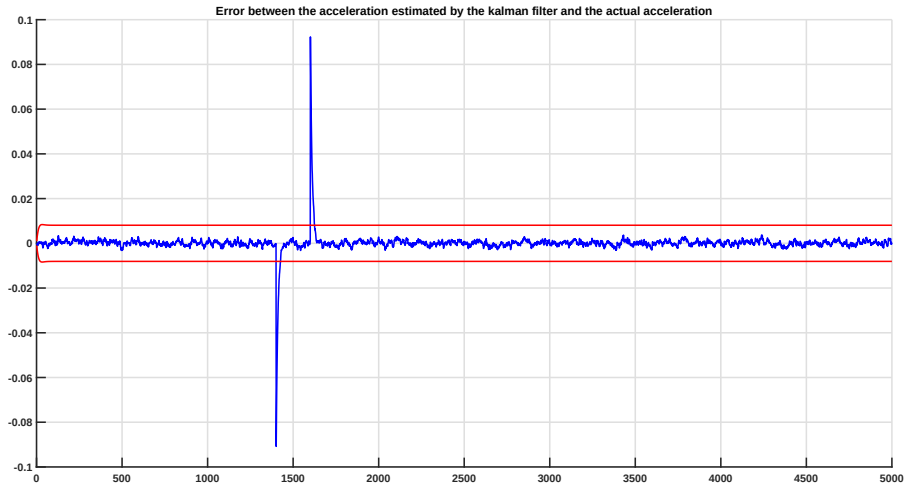

Figure 4.4: *Difference in the reference and predicted acceleration values (blue line) provided by the classical Kalman filter, together with the predicted uncertainty interval (red lines).*

4.4 Example:Velocity and acceleration in the presence of a systematic error

The same example given in Sect. 4.3 is considered, in which a vehicle is moving at a velocity $v_{\rm ref}(t)$, according to the impressed acceleration $a_{\rm ref}(t)$, as shown in Fig. 4.2. But, there is a slight difference. In the previous section, it has been assumed that all the systematic errors have been fully compensated for and the measurements are free from all bias. In this example, it has been assumed that the velocity measurements are affected by a systematic error of magnitude 0.3 m/s which is still inside the 2σ limit for the random contributions to uncertainty since it has been assumed that the velocity

measurements are affected by a gaussian noise with a standard deviation of 0.16 m/s as described in the previous section.

The classical Kalman filter without any additional modifications is used to estimate the velocity and acceleration of the vehicle.

Eq. (4.14) shows the state equations of the model.

Since it is the same example, the state vector is just as before: $\mathbf{x}_k = \begin{bmatrix} v_k \\ a_k \end{bmatrix}$; the *state-transition matrix*, denoted with $\mathbf{A}_{k-1}$ in Fig. 4.1, is constant $\mathbf{A}_k = \mathbf{A} = \begin{bmatrix} 1 & \tau \\ 0 & 1 \end{bmatrix}$; the *control-input matrix*, denoted with $\mathbf{B}_k$ in Fig. 4.1 is zero; the *transformation matrix*, denoted with $\mathbf{H}_k$ in Fig. 4.1, is: $\mathbf{H}_k = \mathbf{H} = \begin{bmatrix} 1 & 0 \\ 0 & 1 \end{bmatrix}$ and the measurement vector is: $\mathbf{y}_k = \begin{bmatrix} v_{mk} \\ a_{mk} \end{bmatrix}$.

The noise covariance matrix $\mathbf{Q}_k$ of the predictions and the noise covariance matrix $\mathbf{R}_k$ of the measurement data are also the same as described in the previous example in Sect. 4.3.

On the other side, at every step k, as far as measurements are concerned, it has been assumed that the measured values are affected by both random and systematic uncertainty contributions. In particular, as far as the velocity is concerned, typical accuracy values have been assumed for the on-board sensor, which are generally one or two orders of magnitude less accurate than a GPS-based speedometer:

- The random contribution is supposed to be normally distributed, with a standard deviation $u^v_{\mathrm{ran}} = 0.16\,\mathrm{m/s}$.
- A systematic error is also supposed to be present, with an estimated value $e^v_{sys} = 0.3\,\mathrm{m/s}$. But this value is supposed to be unknown, so that a systematic contribution is modeled, laying in the interval $\pm b_{\mathrm{sys}} = \pm 0.32\,\mathrm{m/s}$ (which include the true systematic error e^v_{sys}).

On the other hand, as far as the acceleration is concerned, it is supposed that no systematic contributions affect the measurement procedure, while a typical random contribution is considered which is supposed to be normally distributed, with a standard deviation $u^a_{\mathrm{ran}} = 0.005\mathrm{m/s}^2$ that is one order of magnitude less accurate than the model.

Just like the previous section, according to the above assumptions (Sect. 4.3), at $k = 0$:

- $\mathbf{x}^a_0 = \begin{bmatrix} v_{m1} \\ a_{m1} \end{bmatrix}$;
- $\mathbf{P}^a_0 = \mathbf{Q}$.

As far as the measurements are concerned, the value of the measured velocity v_k is simulated, at every step k, as a random extraction from a normal distribution with mean value $v_{\mathrm{ref}}(k) + e^v_{sys}$ and standard deviation u^v_{ran}. The standard uncertainty value associated to the measured value v_k is u_v, which must take into account for both random and systematic uncertainty contributions. As suggested by the GUM [27]:

$$u_v = \sqrt{\left(u^v_{\mathrm{ran}}\right)^2 + \left(u^v_{\mathrm{sys}}\right)^2}$$

where u^v_{sys} is the standard deviation of the pdf associated to the considered systematic contribution. When the GUM [27] is followed and probability theory is employed for uncertainty evaluation, it is a common practice to assign a uniform distribution over the interval of possible variation of the systematic contribution. Under this assumption, it is: $u^v_{\text{sys}} = \frac{b_{\text{sys}}}{\sqrt{3}}\ \text{m/s}$.

Similarly, the simulated measured acceleration a_k at every step k is a random extraction from a normal distribution with mean value $a_{\text{ref}}(k)$ and standard deviation u^a_{ran}. Since only random contributions are supposed to affect the acceleration measurement procedure, the standard deviation associated to a_k is u^a_{ran}.

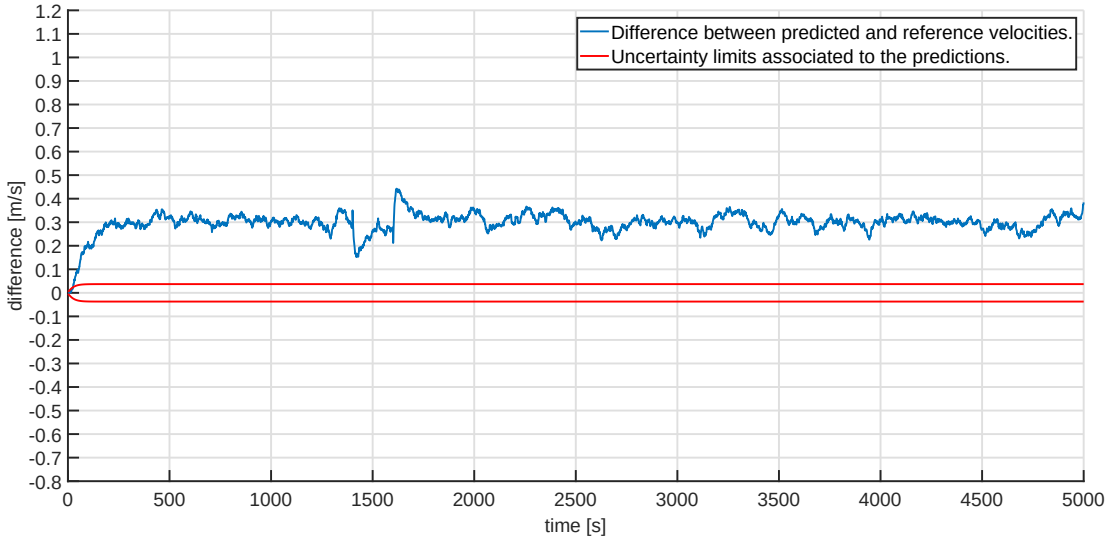

Figure 4.5: *Difference in the reference and predicted velocity values (blue line) provided by the classical Kalman filter, together with the predicted uncertainty interval (red lines).*

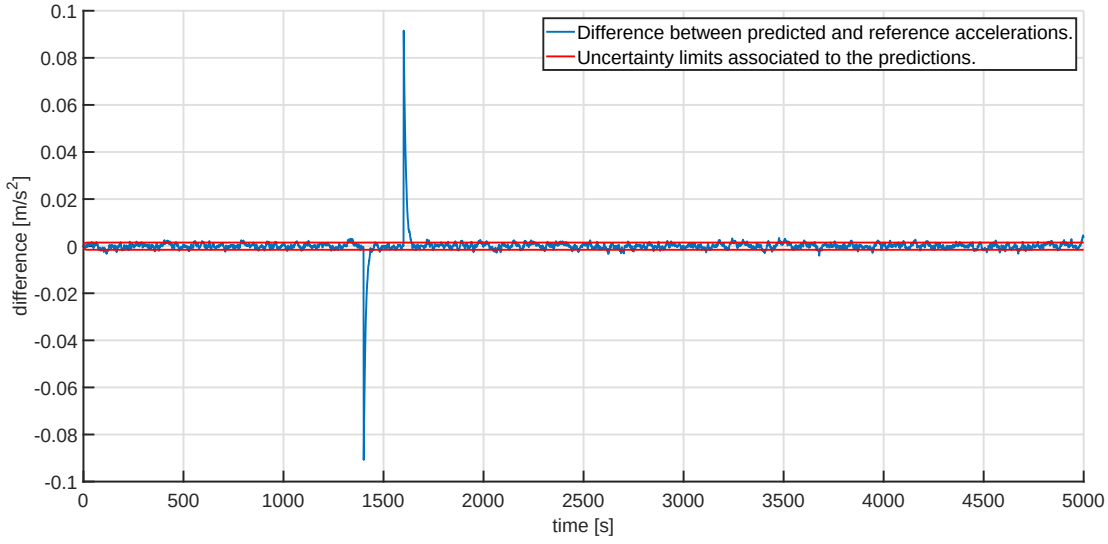

Figure 4.6: *Difference in the reference and predicted acceleration values (blue line) provided by the classical Kalman filter, together with the predicted uncertainty interval (red lines).*

The results of the simulation are reported in Fig. 4.5 and 4.6.

The blue line in Fig. 4.5 represents the difference between the predicted velocity and v_{ref}. This difference is of course not constant but, after a transition of about 250 iterations (i. e. $250\,\mathrm{s}$, since one iteration is done every $1\,\mathrm{s}$) oscillates around the value e_{sys}, as expected, because of the presence of the systematic error in the measurements. On the other hand, the red lines represent the evaluated uncertainty interval. In particular, for each iteration k, the provided interval is the $\pm 3\sigma_k$ interval [27], where σ_k is the standard uncertainty associated to the *a posteriori* value of the velocity at step k, that can be retrieved from the values in the main diagonal of matrix $\mathbf{P}_k^a$.

It can be clearly seen that the difference between the predicted velocity and $v_{\mathrm{ref}}(t)$ is always outside the obtained uncertainty bounds. So, even if the classical Kalman filter can predict quite well the velocity of the vehicle (at steady state), it can be concluded, as expected, that it underestimates the measurement uncertainty and therefore, the theoretical expectation that it is not suitable when also systematic contributions to uncertainty are present is confirmed. Furthermore, the convergence time is quite high.

Fig. 4.6 shows the results obtained for the acceleration and the blue and red lines have the same meaning as in Fig. 4.5. In this case, since only random contributions affect the measured values, the $\pm 3\sigma$ uncertainty intervals contain the measured values except, of course, when the acceleration has a sudden variation.

4.5 Limitations of the classical KF

In its classical formulation, mathematically, KF requires the model uncertainty and the measurement uncertainty to be normal probability distributions [11]. The second limitation is that it is required that the noise is completely unbiased. Or, in other words, all systematic contributions to uncertainty must be compensated for. This is because the Kalman filter simply follows the pattern of the data that is being observed while decreasing the effect of the random contributions to uncertainty using the mathematical model.

In practice, however, this is not possible as sometimes, the systematic errors can not be recognized and therefore are not compensated for.

And as it is confirmed by the example in the previous section, the classical KF is not suitable when there is an uncompensated systematic error in the observed data as can be seen in fig. 4.5. It can be seen that the uncertainty limits have been severely underestimated which is to be expected because the systematic contributions to uncertainty have not been taken into account in a mathematically accurate way.

Modified versions of the classical KF are available and they differ in the way they use different representations of uncertainty to deal with the systematic error in the measurement. In [43], a variation of KF called the Schmidt Kalman filter is proposed which attempts to take into account systematic uncertainty contributions as well, as explained in Sect. 4.6 and applied in this chapter.

Another method would be to implement the Kalman filter as a markov process in the presence of a systematic contribution to uncertainty by considering the systematic error as an ensemble of values from a uniform probability distribution. This has also been explained in the section and has been implemented.

4.6 Schmidt Kalman filter

The Schmidt Kalman filter has been proposed in [43], as a variation of the classical KF, to consider also the systematic uncertainty contributions. The Schmidt Kalman algorithm is as shown in Fig. 4.7. The same example as before has been considered again for the sake of homogeneity in the simulations for easy comparison.

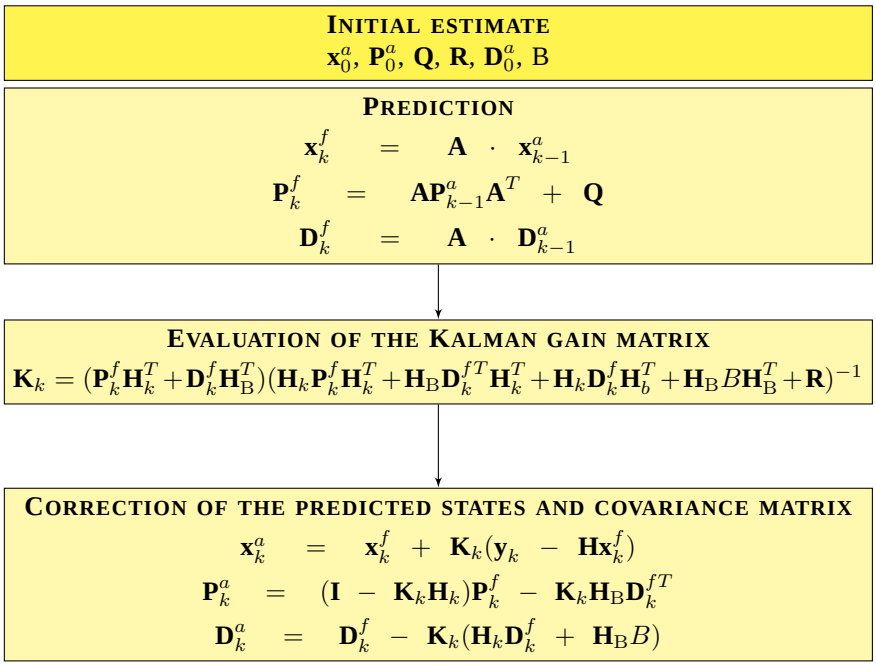

Figure 4.7: *Schmidt Kalman filter algorithm.*

It considers the systematic contribution to uncertainty as an additional state variable. So, the systematic contributions are modeled as a separate matrix of states and the corresponding noise covariance matrix is considered. Therefore, new matrices, in addition to the ones defined in the classical KF have to be defined for modeling the systematic contribution:

- $\mathbf{H}_\mathrm{B} = \begin{bmatrix} 1 \\ 0 \end{bmatrix}$
- $B = {u_{\mathrm{sys}}^v}^2 = 0.32^2/3$
- $\mathbf{D}_0^a = \begin{bmatrix} 0 \\ 0 \end{bmatrix}$

where B is the variance of the systematic contribution and $\mathbf{D}$ is the cross covariance matrix between the random and systematic errors. It is a zero matrix because the systematic and random errors are independent in the considered example. The Readers are addressed to [43] for further details.

The initial values of $\mathbf{x}_0^a$, $\mathbf{Q}$ and $\mathbf{P}_0^a$ are the same as in Sect. 4.3.

Also the simulated measured values v_k of velocity are obtained as in Sect. 4.3 but, in this case, the associated standard uncertainty value is u_{ran}^v, because in the Schmidt Kalman filter, the systematic uncertainty is propagated as a separate matrix.

The simulated measured values of acceleration a_k and the associated standard deviation are also obtained as in Sect. 4.3.

The results of the simulations are reported in Fig. 4.8 and 4.9, where the blue and the red lines have the same meaning as in Figs. 4.5 and 4.6.

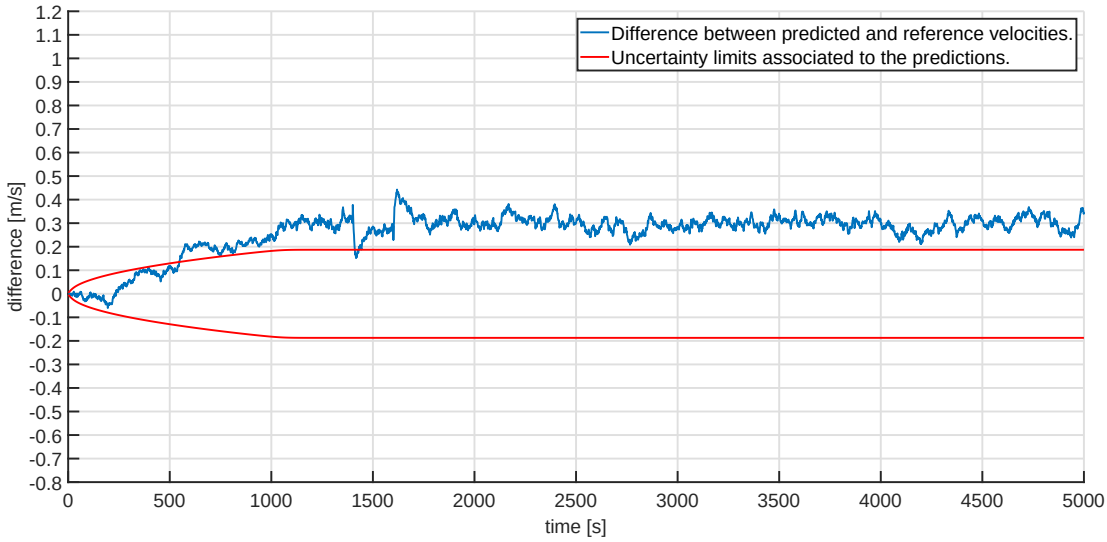

Figure 4.8: *Difference in the reference and predicted velocity values (blue line) provided by the Schmidt Kalman filter, together with the predicted uncertainty interval (red lines).*

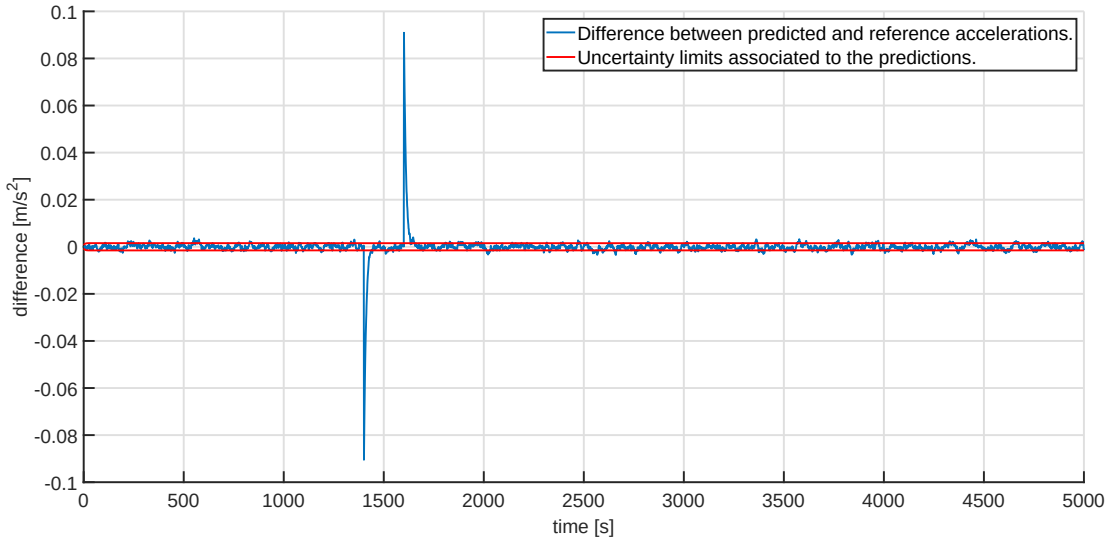

Figure 4.9: *Difference in the reference and predicted acceleration values (blue line) provided by the Schmidt Kalman filter, together with the predicted uncertainty interval (red lines).*

The results obtained for the acceleration are pretty much the same as in the previous case in Sect. 4.3, while a difference can be seen in the velocity.

The Schmidt Kalman filter is aimed at considering systematic uncertainty contributions and indeed the uncertainty intervals are significantly larger than those obtained in Sect. 4.3, but they do not yet contain the actual velocity of the vehicle. Therefore, even if the Scmidt KF provides a better estimation of the measurement uncertainty in the

presence of systematic contributions than the classical KF, uncertainty is still underestimated. This would, in turn, mean that the systematic contributions to uncertainty are still not considered in a completely accurate manner and are underestimated.

4.7 Kalman filter based on a Monte Carlo sampling

The same example as in Sect. 4.4 has been considered again for easy comparison. So, it has been assumed to have a systematic error of 0.3 m/s in the velocity measurement data.

When there is an uncompensated systematic contribution to uncertainty, an interval of values can be estimated where the systematic error lies in. Of course, only an interval can be assumed but the actual value can not be estimated. Otherwise, it could be simply compensated for. So, there is a situation of total ignorance in this interval of values. In the theory of probability, when there is total ignorance, a maximum entropy model is assumed, which leads us to use the uniform probability distribution to represent total ignorance.

In this particular example, the distribution corresponding to the systematic contribution to uncertainty has been assumed to be a uniform distribution with a zero mean and a half-width of 0.32 m/s which is equal to the 2σ interval of the random noise which has been assumed to be gaussian in nature and with a standard deviation of $0.16m/s$. So, the distribution of the velocity would be imposed by both the random and the systematic contributions to uncertainty.

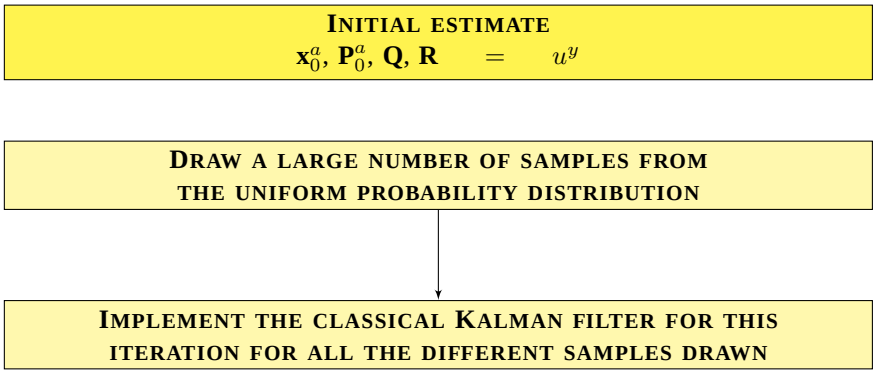

Figure 4.10: *Classical Kalman filter algorithm applied based on monte carlo sampling.*

The classical Kalman filter that has been described in Sect. 4.2 has been used but with a change. The difference is that it is implemented based on a Monte Carlo sampling method. So, the systematic error has been assumed to be an ensemble of values and each of these values belong to the uniform distribution that has been attributed to the systematic uncertainty as explained earlier.

So, every iteration of the Kalman filter has been performed for a large number of samples drawn from the uniform probability distribution so that every possible systematic error in the interval is considered.

The algorithm is as shown in fig. 4.10.

This leads to the consideration of every possible value in the interval so that the maximum value of the obtained state predictions in each iteration can be considered as the uncertainty limit for the particular iteration.

The results are shown in Fig. 4.11.

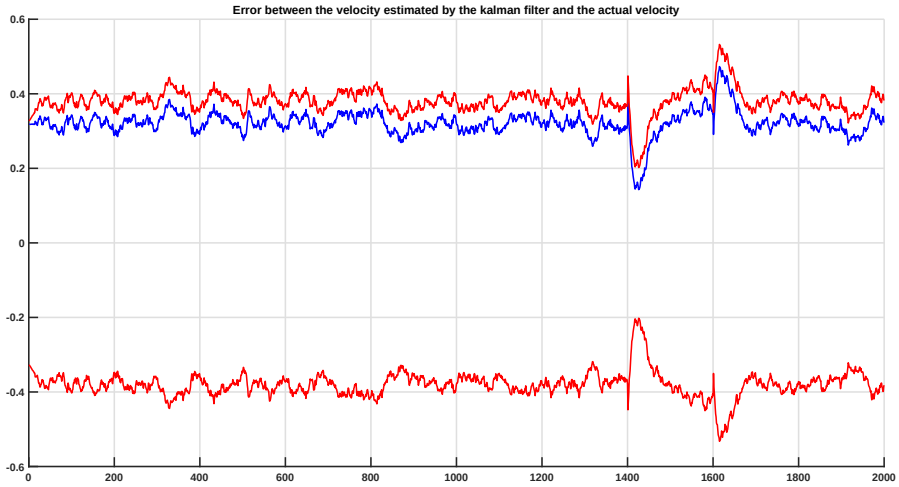

Figure 4.11: *Difference in the reference and predicted velocity values (blue line) provided by the Kalman filter, together with the predicted uncertainty interval (red lines).*

Again, the blue lines represent the error between the predicted states by the Kalman filter and the actual velocity. The plot of acceleration is not reported since it is unchanged with respect to the classical KF since the acceleration does not suffer from any systematic error. It can be seen from Fig. 4.11 that the blue line representing the error between the predicted states by the Kalman filter and the actual velocity still has a mean value of 0.3 m/s. But, the red lines representing the uncertainty are wider apart from each other and the error lies inside the uncertainty interval.

So, implementing a Kalman filter based on Monte Carlo sampling works. But, the number of simulations to be done increases by a very large value and hence, this method is not computationally efficient.

Hence, the theory of possibility and RFVs have been used as explained in the next chapter.

CHAPTER 5

The modified possibilistic Kalman filter.

5.1 Introduction

As it has been explained in the previous chapter, the classical Kalman filter and the theory of probability both are not very suitable to represent and propagate systematic contributions to uncertainty in a mathematically accurate way. As it could also be seen in the previous chapter, there have also been modifications to the Kalman filter as an attempt to consider systematic contributions to uncertainty but they are still inadequate.

The possibilistic KFs defined in [13] and in this chapter also serve the same purpose. There have been other attempts to process systematic contributions to uncertainty using a Kalman filter [42, 52, 53]. Both [52] and [53] propose algorithms to attempt to estimate the systematic error in the measurement and then compensate for the error but do not try to propagate the systematic contributions to uncertainty. Whereas, in [42], an algorithms is proposed to include a systematic error that is of unknown magnitude but is known to be bounded into Bayesian inference and KF using an approach based entirely on probability. However, to achieve this, all the different possible probability density functions over the specified interval with all possible mean values of the corresponding pdfs need to be considered. This makes it quite complex. As explained in chapter 2, a possibility distribution is basically a superior probability distribution. So, it can be seen as inclusive of all possible pdfs. Hence, if possibility distributions could be used in a KF, it would make it a more straight forward implementation of [42].

There are KFs based on the theory of possibility available in the literature [40, 44] but, as per the author's knowledge, uncertainty is considered in a kind of subjective way in those algorithms [13], as is the case with the fuzzy applications. But uncertainty is a well specified concept in metrology and is recommended by [27, 30] to be processed in the same way. Since uncertainty, in metrology, must be considered according to the definition given by [27, 30], this chapter is hence aimed at proposing a possibilistic KF,

whose definition is perfectly framed within the present Standards [27, 30].

As explained earlier in chapter 3, within the mathematical framework of the theory of possibility, Random-Fuzzy variables can be used to represent all contributions to uncertainty in a more accurate way. Therefore, methods and algorithms aimed at fully exploiting the advantages provided by the Random-Fuzzy variables in expressing measurement uncertainty should be capable of processing them. The same goes for the Kalman Filter as well, and the KF proposed in this chapter using the theory of possibility, to be able to process all kinds of uncertainty contributions, is based on these variables (RFVs).

To validate the possibilistic KFs, the same example is considered, where the velocity of a vehicle, along with its associated measurement uncertainty, has to be estimated, with a Kalman filter. This example is described in Sect. 4.4.

Two different approaches to the possibilistic KF are applied and compared with each other: the possibilistic Kalman filter proposed in [13] and a refinement of it, proposed in this chapter. The modified possibilistic KF proposed in this chapter operates with the exact same equations as the classical KF but all output and state variables are RFVs instead of being crisp values as in the classical KF.

Finally, a hybrid KF has also been applied, which combines both the classical KF algorithm and the possibilistic KF algorithm defined in this chapter, for the random and systematic uncertainty contributions respectively.

This last version has been considered, as shown in Sect. 5.5, to validate the proposed possibilistic KF by processing the systematic and random contributions to uncertainty separately, according to their natural mathematical representation [18, 19]. Under these conditions, the highest accuracy is achieved, as shown in Sect. 5.5, at the cost of a higher computational burden that, at present, makes the hybrid KF suitable only as a reference method.

5.2 The considered example

The same example is considered and has been recalled for easy reference, in which a vehicle is moving at a velocity $v_{\mathrm{ref}}(t)$, according to the impressed acceleration $a_{\mathrm{ref}}(t)$, as shown in Fig. 5.1.

Eq. (5.1) shows the state equations of the model:

- v_k and a_k are velocity and acceleration of the vehicle at time k;
- w_k^v and w_k^a are the standard deviation of the noise in velocity and acceleration respectively at time k;
- τ is the time period within two successive measurements

$$\begin{aligned} v_k &= v_{k-1} + \tau \cdot a_{k-1} + w_k^v \\ a_k &= a_{k-1} + w_k^a \end{aligned} \tag{5.1}$$

Since it is the same example as in Sect. 4.4, the state vectors, the measurement vector and the matrices are all the same as given in Sect. 4.4.

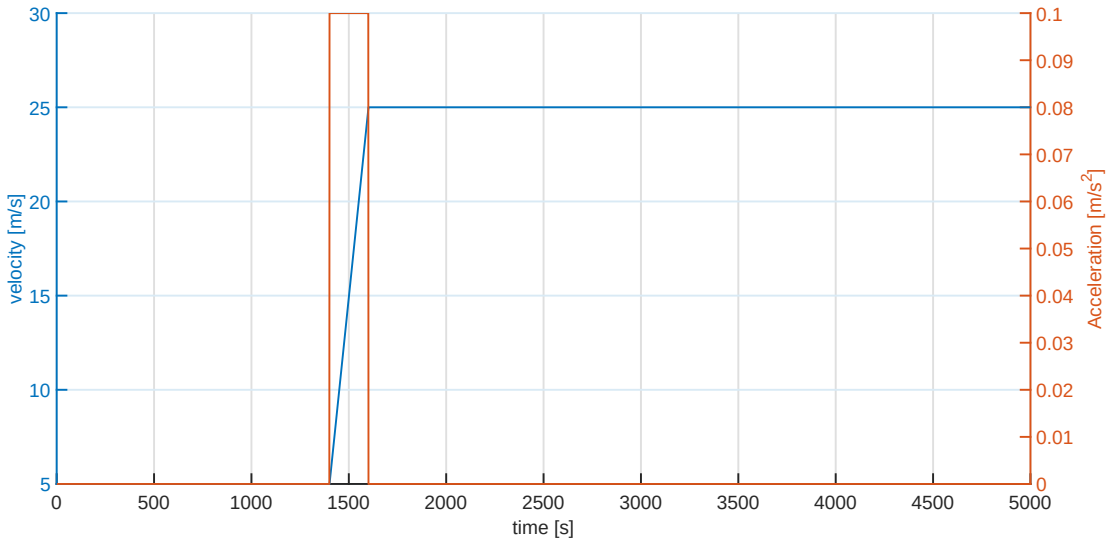

Figure 5.1: *Reference values of velocity (blue line) and acceleration (red line) over time.*

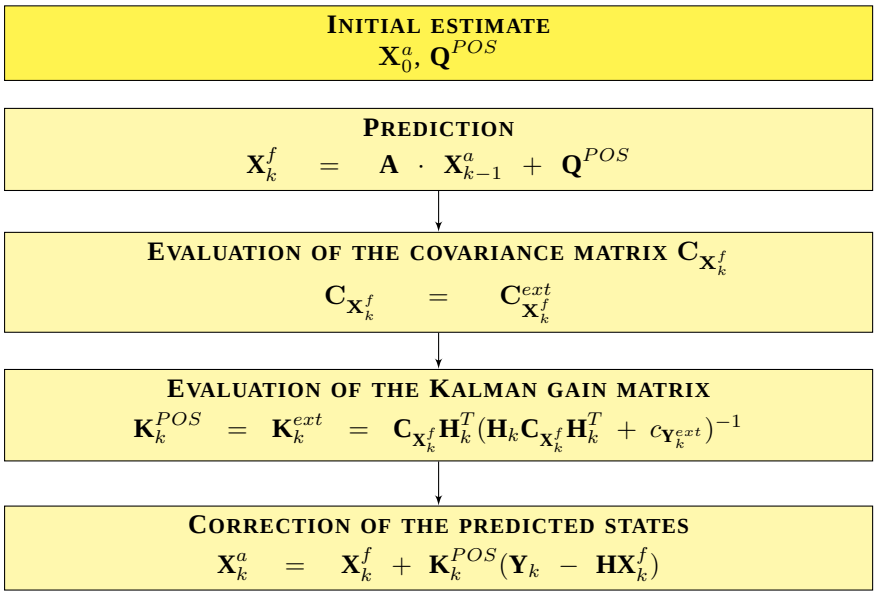

Figure 5.2: *Possibilistic Kalman filter algorithm defined in [13].*

5.3 The possibilistic Kalman filter

This section considers the application of the possibilistic Kalman filter defined in [13], with the aim to consider also the presence of systematic contributions to uncertainty.

The basic equations of this algorithm defined in [13] are given in Fig. 5.2. It can be seen the the equations are very similar to the classical KF equations.

But, in a classical KF, the states are all crisp values and the noise is considered separately using the noise covariance matrix which is propagated separately from the states. This is an important reason for which all the noises need to be strictly gaussian since, otherwise, the equations for the propagation of the noise covariance matrix do not hold true anymore.

In the possibilistic KF, on the other hand, all variables in the state vectors are RFVs and the iterations are performed using RFV mathematics [14, 19, 48], so that both random and systematic contributions can be mathematically represented and combined according to their different nature [19, 48]. Hence, the noise covariance matrix does not need to be propagated separately from the states and is automatically propagated when the states vectors are combined in the form of RFVs. This makes it possible to implement the possibilistic KF for any type of distributions.

Furthermore:

- as for the matrix which considers the model uncertainties (matrix **Q** in the classical Kalman filter), according to the assumptions reported in Sect. 4.4, we define a vector of RFVs $\mathbf{Q}^{POS}$ where:
  - the element related to velocity is an RFV in which there is no internal PD and the random PD is obtained by transforming [48] a zero mean normal pdf with standard deviation w^v in the possibility domain;
  - the element related to acceleration is an RFV in which there is no internal PD and the random PD is obtained by transforming [48] a zero mean normal pdf with standard deviation w^a in the possibility domain;
- as for the initial state vector $\mathbf{X}_0^a$, it is assumed that
  - the initial velocity is an RFV in which there is no internal PD and the random PD is obtained by transforming [8, 15, 16, 36, 48] a normal pdf with mean equal to the first measured value for velocity (v_{m1}) and standard deviation w^v in the possibility domain;
  - the initial acceleration is an RFV in which there is no internal PD and the random PD is obtained by transforming [8, 15, 16, 36, 48] a normal pdf with mean equal to the first measured value for acceleration (a_{m1}) and standard deviation w^a in the possibility domain;
- as for the measured values, for every step k, the RFV associated to the simulated measured velocity is centered on v_k (obtained as in Sect. 4.4) and
  - the internal PD is a rectangular PD with width $\pm b_{sys}$ around v_k;
  - the random PD is obtained by transforming [48] a zero mean normal pdf, with standard deviation u_{ran}^v in the possibility domain.

  On the other hand, the RFV associated to the simulated measured acceleration is centered on a_k (obtained as in Sect. 4.4) and:
  - the internal PD is nil;
  - the random PD is obtained by transforming [48] a normal pdf, with mean a_k and standard deviation u_{ran}^a in the possibility domain.

The RFVs for velocity and acceleration for the initial state vector can be seen in Fig. 5.3. They are both centered at zero because the initial measurements for velocity and acceleration are both assumed to be zero.

The RFVs for velocity and acceleration measured values are as shown in Fig. 5.4.

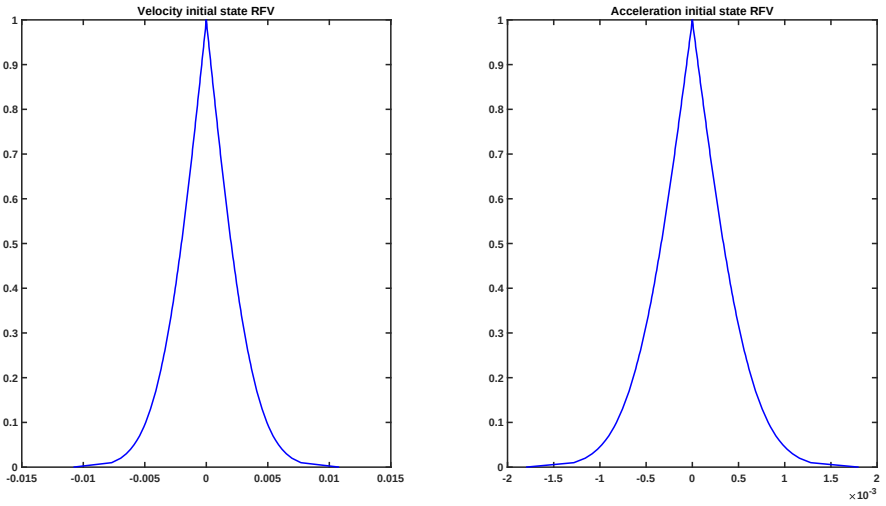

Figure 5.3: *Velocity and acceleration initial state RFVs*

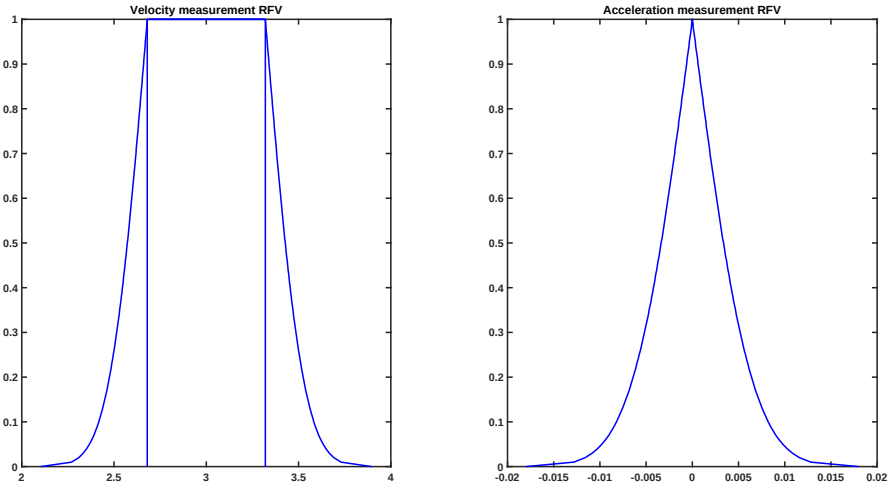

Figure 5.4: *Velocity and acceleration measurement RFVs*

The measured velocity is assumed to be $3m/s$ and the acceleration is assumed to be zero. Hence, they are centered at the corresponding values.

The noise covariance matrix for the state predictions $\mathbf{C}_{\mathbf{x}_k^f}$ can be obtained by calculating the possibilistic variances and the covariances between the system states directly from the respective RFVs of the states.

The obtained results are shown in Figs. 5.5 and 5.6. In the possibilistic approach, the difference between the predicted velocity/acceleration and the corresponding reference values are RFVs[1]. Therefore, the blue lines in Fig. 5.5 and 5.6 represent the mean values of these RFVs. On the other hand, the red lines represent, for every iteration k, the width of the α-cut at level $\alpha = 0.01$ of the predicted velocity/acceleration respectively,

[1] Since the predicted velocity and acceleration are RFVs.

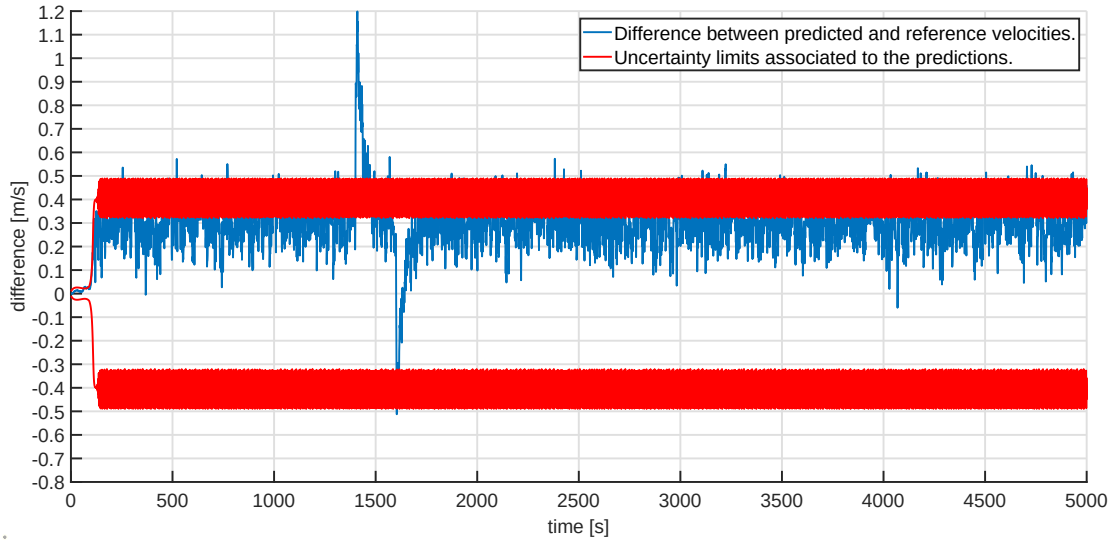

Figure 5.5: *Difference in the reference and predicted velocity values (blue line) provided by the possibilistic Kalman filter defined in [13], together with the predicted uncertainty interval (red lines).*

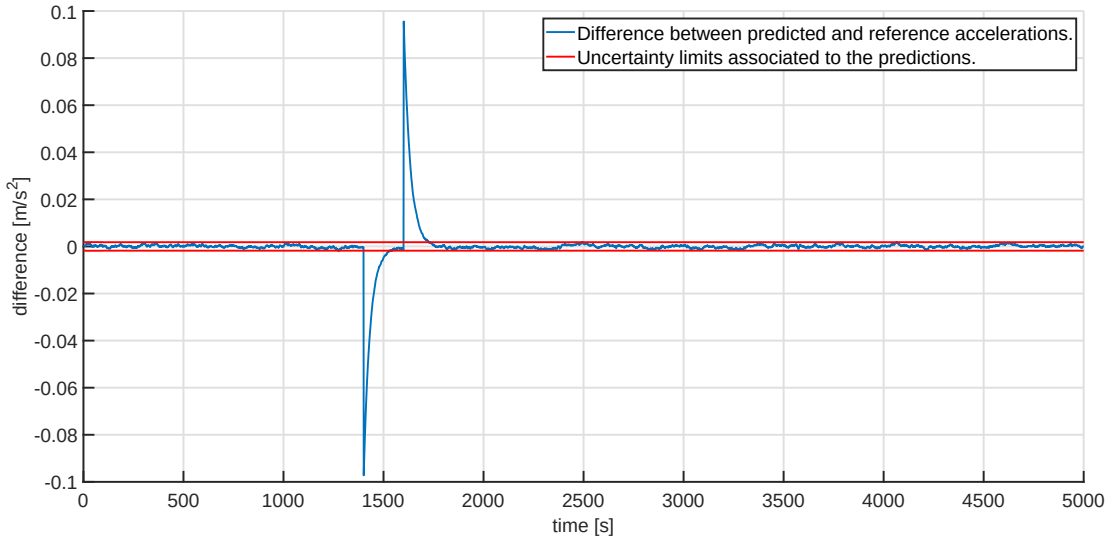

Figure 5.6: *Difference in the reference and predicted acceleration values (blue line) provided by the possibilistic Kalman filter defined in [13], together with the predicted uncertainty interval (red lines).*

i. e. the confidence level at coverage probability 99%.

With respect to the results provided by the classical KF and Schmidt KF, which both underestimate the measurement uncertainty, the possibilistic KF is able to consider correctly also the systematic contribution, so that the provided confidence intervals almost always include the systematic error e_{sys} except during the transient period when there is the sudden change in the acceleration and there is an overshoot till the Kalman filter readjusts to follow the data smoothly. Furthermore, the time of convergence of the possibilistic KF is 117 iterations.

However, Fig. 5.5 also shows a problem in the obtained results, i.e. the non-negligible oscillations. In fact, if, after reaching convergence, the standard deviation

of the results shown in the blue line is evaluated, a value of $88.2 \cdot 10^{-3}\ \mathrm{m/s}$ is obtained, which is much higher than the value obtained when the results of the classical KF ($29.9 \cdot 10^{-3}\ \mathrm{m/s}$) and the Schmidt KF ($26.7 \cdot 10^{-3}\ \mathrm{m/s}$) are considered.

As also summarized in Fig. 5.2, the gain matrix is evaluated according to the covariance matrix $\mathbf{C}_{\mathbf{X}_k^f}$. In [13], it has been suggested that the covariance matrix is evaluated according to the external membership function of the RFVs, so that the overall uncertainty is taken into account. Therefore, under this assumption: $\mathbf{C}_{\mathbf{X}_k^f} = \mathbf{C}_{\mathbf{X}_k^f}^{ext}$ and $\mathbf{K}_k^{POS} = \mathbf{K}_k^{ext}$ [13] (see again Fig. 5.2).

Since, the external membership function of an RFV represents the combined uncertainty of both the random contributions to uncertainty and that of the systematic contributions to uncertainty, the value of the variances and covariances obtained are very high. This results in the Kalman gain ($\mathbf{K}_k^{POS}$) to be very high as well which results in always overcompensating the error between the apriori predicted state and the measurement data obtained. Hence, there are very large oscillations in the predicted states as well as the uncertainty limits evaluated.

This result is not desirable, since the aim of a KF is a good prediction of both the state variable and its uncertainty. However, in this case, the prediction of the uncertainty values is not satisfactory.

5.4 A new definition for the possibilistic Kalman filter

In the previous Sect. 5.3, it has been shown how the possibilistic KF is able to correctly evaluate the measurement uncertainty due to both random and systematic contributions, but it is not as efficient in predicting the velocity values, as proved by the oscillations in the blue line in Fig. 5.5. In this section, a modified possibilistic KF is defined, in order to maintain the advantages of the already defined possibilistic KF but also to improve the state variable prediction.

As stated in previous Sect. 5.3, the oscillations in the blue line in Fig. 5.5 are due to the very high values in the gain matrix $\mathbf{K}_k^{POS}$, which is evaluated according to the possibilistic covariance matrix $\mathbf{C}_{\mathbf{X}_k^f} = \mathbf{C}_{\mathbf{X}_k^f}^{ext}$.

Since the covariance matrix is evaluated starting from the external membership functions of the RFVs representing the state variables, its elements are quite high in magnitude. In the new modified definition for the possibilistic KF, it is proposed to evaluate the possibilistic Kalman gain matrix, according to the possibilistic covariance matrix $\mathbf{C}_{\mathbf{X}_k^f} = \mathbf{C}_{\mathbf{X}_k^f}^{ran}$. This means that the possibilistic variances and covariances are evaluated from the random PDs of the RFVs of the state variables.

Similarly, also the possibilistic variance of measurements $\mathbf{Y}_k$ is evaluated for its random PD $\mathbf{Y}_k^{ran}$. In this way, since the possibilistic variance and covariance decrease, also the elements in the Kalman gain matrix decrease.

To understand the motivation behind this, let us go back to the basics of the Kalman filter as explained in Sect. 4.2. It is known that the Kalman gain is evaluated in such a way that the variances of the errors between the predicted states and the measurement data is minimized. Hence, it is a weighted ratio of the variances of the state predictions and the variances of the measurement data.

Now, if the measurement data is affected by purely the random contributions to uncertainty, the variance of the data represents the magnitude of variation around the mea-

sured value. Now, if we consider that there is an unknown systematic error and hence a systematic contribution to uncertainty, it still means that the magnitude of variation around the measured value is still purely from the random contributions to uncertainty. The systematic contributions to uncertainty only mean that the expected value of the data is not the true mean value of the distribution, rather, it is shifted by a certain value which is the systematic error.

But, in the previous definition of the possibilistic Kalman filter algorithm, the possibilistic variance associated to the state has been evaluated using the external membership functions of the RFVs which includes both the systematic and random contributions to uncertainty. Hence, the possibilistic variance calculated from the external membership function of the RFVs includes the effect of both the variation around the measured value and the effect of the shift of the expected value from the true mean. This is not desirable for the calculation of the Kalman gain.

Hence, if the possibilistic variance of just the random part of the RFV is calculated, that again accurately represents the variation around the measured value, whatever the expected value might be, which is what we want to use for the calculation of the Kalman gain.

Under this new assumption, the algorithm for the possibilistic Kalman filter is schematically represented in Fig. 5.7. With respect to the algorithm in Fig. 5.2, the different evaluation of the covariance matrix can be readily perceived and, consequently, the different Kalman gain matrix can be also seen.

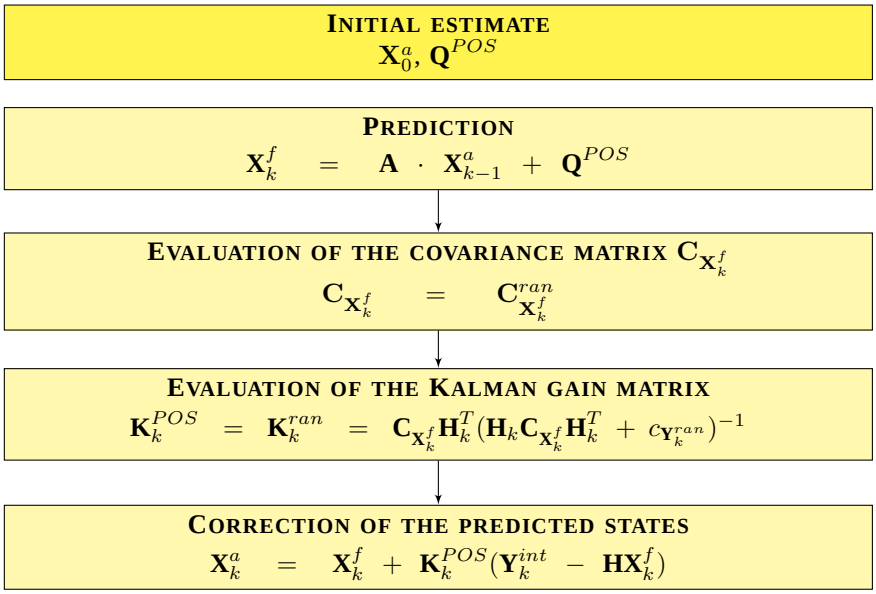

Figure 5.7: *The defined possibilistic Kalman filter algorithm.*

There is also another difference between the two algorithms in Figs. 5.2 and 5.7, shown in the last equation. In the new definition, the correction of the state variables is done by considering, in the given equation, only the internal PD of the RFV associated to the measurement value. This is more coherent with the classical KF, in which the correction of the state variables only depends on the value v_k of the measured velocity and not on its uncertainty. In the same way, by processing $\mathbf{Y}_k^{int}$, all possible values of the measured velocity caused by the presence of a systematic error are taken into account,

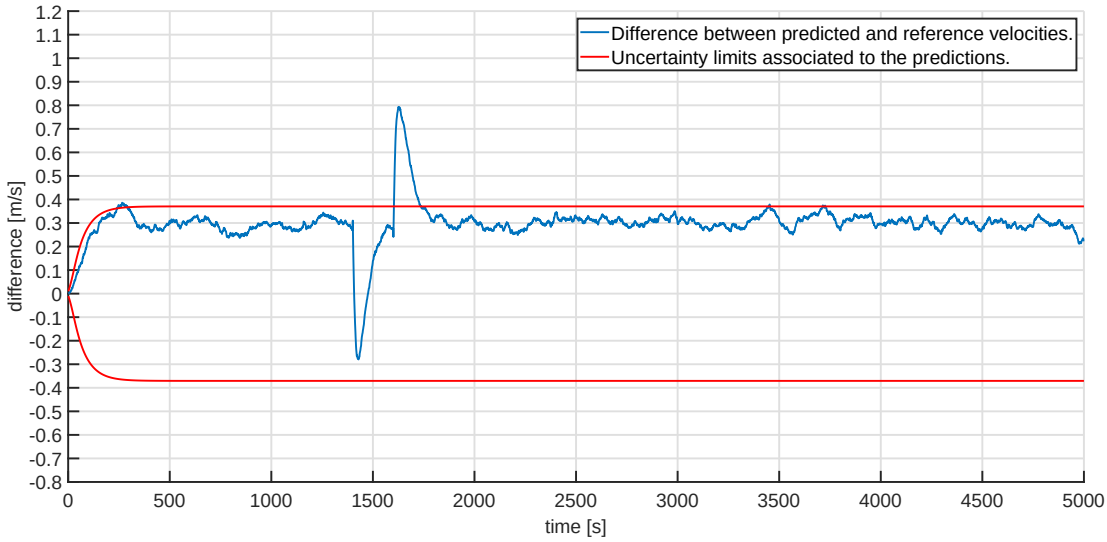

Figure 5.8: *Difference in the reference and predicted velocity values (blue line) provided by the possibilistic Kalman filter defined in this chapter, together with the predicted uncertainty interval (red lines).*

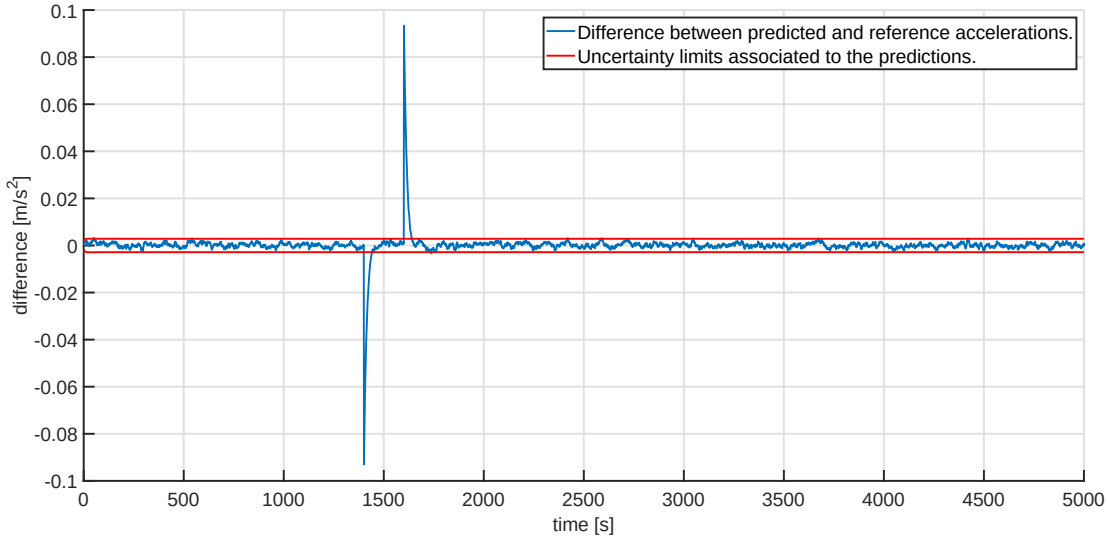

Figure 5.9: *Difference in the reference and predicted acceleration values (blue line) provided by the possibilistic Kalman filter defined in this chapter, together with the predicted uncertainty interval (red lines).*

but the random variability about this value is not considered in the state prediction.

This is equivalent to considering all possible values for the expected value inside the interval of values represented by the internal membership function of the RFVs. This is similar to the implementation of the classical KF algorithm based on Monte Carlo sampling as explained in Sect. 4.7. But, using the theory of possibility and RFVs makes it much more direct and computationally efficient thanks to the RFV mathematics.

The obtained results are shown in Figs. 5.8 and 5.9, where the red and blue lines have the same meaning as in Figs. 5.5 and 5.6. Fig. 5.8 clearly shows that the oscillations reported in Fig. 5.5 have been completely eliminated. Convergence is obtained

after about 153 iterations, so convergence is slower than with the original possibilistic Kalman filter, but the results are really improved. If, after reaching convergence, we evaluate the standard deviation of the results in the blue line, we obtain a value of $22.4 \cdot 10^{-3}\,\mathrm{m/s}$, which is lower than in all previous cases.

The good estimation of uncertainty is also confirmed, since the predicted values of velocity are well inside the predicted coverage interval (red lines). The improvement, with respect to the implementation shown in Sect. 5.3 is, once again, the absence of oscillations.

It can be concluded that the defined possibilistic KF improves the behavior of the possibilistic Kalman filter defined in [13], since both predictions and uncertainty are correctly evaluated.

5.5 Validation of the proposed possibilistic Kalman filter

In order to validate the possibilistic Kalman filter defined in this chapter, this section shows the results obtained by employing an hybrid KF, in which the variables are partly processed according to the theory of possibility, and partly according to the theory of probability. In particular, the random contributions to uncertainty have been processed according to the classical KF equations, while the systematic contributions to uncertainty have been modeled and processed as internal PDs of RFVs, by applying the RFV mathematics. In this way, the systematic contribuitions can be correctly propagated [18, 19, 48]. The algorithm in this case is schematically described in Fig. 5.10.

As far as the classical KF is concerned, the same assumptions are done as in Sect. 4.4 except that, in this case, the standard uncertainty associated to the simulated measured velocity is u^v_{ran} (and not u^v), since only the random contributions are now considered. As for the RFV part, it is sufficient to consider only the initial internal PDs of velocity and acceleration in the initial state $\mathbf{X}_0^{a\_\mathrm{int}}$, as defined in Sect. 5.3.

The obtained results are shown in Figs. 5.11 and 5.12.

The blue line in Fig. 5.12 shows the differences between the reference and the predicted accelerations and the red line gives the evaluated uncertainty intervals.

The blue line in Fig. 5.11 represents the difference between the predicted velocity (directly provided by the classical KF, at the left side of the algorithm's model) and $v_{\mathrm{ref}}(k)$. On the other hand, the red intervals represent, for every iteration, the 99% confidence interval of the RFV associated at the *a posteriori* velocity. In order to obtain this RFV, at every iteration, it is possible to combine the internal PD (obtained with the RFV mathematics, at the right side of the algorithm's model in Fig. 5.10) with the random PD built according to the results given by the classical KF at the same step (obtained by applying the probability-possibility transformation to the pdf given at the left side of the algorithm's model in Fig. 5.10). In particular, we obtain the random PD by applying the probability-possibility transformation [48] to the normal pdf whose mean value is the first element in $\mathbf{x}_k^a$ and whose standard deviation is given by the element $(1,1)$ in the covariance matrix $\mathbf{P}_k^a$.

In this case, we have convergence after about 85 iterations and the standard deviation of the blue line in the results is $30.8 \cdot 10^{-3}\mathrm{m/s}$ after reaching convergence.

By comparing Fig. 5.8 with Fig. 5.11, it can be immediately seen that we have obtained very similar results, thus confirming the validity of the proposed possibilistic

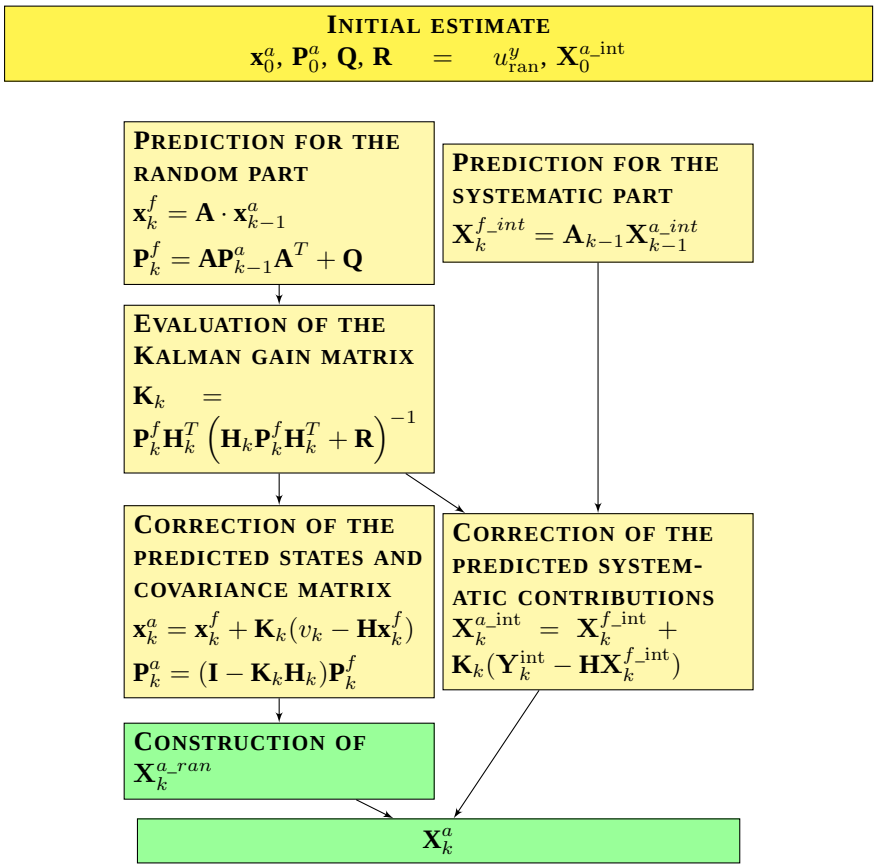

Figure 5.10: *The employed algorithm to validate the proposed possibilistic Kalman filter.*

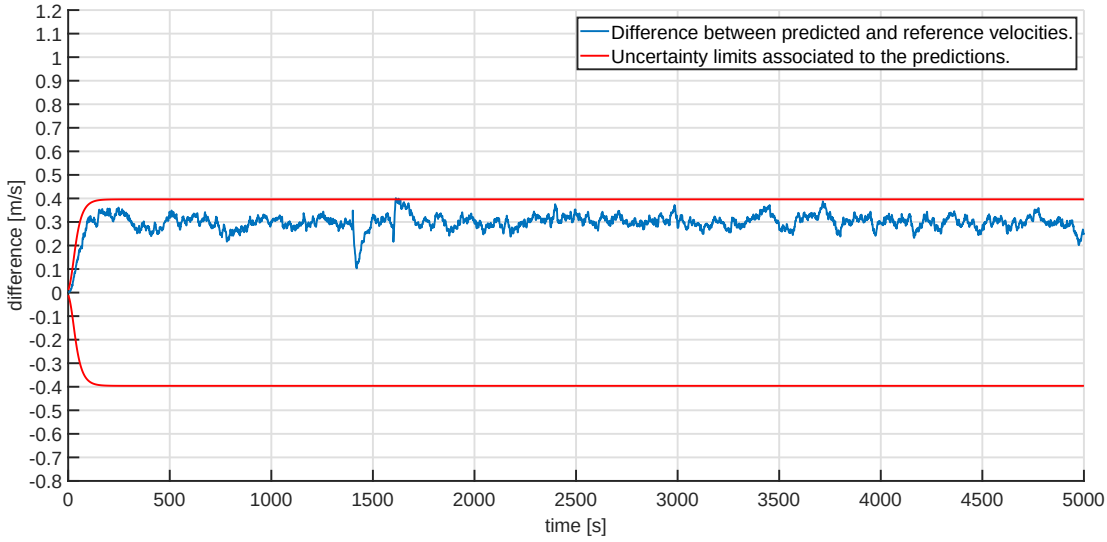

Figure 5.11: *Difference in the reference and predicted velocity values (blue line) provided by the hybrid Kalman filter, together with the predicted uncertainty interval (red lines).*

KF. Of course, the application of the possibilistic KF is much more immediate than the application of the Hybrid KF.

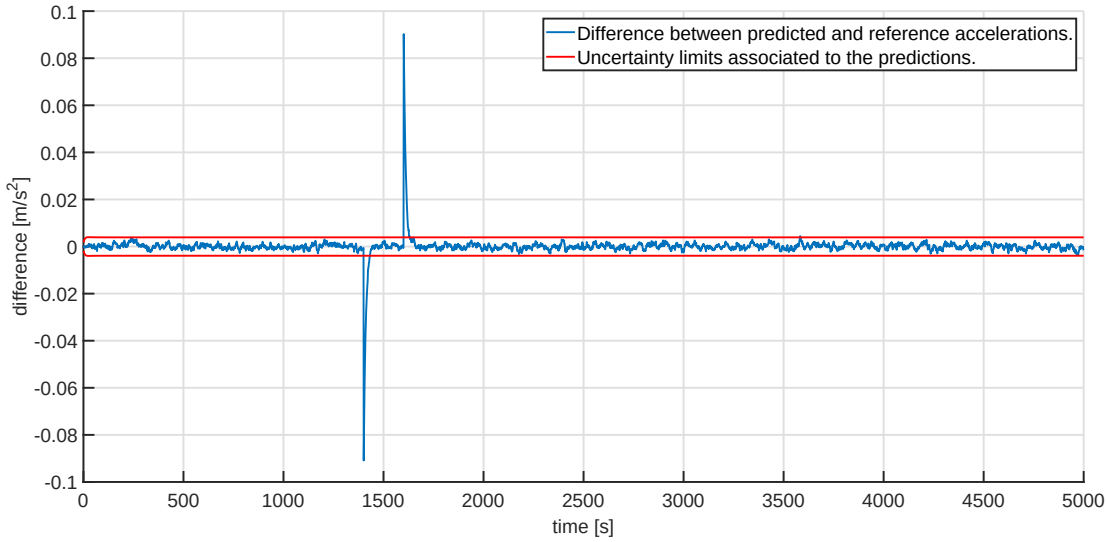

Figure 5.12: *Difference in the reference and predicted acceleration values (blue line) provided by the hybrid Kalman filter, together with the predicted uncertainty interval (red lines).*

5.6 Further tests and comparison

In order to achieve a more comprehensive validation of the proposed possibilitic KF, similar simulations as those reported in Sect. 5.2 and 5.5 have been repeated by considering the pattern shown in Fig. 5.13 for velocity and acceleration.

The results obtained are quite similar to those shown in Fig. 5.5, 5.8, 5.11 for velocity and to those shown in 5.6, 5.9, 5.12 for acceleration. The results for velocity are shown in Fig. 5.14, 5.16, 5.18 for the original possibilistic KF, modified possibilistic KF and the hybrid KF respectively. The results for acceleration are shown in Fig. 5.15, 5.17, 5.19 for the original possibilistic KF, modified possibilistic KF and the hybrid KF respectively.

A few synthetic indexes have been extracted from the obtained results, for a more immediate comparison of the different considered KFs. In particular:

- Convergence time. It is the time taken to reach the 90% of the steady-state value of the prediction.
- Steady-state error. It is the difference between the average predicted value and the reference value, once steady state is reached.
- Error variation. It is the standard deviation of the error once steady state is reached.
- Uncertainty limits. It is the width of the coverage interval that is supposed to encompass the error on the predicted value with a 99% coverage probability, once steady-state is reached. When the classical KF is employed, this is the $\pm 1.96\sigma$ interval. When the possibilistic KF is employed, this is the width of the α-cut at $\alpha = 0.01$ level of the RFV of the predicted values.
- Variation of uncertainty limits. It is the standard deviation of the width of the interval considered above, for the predicted values, once steady state is reached.

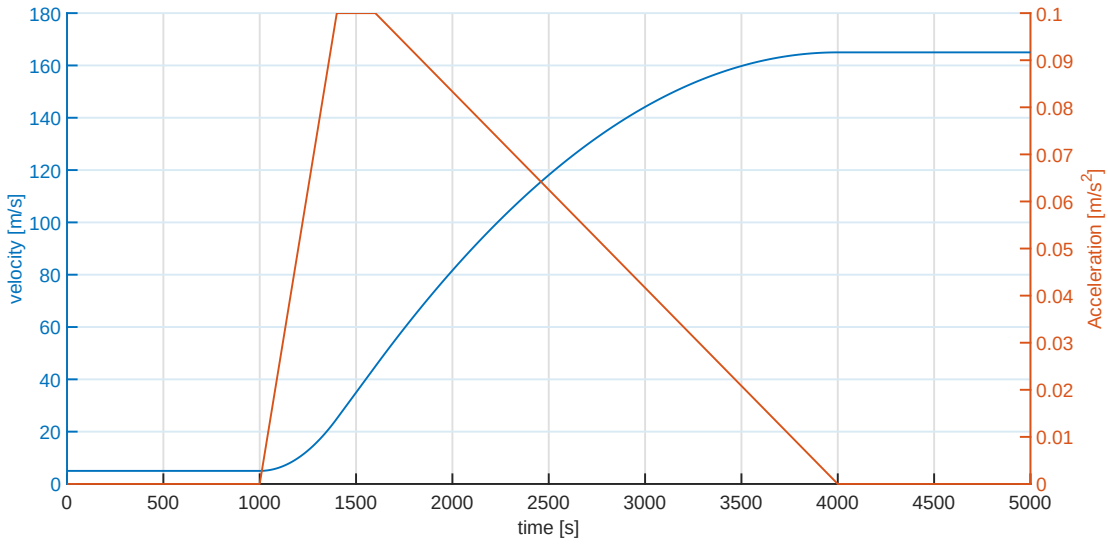

Figure 5.13: *Reference values of velocity (blue line) and acceleration (red line) over time for the new considered case.*

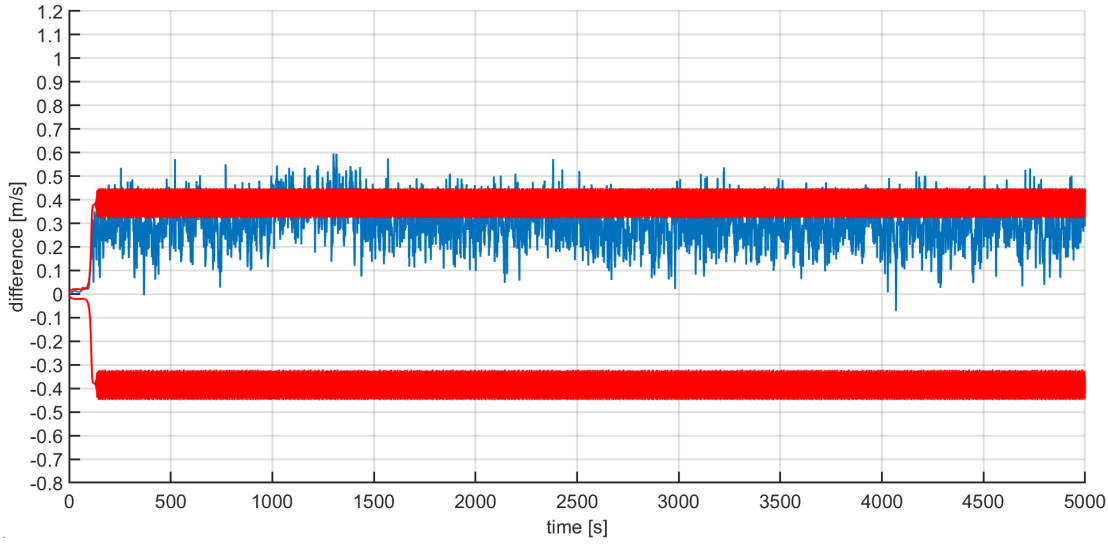

Figure 5.14: *Difference in the reference and predicted velocity values (blue line) provided by the original possibilistic KF, together with the predicted uncertainty interval (red lines).*

- Percentage of values inside the uncertainty limits. It is the relative number of predicted values whose error falls inside the above interval. This value should be, theoretically, 99%. The closer it approximates this value, the more accurate is the prediction provided by the considered KF.

All above indexes have been computed and reported in Table 5.1 (velocity) and Table 5.2 (acceleration) for the simulated pattern shown in Fig. 5.1, and in Table 5.3 (velocity) and Table 5.4 (acceleration) for the simulated pattern shown in Fig. 5.13.

It is, of course, known that the classical KF has been applied outside its theoretical assumptions and hence, the results obtained from the classical KF are inaccurate. The results from the classical KF have still been reported purely for the sake of comparison.

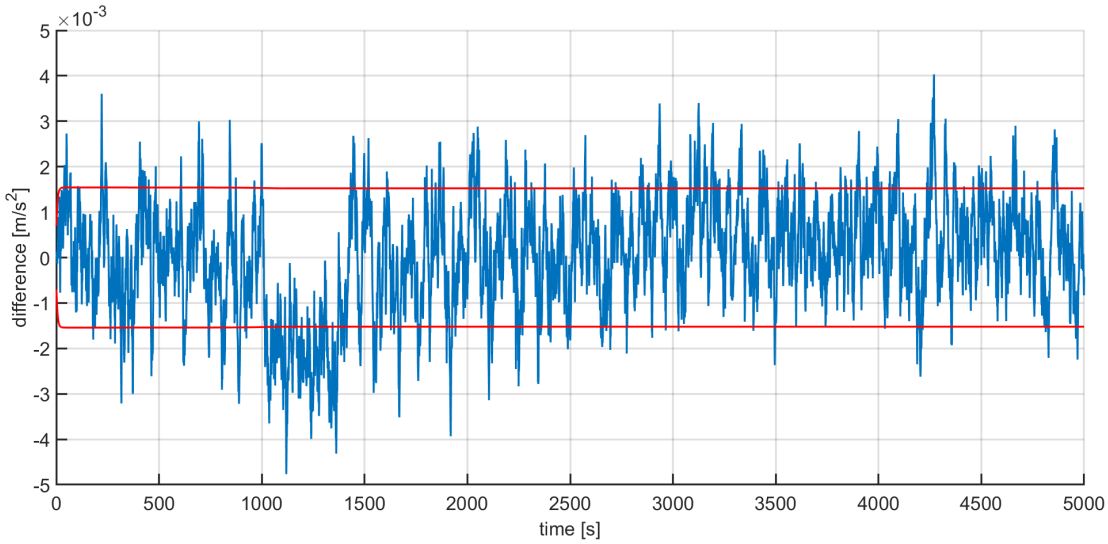

Figure 5.15: *Difference in the reference and predicted acceleration values (blue line) provided by the original possibilistic KF, together with the predicted uncertainty interval (red lines).*

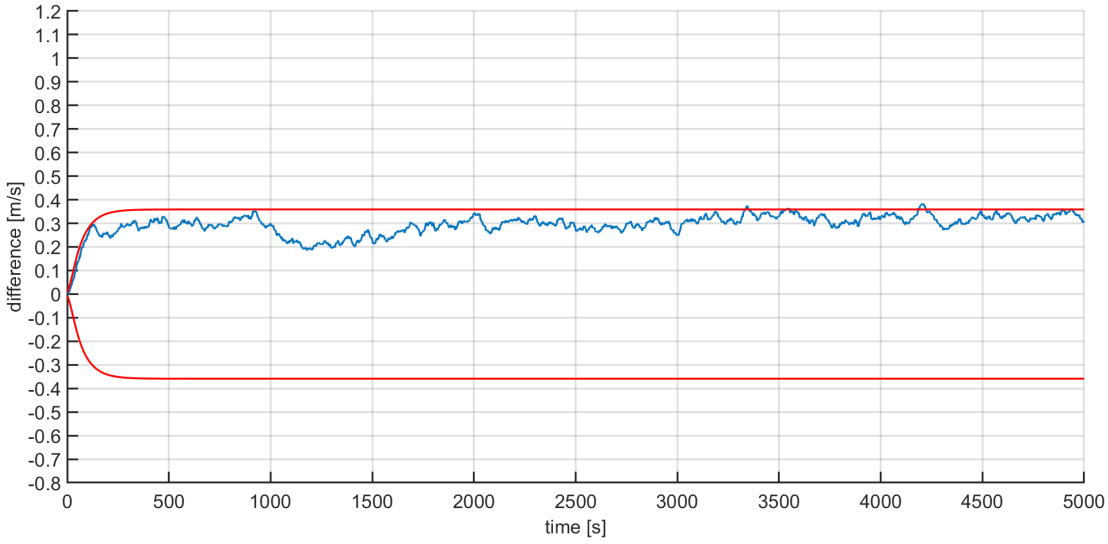

Figure 5.16: *Difference in the reference and predicted velocity values (blue line) provided by the modified possibilistic KF, together with the predicted uncertainty interval (red lines).*

The reported data confirm that the proposed possibilistic KF provides good results in the presence of systematic contributions to uncertainty and that the hybrid KF can be considered as a reference method.

Applications of the proposed KF have been presented in the following chapters.

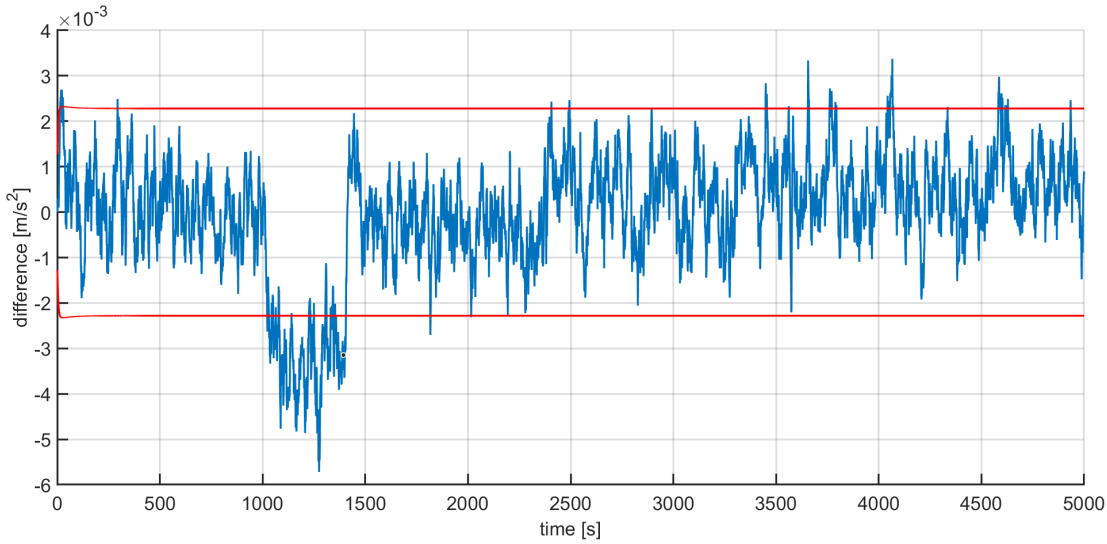

Figure 5.17: *Difference in the reference and predicted acceleration values (blue line) provided by the modified possibilistic KF, together with the predicted uncertainty interval (red lines).*

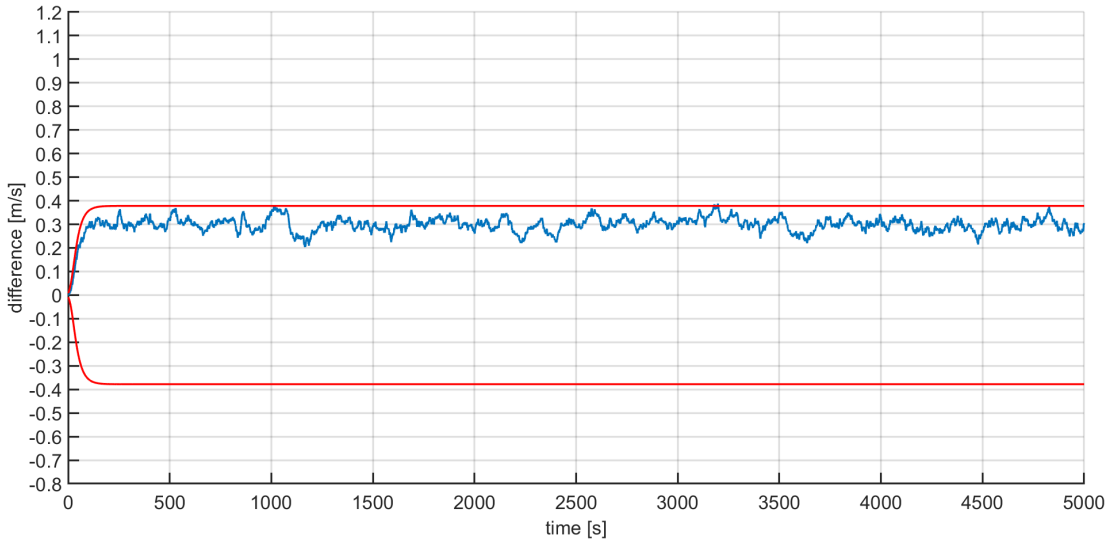

Figure 5.18: *Difference in the reference and predicted velocity values (blue line) provided by the hybrid KF, together with the predicted uncertainty interval (red lines).*

KF	Classical	Schmitt	Original Possibilistic	Modified Possibilistic	Hybrid
Convergence(s)	54	847	117	151	85
Steady-state error	0.2961	0.2968	0.3016	0.3024	0.2997
Variation of error	0.0299	0.0267	0.0847	0.0224	0.0308
Uncertainty limits	± 0.0371	± 0.1871	± 0.4056	± 0.3706	± 0.3961
Variation of uncertainty limits	0	0	0.0656	0	0
Percentage inside the uncertainty limits	0.34	5.14	82.36	97.38	99.92

Table 5.1: *Synthetic indexes for velocity for case 1 as seen in Fig. 5.1.*

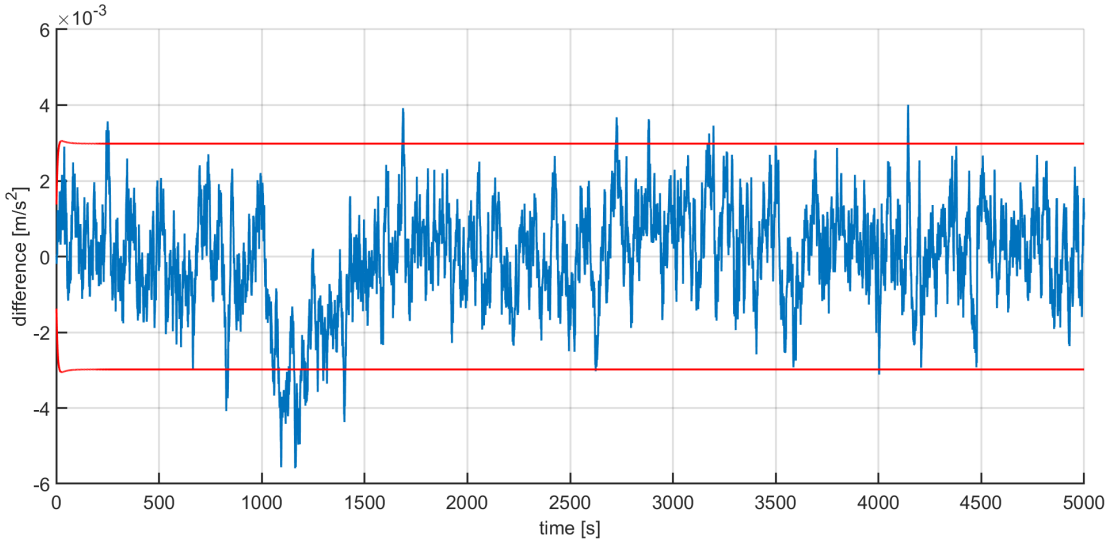

Figure 5.19: *Difference in the reference and predicted acceleration values (blue line) provided by the hybrid KF, together with the predicted uncertainty interval (red lines).*

KF	Classical	Schmitt	Original Possibilistic	Modified Possibilistic	Hybrid
Convergence(s)	10	10	3	7	9
Steady-state error	-0.00009	0.00003	0.00052	0.00002	-0.00007
Variation of error	0.0012	0.0011	0.00086	0.00084	0.0011
Uncertainty limits	± 0.0015	± 0.0015	± 0.0018	± 0.0028	± 0.0039
Variation of uncertainty limits	0	0	0	0	0
Percentage inside the uncertainty limits	81.14	83.70	93.88	98.42	98.72

Table 5.2: *Synthetic indexes for acceleration for case 1 as seen in Fig. 5.1.*

KF	Classical	Schmitt	Original Possibilistic	Modified Possibilistic	Hybrid
Convergence(s)	54	847	117	151	85
Steady-state error	0.2969	0.3138	0.2913	0.3036	0.3032
Variation of error	0.0251	0.0316	0.0843	0.0276	0.0287
Uncertainty limits	± 0.0371	± 0.1871	± 0.4056	± 0.3706	± 0.3961
Variation of uncertainty limits	0	0	0.0656	0	0
Percentage inside the uncertainty limits	0.2	11.96	83.10	99.76	99.88

Table 5.3: *Synthetic indexes velocity for case 2 as seen in Fig. 5.13.*

KF	Classical	Schmitt	Original Possibilistic	Modified Possibilistic	Hybrid
Convergence(s)	10	10	3	7	9
Steady-state error	0.000075	0.0020	0.00062	0.00012	0.00028
Variation of error	0.0011	0.0024	0.0018	0.00096	0.0010
Uncertainty limits	± 0.0015	± 0.0015	± 0.0010	± 0.0028	± 0.0039
Variation of uncertainty limits	0	0	0	0	0
Percentage inside the uncertainty limits	79.40	37.72	77.88	95.96	99.18

Table 5.4: *Synthetic indexes for acceleration for case 2 as seen in Fig. 5.13.*

CHAPTER 6

Application of the modified possibilistic KF in Precision time protocol

6.1 Importance of time synchronization

The distribution of a common time reference among the nodes of a given distributed system represents a fundamental issue in several contexts, i.e. smart grids, Industry 4.0 and Internet of Things (IoT). In IoT, a large network of sensors and other devices should be able to interact with each other to be able to implement higher level applications collectively.

With the increasing level of complexity in IoT, these devices need to be highly dynamic and be able to self-configure such that a single device can operate in multiple different scenarios with different partner devices. This represents one of the challenges in IoT to be able to provide the device with "high level of intelligence" for a high fliexibility in operation.

With such a complex network, the IoT devices also need to be time-aware, since an accurate time is necessary to be able to coordinate with multiple devices. This is because accurate timestamps of events or data are required so that the data from different nodes can be processed together and also these time stamps are used for latency measurements.

For example, in finance, especially in high frequency trading networks, traders buy and sell equities and securities. The trading operations that should occur in these networks should be very fast and accurate and should occur in a predefined window of time to be valid. The speed and accuracy of operations are very important since the prices change really fast in the financial markets which are highly volatile. So, for large trading companies that have transactions involving a huge sum of money, any small time delay which results in an increase or decrease of the equity price would amount to

huge difference in the revenue. Also, it is important that there is a saved record of all trading activities so that the portfolio of a particular trader can be known at all instants in time. So, not only do the trading operations need to occur at a high speed but they also need to be timestamped accurately.

Similarly, in banking, all financial transactions need to be accurately timestamped to keep track of the money being exchanged. Timestamps on financial documents are another example where accurate time synchronization is very important. Without that, there would be numerous mishaps in proving that the exchange of money occurred, or an agreement was signed or other business operations took place when they were alleged to have taken place to avoid any financial scams.

Other examples where accurate time synchronization is highly important would be the internet, mobile networks, power systems etc.

Given the importance of time synchronization, there are various protocols that have been defined with different levels of accuracy in synchronization. The most common protocol in use is the Network time protocol (NTP). The first specification document for NTP was released in 1985. It was first devised by D.L. Mills, an American scientist. It operates using the User Datagram Protocol (UDP). After the first version, there have been several versions released over time. Currently, it is the fourth version of NTP that is being run and the specifications for NTPv4 have been defined in 2010. The fifth version for NTP is currently under work.

Most of the household computers around the world are synchronized to the Coordinated Universal Time (UTC) using NTP. However, the synchronization accuracy using NTP is around 1 millisecond under good conditions and can be tens or even hundreds of milliseconds depending on the operating network conditions.

For an industrial scenario, this accuracy may not be good enough. Especially in high frequency settings, the synchronization needs to be much more accurate. This can be achieved by either a Global positioning system (GPS) based clock or a Precision time protocol (PTP) network. Since GPS based clocks are quite expensive, they are usually used as either reference clocks in a time network or as a time source for a stand-alone node. On the other hand, for an industry where there are multiple nodes in the same local network, having a GPS clock for each node becomes quite expensive. So, in this scenario, arranging a PTP network becomes a more feasible option.

6.2 Precision time protocol

Precision Time Protocol (PTP), either as an alternative to Global Positioning System (GPS) or as a synchronization back-up, is a widely accepted solution for the synchronization of nodes in a time network. PTP provides a synchronization accuracy of the order of nanoseconds under ideal conditions, as given below. The specification for PTP protocol, also known as the IEEE 1588 standard has been initially released in 2002 and the second version which is currently in use has been released in 2008.

A PTP network operates using a Master-slave hierarchy system in different layers in increasing order of accuracy of the clock. The clock with the highest accuracy that provides the reference time to the rest of the network is called the grandmaster clock. This is usually a clock that is synchronized to the UTC with a high degree of accuracy. Usually, a GPS based clock is used as the grandmaster in the network.

There are two types of message exchanges that happen between the master clock and the slave. Event messages are the messages that are used primarily for the synchronization between the clocks and highly accurate timestamps are generated at the sender end when an event message is transmitted from a node and also when the message is received at the receiving end.

General messages instead are the messages which do not require the generation of an accurate timestamp. Usually, the timing information of the event messages is relayed using the general messages.

There are several requirements for the PTP network that have been prescribed for an optimal functioning of the network, as given in the IEEE1588 standard:

- Cyclic forwarding of the PTP messages within the same communication path needs to be eliminated by the network using suitable algorithms because PTP assumes that it is done and only takes care that PTP messages are not cyclic forwarded between different communication paths.

- The event that there is a missed message occasionally, duplicated messages or a message that arrives out of order needs to be rare although PTP is tolerant to such occurrences if occasional.

- PTP assumes that the network is operating in a multicast communication mode. So, it is assumed that announce messages are sent in regular intervals by one port and the message is received by all the other ports of the ordinary or boundary clocks in the communication path. PTP ports discover other ports when they receive the multicast announce messages in a network.

  So, if it is not possible to use multicast mode in a network, care should be taken that the PTP behavior is preserved in the mode. So, the announce message needs to be replicated to all the ports in the communication path using unicast messages. Discovery is not possible if not using multicast. So, an alternative method like configuration needs to to be used to facilitate the discovery of clocks.

- Like any other synchronization algorithm, the accuracy obtained in PTP is dependent on the error in calculating the offset which is in turn dependent on the asymmetry in the forward and return paths of the message. This error is not detectable by PTP.

- Two step clocks are the devices that use two messages to provide the timing information to a port. The first message is called an event message, which relays the information about the request, and the net message is called a general message, that contains the information about the time when the event message was generated. In such cases, if the event message and general message travel to the node through different paths in the network, that would result in an error in the calculation of the path delay and this introduces jitter and additional error in the offset calculation.

- It is assumed that the number of boundary clocks used in the master slave synchronization hierarchy from the grandmaster to any slave in the network is less than 255.

- Components in the network like bridges cause unwanted jitter which results in error. The jitter is dependent on the traffic in the network. So, care should be taken that the network is designed in such a way to minimize the traffic in the network. PTP messages should also be set to be processed at a high priority with respect to other messages at the device.
- The protocol in the network should be structured in such a way that the message timestamp point can be defined. Message timstamp point is the point within the PTP event message which, when passes the reference plane of a clock generates a timestamp. A PTP message is a data packet. So, the message timestamp point refers to the part of the data in the datapacket which when being processed by the clock triggers the generation of the timestamp at the clock. It is like a trigger command in the data packet. So, it should be clearly defined where this trigger command is placed in the PTP message.

The clock synchronization of a slave clock in a PTP network occurs at the beginning of every UTC second and is initiated by the master clock.

Let us suppose that the sync message is received at a time instant (t_{sync}) by the slave which triggers the clock synchronization. The clock synchronization in a PTP network occurs as given below and shown in the fig. 6.1:

- The slave receives a $sync$ message from the master and the time $T^M(t_{sync})$ is recorded which is the timestamp denoting the time at which the sync message is sent from the master.
- The master sends the information about $T^M(t_{sync})$ either by sending a $Follow\ up$ message if it is a two-step clock or by embedding the timestamp in the sync message that was sent in the first step if it is a one-step clock.
- The time of reception of the sync message is recorded by the slave the moment the sync message is received at the node. Let the timestamp recorded by the slave be $T^S(t_{sync})$.
- The slave sends a $Delay - Request$ message to the master and the time at which the message has been transmitted is recorded by the slave. Let the timestamp be $T^S(t_{delay})$.
- The master receives the message and records the time at which this message has been received from the slave. Let the corresponding timestamp be $T^M(t_{delay})$.
- The timestamp $T^M(t_{delay})$ is sent to the slave by the master using a $Delay - Response$ message, so that, at the slave, all four timestamps $T^M(t_{sync})$, $T^S(t_{sync})$, $T^S(t_{delay})$ and $T^M(t_{delay})$ are available.

The propagation delay and the time offset are calculated using the four timestamps. In particular, the propagation delay $\hat{d}$ is calculated by:

$$\hat{d} = (T^S(t_{delay}) - T^M(t_{sync})) - (T^S(t_{delay}) - T^M(t_{delay}))/2 \tag{6.1}$$

While the time offset $\hat{\theta}_{t_{sync}}$ at the time instant t_{sync} is given by:

$$\hat{\theta}(t_{sync}) = T^S(t_{sync}) - T^M(t_{sync}) - \hat{d} \tag{6.2}$$

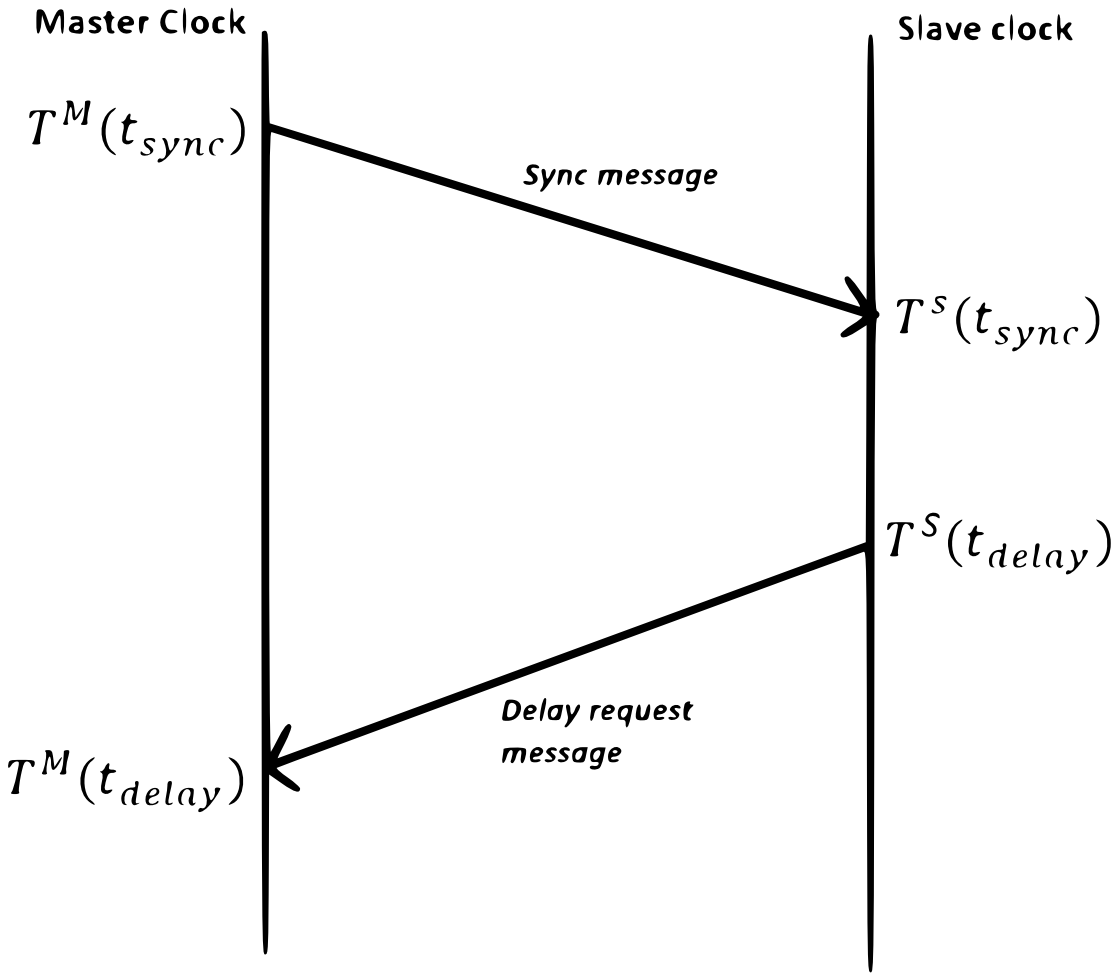

Figure 6.1: *Message exchange in a PTP network.*

This offset is then used to correct for the error in time between the slave clock and the master clock. The error is produced because there is a drift in any clock in the world. So, the slave clock is constantly drifting away from the reference time. Hence, to always maintain a high degree of accuracy in the time synchronization, it is very important that the synchronization process is continuously repeated at regular intervals in time. So, essentially, synchronization is like a constant calibration that is being done on the slave clock.

Just like any other measurement process, also synchronization has several sources of error. Some sources are of random nature like the noise in timestamping or the random delay in the transmission of the messages. Other sources are of systematic errors like error in offset calculation due to asymmetricity.

6.2.1 Uncertainty in PTP networks

As mentioned earlier, any timestamping process is effected by a random noise in timestamping. For the sake of simplicity, we assume in the following that the uncertainty contribution affecting master timestamps can be neglected when compared to other un-

certainty sources; this leads to:

$$T^M(t_{sync}) = t_{sync} - d \tag{6.3}$$

where d is the actual propagation delay between master and slave.

Let us assume that the timestamp $T^S(t_{sync})$ measured by the slave is affected by a timestamping noise ν_T. But, it is also affected by the current value of time offset $\theta(t_{sync})$ between the local clock and the time reference:

$$T^S(t_{sync}) = t_{sync} + \theta(t_{sync}) + \nu_T \tag{6.4}$$

By substituting (6.4) and (6.3) in (6.2) we can obtain the relationship between estimated and the actual offset values:

$$\hat{\theta}(t_{sync}) = \theta(t_{sync}) + \nu_T + (d - \hat{d}) \tag{6.5}$$

Assuming a hardware timestamping mechanism, and hence assuming that there has been no latency in the generation of the timestamp, the measurement uncertainty in the timestamp is essentially due to the finite clock resolution. The clock resolution can be modeled as a zero-mean white noise with a uniform distribution and variance $\sigma_\nu^2 = 1/(12 f_0^2)$, where f_0 is the nominal frequency of the local oscillator [12].

The second contribution $d - \hat{d}$ instead depends on the accuracy of the delay estimation procedure. This procedure is based on the assumption that the direct link delay d_{MS} from master to slave, and the inverse link delay d_{SM} from slave to master are symmetric and time-invariant. Several hardware solutions can be adopted to guarantee the fulfillment of this requirement, such as the use of boundary clocks or transparent clocks. These solutions however present a high cost and they can be implemented only on proprietary networks. Typical examples can be found in industrial applications, where IEEE 1588 compliant network devices are employed.

So far, the contributions to uncertainty are only of random nature. So, suitable servo clocks have been proposed in the literature for further reducing measurement uncertainty in offset and propagation delay estimations provided by the PTP, before using them for the correction of the local clock. Among the available servo clocks, servo clocks based on Kalman filter have also the advantage to provide information about the accuracy of the local clock, thus providing a self-aware local clock [22].

But, propagation delays over the Internet strongly depend on routing protocols, which might select different network paths from direct and inverse links, and on network traffic load. In general, propagation delays can be modeled by the sum of two contributions: a constant term D_{MS} (or D_{SM}) and a random term q_{MS} (or q_{SM}) representing the packet delay variability. In general [24]:

$$d = D + q \tag{6.6}$$

where the subscripts MS and SM are omitted for the sake of simplicity. The first contribution is mainly associated to the length of a propagation path and it varies only when the packet routing is changed. In this case, D presents an abrupt variation, either increasing or decreasing; anyway the rate of occurrence of these events is typically low and it can be managed in order to keep the behavior of the servo clock unaffected.

The second random contribution q is associated instead to queuing phenomena and strongly depends on the traffic load, the kind of traffic (video, voice, best-effort), the

number of switches along the path and so on. A widely accepted statistical model for this random component consists in modeling its probability density function (pdf) by a Gamma distribution:

$$f_q(a) = \frac{\exp\left(-\frac{a}{\beta}\right)}{\beta\Gamma(k)}\left(\frac{a}{\beta}\right)^{k-1} 1(a) \tag{6.7}$$

being $k, \beta > 0$. The function $1(a)$ is the unit step, that is, $1(a) = 1$ for $a > 0$ and $1(a) = 0$ otherwise. This distribution is parameterized in terms of shape parameter k and scale parameter β, which depend on the traffic load, packet size profile and number of switches, as specified in the ITU-T G.8261 recommendation. The mean and variance are, respectively: $\mathrm{E}[q] = k\beta$ and $\mathrm{var}[q] = k\beta^2$.

The propagation delay, estimated by the PTP engine, corresponds to the one-way delay, that is:

$$\hat{d} = \frac{d_{MS} + d_{SM}}{2} = \frac{q_{MS} + D_{MS} - q_{SM} - D_{SM}}{2} \tag{6.8}$$

It follows that it depends on the difference between two Gamma random variables and two constant contributions. Therefore, the uncertainty contribution $d - \hat{d}$ depends on the traffic load differences between direct and inverse link and, in general, it presents a non-zero mean value $E[d - \hat{d}] \neq 0$. So, along with a random errors, there is the possibility of a systematic error.

When PTP messages are exchanged through a network infrastructure subjected to an intense traffic load, the performances of this synchronization system are affected by the packet delay variability (PDV). PDV is the difference in end-to-end one-way delay between selected packets in a flow with any lost packets being ignored. PDV may lead to significant asymmetries between the direct and inverse path between master and slaves, thus causing a degradation in PTP performances. A solution consists in adopting PTP-aware devices, as for instance preemptive network switches able to manage packets having different priorities. Nonetheless, a systematic uncertainty contribution due to the asymmetries in the traffic load between direct and inverse path still remains and current servo clocks, which are based on the assumption of having a symmetric path, cannot deal with this error contribution.

Some articles can be found in the literature [38, 39, 41, 46, 49], where some algorithms have been proposed to deal with asymmetric loads. However, all these algorithms only try to lessen the systematic error due to the asymmetric loads as much as possible. But, they do not propagate the uncertainty limits associated to the measurements due to asymmetricity, which is an important result because even if the systematic error is lessened, there is still some residual error. So, the overall uncertainty of the clock is affected by both random and systematic contributions to it. Hence, it is very important to correctly propagate it, to properly estimate the accuracy of the clock.

The Kalman filters available in the possibility domain allow to propagate all kinds of uncertainty contributions, included the systematic contributions.

It is proposed in this chapter first to characterize the PTP network and then use the possibilistic KF proposed in chapter 5 [20] to propagate the systematic contributions to uncertainty due to asymmetric delays and evaluate the overall uncertainty associated to the offset calculations between the master and the slave.

6.3 KF-based servo clock

The Kalman filter is based on a set of equations that provide a recursive solution to a least-squares problem. A KF-based servo clock was introduced in [23] and refined in [22]. Its implementation, here recalled for completeness, is based on the two-state discrete-time clock model introduced in [23]. Let $\theta(n)$ be the time offset and $\gamma(k)$ the fractional frequency deviation. Equations describing the evolution of clock state with a time step τ are:

$$\begin{cases} \theta(k) &= \theta(k-1) + \gamma(k) \cdot \tau + \omega_\theta(k) \\ \gamma(k) &= \gamma(k-1) + \omega_\gamma(k) \end{cases} \tag{6.9}$$

where $\omega_\theta(k)$ and $\omega_\gamma(k)$ are two uncorrelated zero-mean random processes with variances respectively σ_θ^2 and σ_γ^2 [23]. $\omega_\theta(k)$ corresponds to the random noise effecting the offset between the slave and the master. $\omega_\gamma(k)$ corresponds to the random noise affecting the skew which is the normalized difference between the frequency of the local clock and the frequency of the reference clock. σ_θ and σ_γ depend on the different noises like the Weiner noise which contribute to the overall noise in the offset and the skew in the clock model [23, 55].

The classical Kalman filter as has been explained in Sect. 4.2 has been employed to filter the offset calculations and provide the state estimations for a slave clock in the PTP network. The Kalman filter algorithm is recalled in Fig. 6.2 for easy reference.

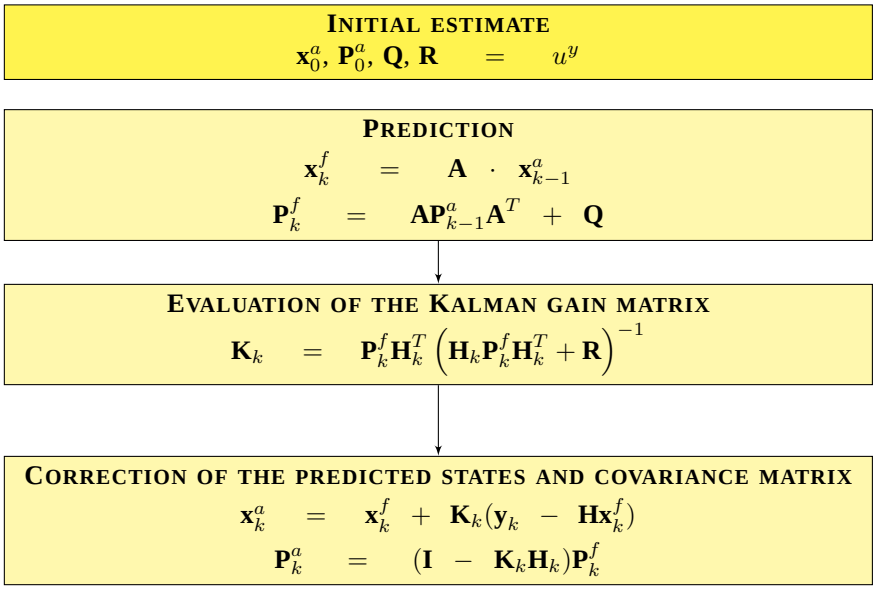

Figure 6.2: *Classical Kalman filter algorithm.*

So, the offset calculations made by the slave clock are fed to the Kalman filter to further filter the noise associated to the calculated offset and provide more accurate predictions of time for the slave clock.

The filter parameters can be obtained from (6.9) and are as given below:

- **State vector**: $\mathbf{x}_k = \begin{bmatrix} \theta(k) & \gamma(k) \end{bmatrix}^T$. $\theta(k)$ and $\gamma(k)$ represent the time offset and the frequency deviation.

- **State transition matrix**: $\mathbf{A} = \begin{bmatrix} 1 & \tau \\ 0 & 1 \end{bmatrix}$.
- **Measurement**: $z_k = [\hat{\theta}(t_{sync})]$. $\hat{\theta}(t_{sync})$ is the time offset measured in correspondence to the k-th synchronization time instant $t_{sync} = k\tau$.
- **Measurement matrix**: $\mathbf{H} = \begin{bmatrix} 1 & 0 \end{bmatrix}$since only the offset is being measured.
- **Process noise covariance matrix**: $\mathbf{Q} = \begin{bmatrix} \sigma_\theta^2 & 0 \\ 0 & \sigma_\gamma^2 \end{bmatrix}$. This is the noise covariance matrix that corresponds to the offset and skew states in the model given in (6.9).
- **Measurement noise variance**: $R = \sigma_{\hat{\theta}}^2$. This is the noise that affects the offset measurement made by the slave clock.

The Kalman filter operates in two phases. During the prediction phase, the a-priori estimate of the state $\mathbf{x}_k^f$ is obtained from the knowledge of the state at the previous time instant $\mathbf{x}_{k-1}^a$:

$$\mathbf{x}_k^f = \mathbf{A}\mathbf{x}_{k-1}^a \tag{6.10}$$
$$\mathbf{P}_k^f = \mathbf{A}\mathbf{P}_{k-1}^a\mathbf{A}^{\mathrm{T}} + \mathbf{Q} \tag{6.11}$$

where $\mathbf{P}_k^f$ is the $apriori$ estimate error covariance matrix.

During the correction phase, a refined $aposteriori$ state estimate $\mathbf{x}_k^a$ is obtained by using the new measurement:

$$\mathbf{x}_k^a = \mathbf{x}_k^f + \mathbf{K}_k(z_k - \mathbf{H}\mathbf{x}_k^f) \tag{6.12}$$
$$\mathbf{P}_k^a = (\mathbf{I} - \mathbf{K}_k\mathbf{H})\mathbf{P}_k^f \tag{6.13}$$

where:

$$\mathbf{K}_k = \mathbf{P}_k^f\mathbf{H}^T(\mathbf{H}\mathbf{P}_k^f\mathbf{H}^T + R)^{-1} \tag{6.14}$$

is the Kalman gain.

As has been explained in chapter 4, in Sect. 4.4, a classical Kalman filter works perfectly fine when there are only random contributions to uncertainty. So, it is the same also for PTP networks. Under, ideal conditions, PTP networks are in fact free from systematic errors. But, as explained in the Sect. 6.2.1, there are cases especially when there is an asymmetry in the paths between the master and the slave. In such situations, there is a bias that is introduced in the offset calculated by the slave clock. Such a case is considered here as an example.

It has been considered that there is an asymmetry in the traffic loads between the path from the master to the slave and the path from the slave to the master. Due to the difference in traffic loads, the delay in the transmission of the packets in the path from the master to the slave is different from that between the slave and the master. It has

been assumed that, in this example, the traffic load is equal to 20% of the bandwidth in the path from master to slave and 60% of the bandwidth in the path from slave to master. This introduces a significant bias in the calculation of the offset.

So, when the classical KF shown in Fig. 6.2 is employed to predict the time of the slave clock in this situation, the results are as shown in Fig. 6.3. The blue line represents the residual offset between the master and the synchronized slave clocks, while the red lines represent the uncertainty intervals corresponding to a 99% interval [27]. The uncertainty interval can be evaluated from the noise covariance matrix of the states that is also estimated by the Kalman filter. The noise covariance matrix contains the variances of the states and the covariances between the states. So, the standard deviation of each state can be evaluated by making a square root of the corresponding variance. Since the noises that affect a clock has been said to be gaussian, the 99% confidence interval corresponds to the $\pm 3\sigma$ interval. It can be easily noted that, due to the presence of systematic errors originated by the traffic asymmetry, the confidence interval is underestimated.

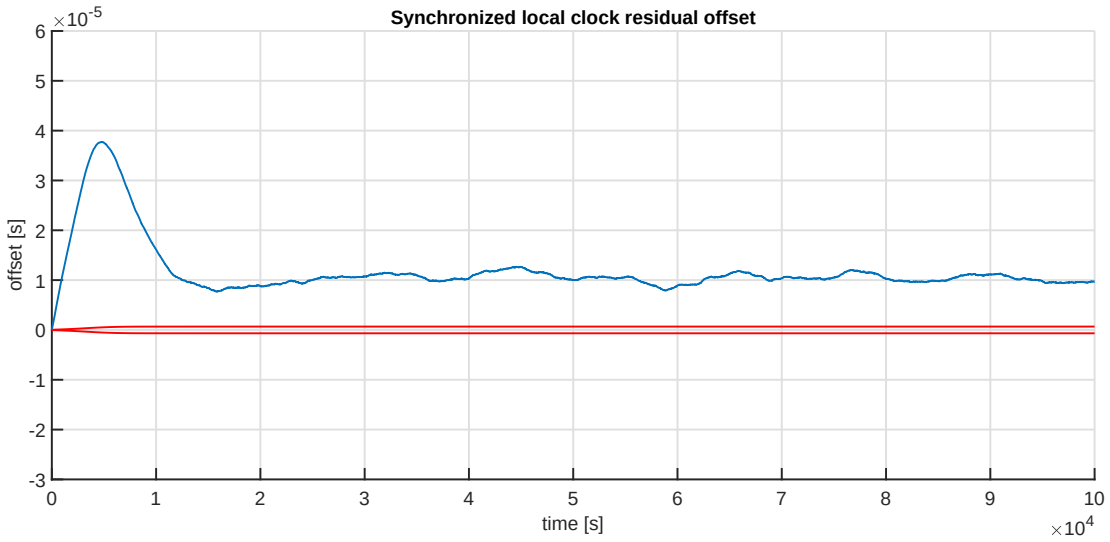

Figure 6.3: *Results obtained with the classical Kalman filter, with constant traffic load. The blue line represents the residual offset between the master's and slave's clocks. The red lines represent, for each iteration, the uncertainty limits.*

Another example has also been considered, where the traffic loads between the master and the slave are varying as shown in Fig 6.4. It can be seen that till the time instant $t = 40000s$, the traffic loads in the path between the master and the slave and in the path between the slave and the master are both at 20%. After that, the traffic load in the path between the slave and the master constantly increases till $t = 80000s$ and then it becomes constant while the traffic load in the path between the master and the slave is always constant at 20%.

The classical Kalman filter shown in Fig. 6.2 is again applied to this case and the results have been reported in Fig. 6.5. Again, the blue line represents the residual offset between the master and the synchronized slave clocks. It can be immediately seen that till time $t = 40000s$, the residual offset has a zero mean value. This is to be expected as the traffic loads in the onward and the return paths have been equal till now. And

then, it can also be seen that, after this point, the residual offset starts increasing till $t = 80000s$. This is because the asymmetry between the traffic loads in the onward and the return paths keeps increasing till that point.

The red lines represent the uncertainty intervals corresponding to a 99% interval. It can be immediately seen how the uncertainty limits are underestimated as soon as there is an uncompensated systematic error that is introduced because of the asymmetric traffic loads.

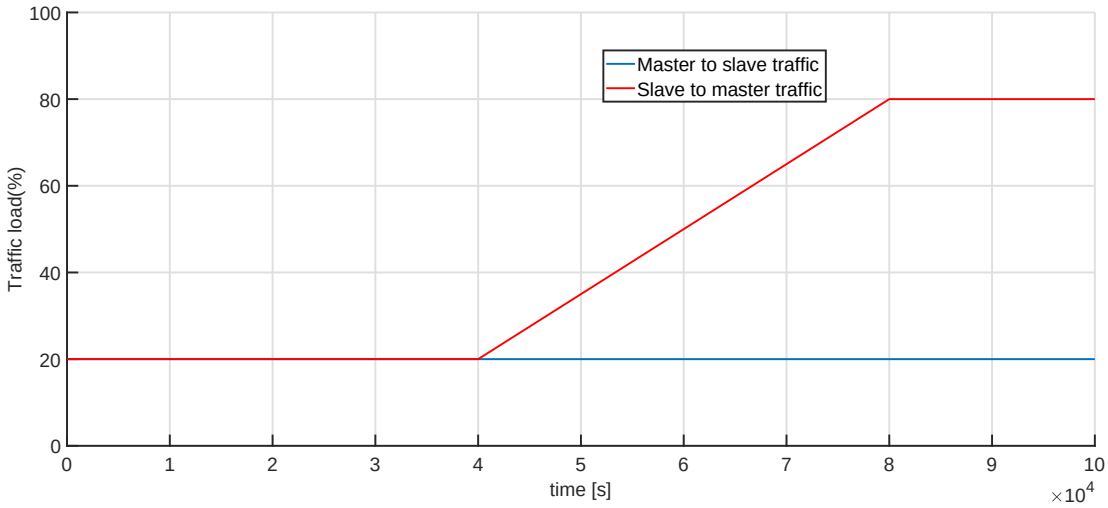

Figure 6.4: *The variable traffic load simulated in the network.*

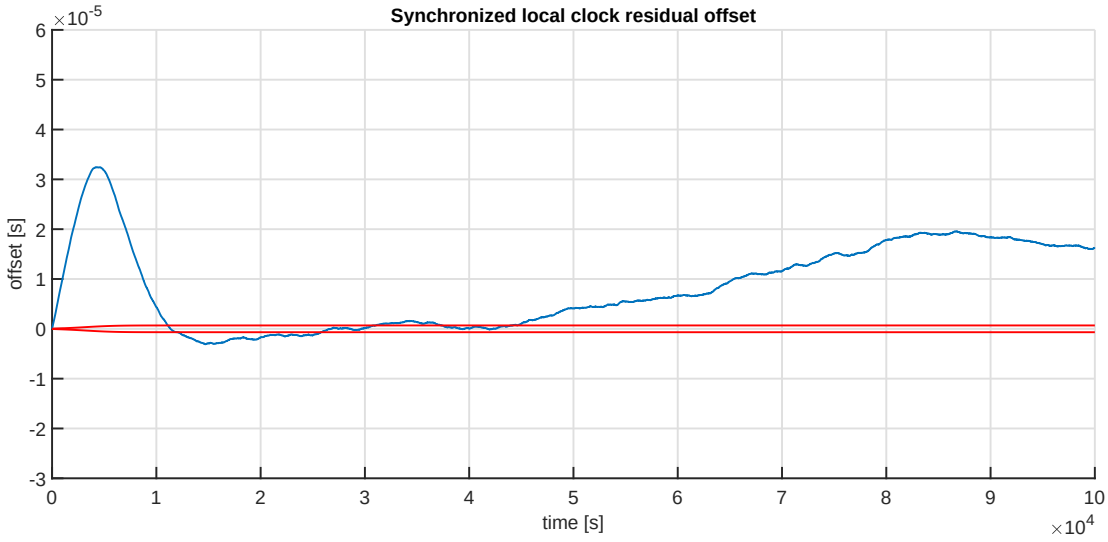

Figure 6.5: *Results obtained with the classical Kalman filter, with varying traffic load, according to Fig. 6.4. The blue line represents the residual offset between the master's and slave's clocks. The red lines represent, for each iteration, the uncertainty limits.*

6.4 The servo clock with the modified possibilistic Kalman filter

As can be recalled from chapter 5, the possibilistic Kalman filter provides a good solution to correctly estimate the uncertainty interval associated to the states when there are systematic contributions to uncertainty in the measurements.

So, the possibilistic KF would be perfect for the two examples considered in the previous section.

Fig. 6.6 shows the possibilistic KF equations. Let us consider here how the different matrices and RFVs are defined, according to the given metrological assumptions.

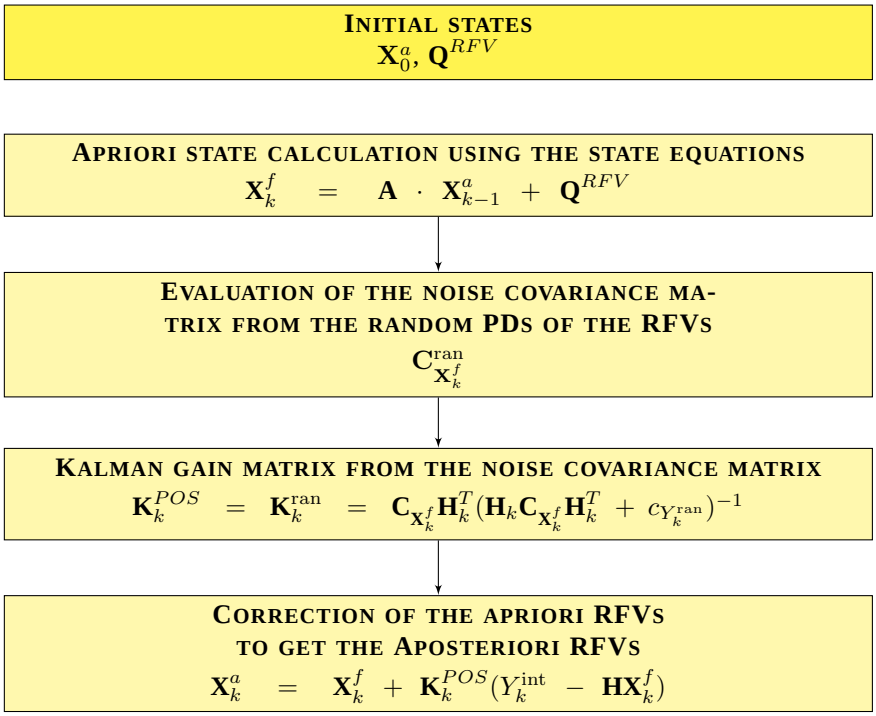

Figure 6.6: *The modified possibilistic Kalman filter algorithm.*

$\mathbf{Q}^{RFV}$ is the noise vector of the state RFVs. Since it is assumed that offset and skew of a clock are affected by random noises which distribute according to gaussian pdfs, with standard deviation σ_θ and σ_γ respectively. Therefore:

- The RFV corresponding to the noise affecting the offset is centered at zero; its internal PD is nil, since no systematic contributions are assumed in the model, while its random PD (which in this case is also the external one) is the PD which contains the same metrological information of the assumed pdf by making a probability-possibility transformation on the pdf that is the Gaussian distribution with standard deviation σ_θ.
- The RFV corresponding to the noise affecting the skew is centered at zero; its internal PD is also nil, since no systematic contributions are assumed in the model, while its random PD (which in this case is also the external one) is the PD which contains the same metrological information of the assumed pdf, that is the Gaussian distribution with standard deviation of σ_γ.

$\mathbf{X}_0^a$ is the vector of the state RFVs Θ_0^a and Γ_0^a, associated to the initial offset and skew. Since the states in the process model are affected only by the random noise given by the noise vector $\mathbf{Q}^{RFV}$ and since there is no available prior information about the offset and skew, it is assumed that the values of the initial offset and skew are zero. This means that the RFVs of the offset and skew Under this assumption, the initial RFVs associated to offset and skew are simply the RFVs associated to their affecting noises, so that: $\mathbf{X}_0^a = \mathbf{Q}^{RFV}$. The resulting RFVs Θ_0^a and Γ_0^a are given in Fig. 6.7 and 6.8 respectively. The red line is the internal PD. The blue line is the external PD. It is worth to underline that the initial RFVs Θ_0^a and Γ_0^a are not complete RFVs, since the internal PDs are nil, but, after one step they become complete RFVs, because of the presence of the measurement Y_k in the possibilistic KF equations.

As explained in chapter 5 in Sect. 5.4, $\mathbf{C}^{\text{ran}}_{\mathbf{X}_k^f}$ is the possibilistic noise covariance matrix and it is the equivalent of matrix $\mathbf{P}_k^f$ in the probability domain. However, in probability, $\mathbf{P}_k^f$ is evaluated thanks to an *ad hoc* iterative formula (see (6.14)), while, in the possibilistic KF, $\mathbf{C}^{\text{ran}}_{\mathbf{X}_k^f}$ is evaluated directly from the random PDs of the RFVs in the state vector at step k. This is because during the evaluation of the state vector at each iteration, since the states are all RFVs, they already include the effects of the different contributions to uncertainty in them. So, the noise covariance matrix does not need to be propagated separately like in probability. So, it can simply be evaluated in each step directly from the RFVs. In particular, the definitions of possibilistic variance and covariance are applied to the random PDs in $\mathbf{X}_k^f$.

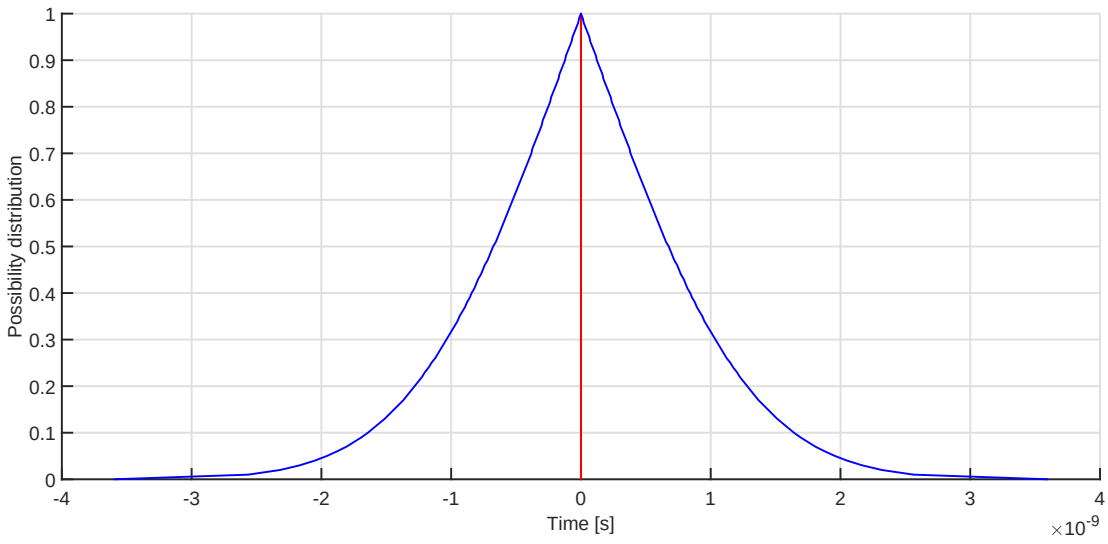

Figure 6.7: *Initial RFV of the state variable theta:* Θ_0^a

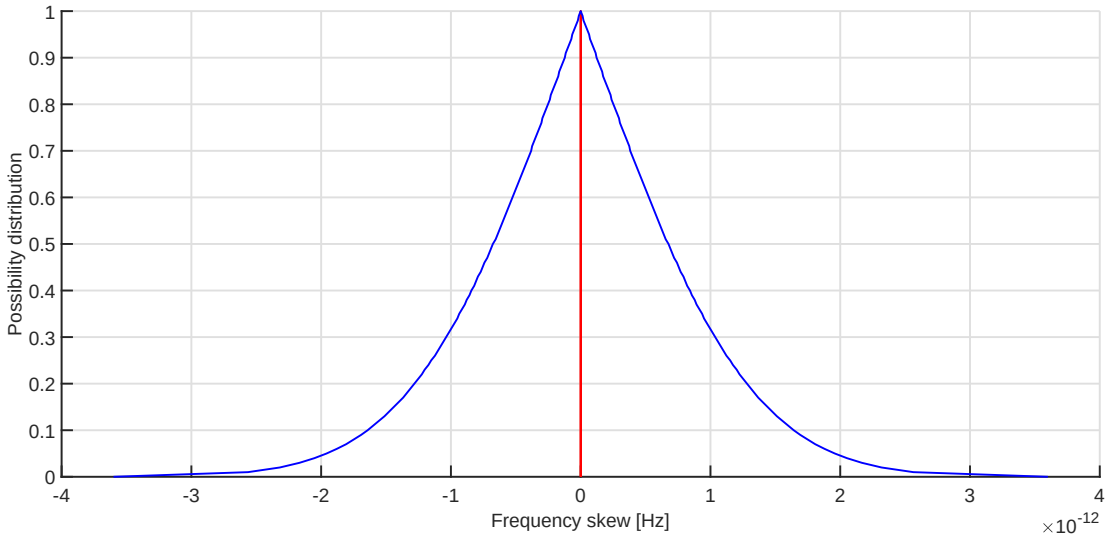

Figure 6.8: *Initial RFV of the state variable gamma:* Γ_0^a.

Similarly, $c_{Y_k^{\text{ran}}}$ is the possibilistic variance associated to the measurement RFV, Y_k^{ran}.

As explained in chapter 3, for an RFV described by an infinite number of α-cuts, α being a real variable, operatively, it can be represented by a finite discrete number of α-cuts. If N α-cuts α_i, with $i = 1...N$, are considered, mean value and variance of an RFV **X** are defined as given below:

$$M(\mathbf{X}) = \frac{1}{N} \cdot \sum_{i=1}^{N} \alpha_i \left(x_2^{\alpha_i} - x_1^{\alpha_i}\right)$$

$$Var(\mathbf{X}) = \frac{1}{2 \cdot N} \cdot \sum_{i=1}^{N} \alpha_i \left(x_2^{\alpha_i} - x_1^{\alpha_i}\right)^2$$

where $\alpha_i = \frac{1}{N-1} \cdot (i-1)$.

Where as the covariance of two RFVs A, B is given as below:

$$Covar(\mathbf{A, B}) = \frac{1}{2 \cdot N} \cdot \sum_{i=1}^{N} \alpha_i \left(x_2^{\alpha_i} - x_1^{\alpha_i}\right)\left(y_2^{\alpha_i} - y_1^{\alpha_i}\right)$$

where $\alpha_i = \frac{1}{N-1} \cdot (i-1)$.

After evaluating the noise covariance matrices of both the states and the measurements, the formula for the evaluation the possibilistic Kalman gain matrix $\mathbf{K}_k^{POS}$ is seen in fig. 6.6.

Y_k is the RFV associated to the offset measurement at step k. By assumption, both random and systematic contributions to uncertainty affect the measurement procedure; therefore Y_k is always (at every step k) a complete RFV, with well defined internal and random PDs: the internal one which takes into account the effects of the systematic contributions; the random one, which takes into account the effects of the random ones. Hence:

- the random PD Y_k^{ran} is the PD corresponding (obtained by applying a probability-possibility transformation as given in Sect. 2.3.2) to a gaussian pdf with mean the measured value $\hat{\theta}_k$ and standard deviation $\sigma_{\hat{\theta}}^2$.

- the internal PD Y_k^{int} is a uniform PD. The mean value of this PD is zero, while the width depends on the considered assumption. In fact, the PTP network has been simulated for different combinations of loads in the direct and inverse paths, both constant and variable (as shown in Fig. 6.4) and, for every different simulation, the width of the rectangular PD is assumed to be twice the maximum observed offset.

Fig. 6.9 shows an example of RFV Y_k, when the traffic is 20% from master to slave and 60% from slave to master. The red line corresponds to the internal PD Y_k^{int}, while the blue line corresponds to the external PD, which combines the internal PD with the random one.

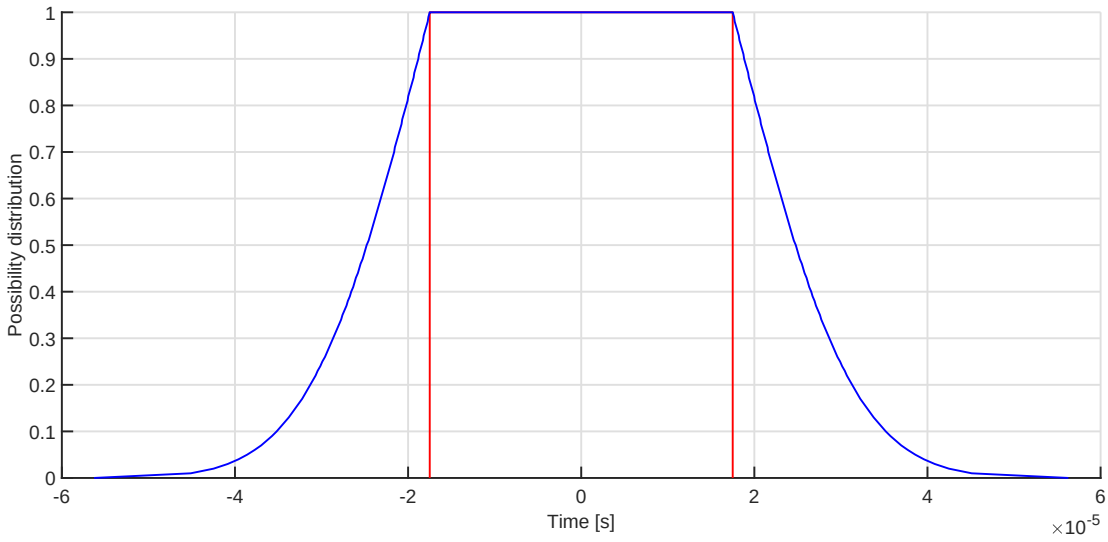

Figure 6.9: *Example of RFV Y_k, representing the measured offset.*

6.5 Simulation Results with the possibilistic KF

In order to make an easy comparision between the results obtained by the classical KF in Sect. 6.3, the modified possibilistic KF defined in chapter 5, sec. 5.4, is applied for the same two cases of traffic load as assumed in Sect. 6.3. The results are shown in Fig. 6.10 and 6.11.

Fig. 6.10 shows the residual offset between the master and slave's clocks when constant traffic load is considered. Since, when the servo clock based on the possibilistic KF is applied, the residual offset is an RFV, the mean value of the RFV is plotted (blue line). On the other hand, the red lines show, for every time step, the α-cut at level $\alpha = 0.01$ of the *a posteriori* RFVs Θ_k^a, which corresponds to the confidence interval at confidence level 99%.

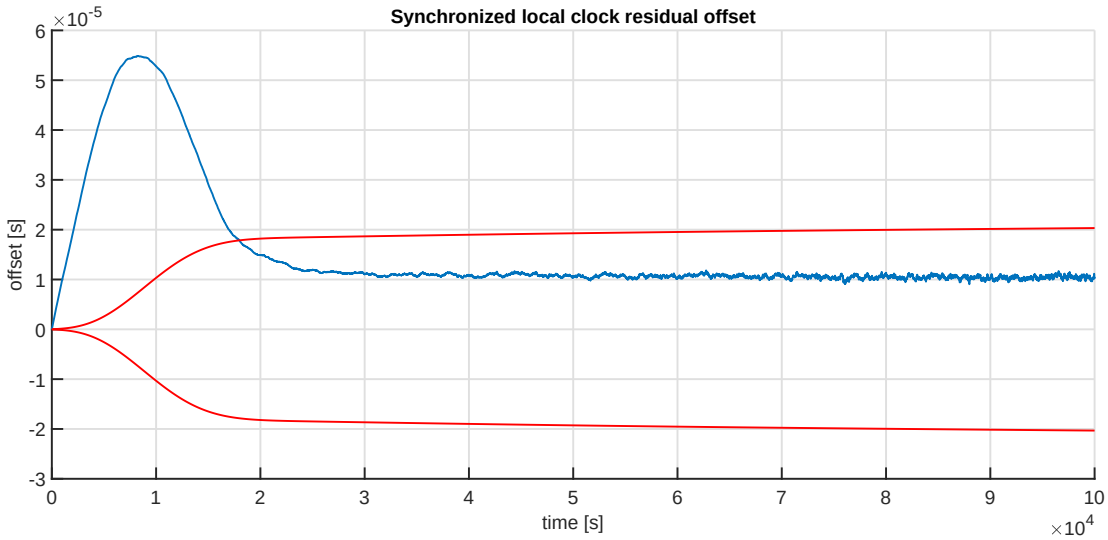

Figure 6.10: *Results obtained with the possibilistic Kalman filter, with constant traffic load. The blue line represents the residual offset of the servo clock after the synchronization procedure (mean value of the RFV Θ_k^a). The red lines represent, for each iteration, the width of the 99% confidence interval, which corresponds to the α-cut at level $\alpha = 0.01$ of Θ_k^a.*

This figure has to be compared with the corresponding figure 6.3, obtained when the classical KF is applied. It can be noted that the servo clock based on the possibilistic Kalman filter provides a correct estimate of the uncertainty intervals. The disadvantage is that the convergence is lower than that of the classical KF.

Fig. 6.11 shows the results given by the servo clock based on the possibilistic KF, when the variable traffic load, as given in Fig. 6.4, is considered. In particular, Fig. 6.11 shows the residual offset (the meaning of the blue and red lines is the same as in Fig. 6.10). This figure has to be compared with the corresponding figure 6.5, obtained when the classical KF is applied. It can be seen that the possibilistic KF is able to evaluate the uncertainty also in the case of a variable traffic load.

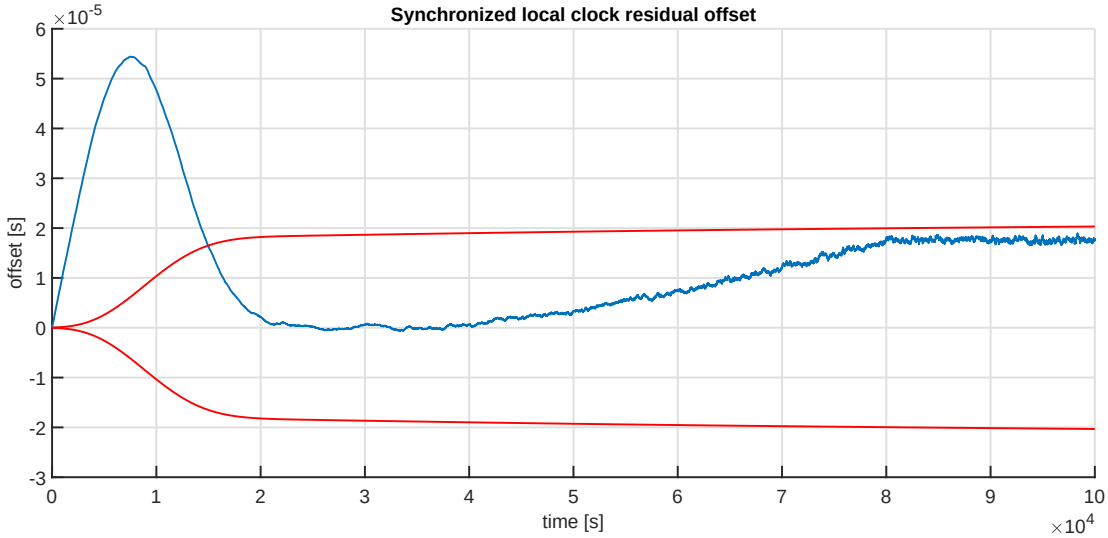

Figure 6.11: *Results obtained with the possibilistic Kalman filter, with varying traffic load, according to Fig. 6.4. The blue line represents the residual offset between the master's and slave's clocks (mean value of the RFV Θ_k^a). The red lines represent, for each iteration, the width of the 99% confidence interval, which corresponds to the α-cut at level $\alpha = 0.01$ of Θ_k^a.*

CHAPTER 7

Defense against malicious attacks on a PTP network using the possibilistic Kalman filter

As it has been established, accurate time synchronization is extremely important in the modern world. It is important in everywhere including power grids, defense etc.

If there is any problem with the time synchronization, depending on the severity, it can cause problems as small as in accurate navigation for a car driver to something as serious as a blackout or a plane crash.

So, malicious attacks on a time network are of serious concern for any entity. Hence, defense against such attacks on the time network is of utmost importance. This chapter proposes one possible solution to malicious attacks especially on a PTP network. As explained in the previous chapter, the possibilistic KF is capable of propagating all contributions to uncertainty in a PTP network including the systematic contributions to uncertainty accurately. So, a possible defense strategy based on this uncertainty attacks is described in this chapter.

7.1 Malicious attacks on the PTP network

There are numerous types of attacks that could be used to attack a PTP network.

7.1.1 Asymmetric delay attack

A PTP network works based on the assumption that the packet transfer delays between the master and the slave are symmetrical for a highly accurate synchronization. When the transmission delays are equal, they cancel each other during the offset calculation as shown in Sect. 6.2.1. When they are not symmetrical, they introduce a bias in the offset measured by the slave.

This is what is taken advantage of in an asymmetric delay attack. As the name suggests, the attacker manipulates the transmission of the data packets between the master and slave. This can be done by hacking the switches and manipulating the switch in such a way that the messages from the master to the slave are held at the switch for a certain duration before transmitting it to the slaves that are connected to the master through the particular switch.

This would make the delay in the transmission of the messages from the master to the slaves higher than the delay from the slaves to the master. This way, an asymmetry is introduced in the delays and thereby a bias is introduced in the offset measured by the slaves. This way, all the slaves that are connected to the master through the particular switch are affected by the attack and they all fall out of synchronization.

7.1.2 Denial of service

For synchronization to occur between the master and the slave clocks in the PTP networks, there needs to be an exchange of messages between the two of them. When the attackers try to shut down a node in a network or the network itself so that others can not access it, it is called denial of service. Usually, this is done by flooding the target with heavy traffic.

7.1.3 Spoofing

In spoofing, the attacker mimics an actual master clock. So, the attacker creates similar packets as the master clock and transmits them to the slaves. Except that the information in the packets is modified to include wrong information about the timestamp. The slave keeps thinking that the packets are being received from the master and hence falls out of synchronization.

7.1.4 Replay attack

In this type of attack, some of the messages from the master are recorded and then they are replayed at a later time. So, in this type of attack, the packets are entirely legitimate but since they are replayed at a later time, the time information in them is completely wrong. This would make the offset calculated by the slave wrong and makes it fall out of synchronization.

7.1.5 Jamming attack

In jamming, some or all of the protocol packets are intercepted by the attackers and they are not transmitted to the destination.

7.2 Proposed Defense strategy using the possibilistic KF

A Kalman filter, in general, can not only predict the system states but also evaluate the uncertainty associated to the states. The same is true also for PTP networks. The uncertainty associated to the slave clock can be evaluated by also the classical Kalman filter.

So, what happens if we use this uncertainty limits to selectively use the offset data without using everything blindly? The answer is that it would absolutely work if we

do not have any systematic contributions to uncertainty in the data. In this particular scenario, all the data that lie outside the uncertainty limits evaluated by the classical KF could be discarded as faulty data.

But, as shown in Chapter 4, the classical KF algorithm underestimates the uncertainty associated with the states in the presence of a systematic error in the measurement data. So, if the uncertainty limits are used to discard the data outside the uncertainty limits, it would mean that also the correct timestamps from the reference clock would be discarded if there were a systematic error in the calculation of the offset. This is especially important in PTP networks that use optical transport network (OTN), since these networks have static asymmetries for long intervals of time before changing abruptly. So, in these networks, the asymmetries are simply a part of the network and they do introduce systematic error in the offset. So, if all these timestamps are rejected, this would mean that the slave will not use any of the timestamp from the reference clock and this would mean that there would be no synchronization and it would keep drifting and falling out of synchronization. This is equivalent to actually performing a denial of service attack on the target. This is the main hurdle to be able to use the uncertainty limits obtained by a classical KF algorithm to defend against malicious attacks.

But, the above mentioned problem would be solved if the systematic uncertainty in the network could also be propagated. As seen in chapter 6, the possibilistic KF is capable of propagating also the systematic contributions to uncertainty accurately in a PTP network. So, if the PTP network is characterized accurately, the uncertainty evaluated by the possibilistic KF would include any possible offset that could result from an actual asymmetry in the traffic loads in the network.

Now, in the case of an attack on the PTP network that involves the modification of the timestamp like an asymmetric delay attack or a spoofing attack, the offset that would be measured by the slave would fall out of the uncertainty intervals evaluated by the possibilistic KF.

So, if the measured offset is outside the uncertainty limits, the timestamp would be deemed invalid and would not be used to correct the slave clock. In Fig. 6.6, the final step of the possibilistic KF algorithm should only be used when there is a valid measured offset available to refine the offset prediction calculated in step 2 of the algorithm. Instead, when the measured offset falls outside the uncertainty limits, it is deemed invalid. So, the offset calculated by the possibilistic KF in step 2 would be directly used till the attack stops and the offset between the slave and the master again falls inside the uncertainty limits. Then, the normal operation of the KF would be resumed.

When the measured offset values fall outside the uncertainty limits for a long duration, it is also possible to alert the system about the possibility of the attack, of course.

7.3 Simulation results against an attack

The PTP network example with constant traffic load as explained in Sec. 6.3 has been used also in this chapter. So, the traffic load from the master to slave is 20% and the traffic load from the slave to master is 60%.

Two case studies of asymmetric delay attack have been performed, as explained below. For each of the case studies, two situations have been considered:

- Situation I: the Possibilistic KF that has been described in Sect. 5.4 has been used

according to the procedure described in Sect. 6.4 but without using the uncertainty limits to validate the measured offset.

- Situation II: The uncertainty limits have been used to dispose of the invalid timestamps during the duration of the attack, as explained in Sect. 7.2.

7.3.1 Asymmetric delay attack case study A

An asymmetric delay attack on the PTP network has been simulated where the offset between the slave and the master has a bias of about 800 μs starting from 25000 s till the rest of the simulation.

The results for situation I can be seen in Fig. 7.1. The residual offset between the slave and the master clock is shown in the blue line. The uncertainty limits evaluated by the possibilistic KF are given in red lines. It can be seen that the residual offset is quite high and goes to 800 μs as expected from the attack and is completely outside the uncertainty limits evaluated by the possibilistic KF.

The results for situation II can be seen in Fig. 7.2. In this situation, invalid timestamps falling outside the uncertainty limits are discarded. Again, the residual offset between the slave and the master clock is shown in the blue line. The uncertainty limits evaluated by the possibilistic KF are given in red lines. It can be clearly seen that the residual offset between the slave and the master clock is well within the uncertainty limits (red lines) evaluated by the possibilistic KF and is almost the same as seen in Fig. 6.10. So, it can be clearly seen that the proposed defense strategy is quite effective to defend in the case of a malicious attack on the PTP network.

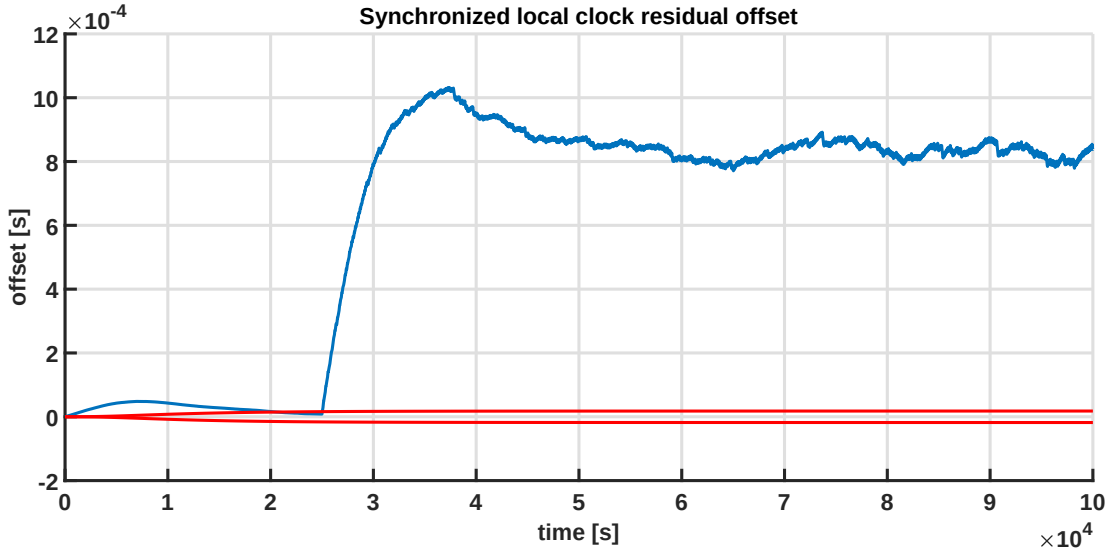

Figure 7.1: *Residual offset between the slave and the master clock shown in the blue line with the uncertainty limits evaluated by the possibilistic KF given in red lines when the clock is not defending against the attack.*

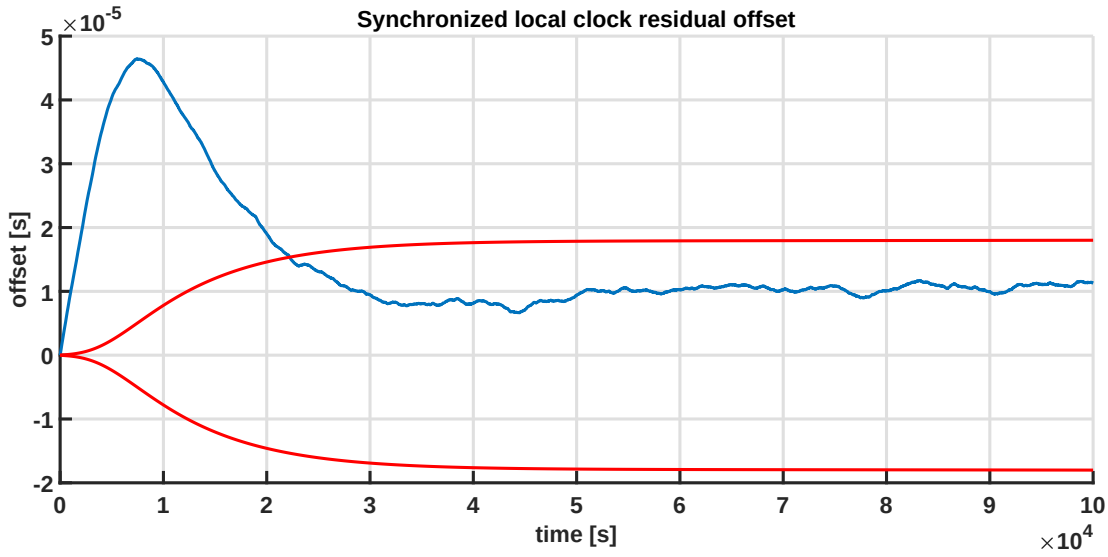

Figure 7.2: *Residual offset between the slave and the master clock shown in the blue line with the uncertainty limits evaluated by the possibilistic KF given in red lines when the defense strategy is employed.*

7.3.2 Asymmetric delay attack case study B

In the second case study, an asymmetric delay attack on the PTP network has been simulated at random instants during the simulation. The offset between the slave and the master increases constantly at the rate of 20 μs every second for 50 s which is the duration of the attack. The randomness of the attack has been simulated by generating a random integer from 1 to 500 and the attack starts whenever the number generated is 1. Every time the attack starts, it continues for 50 s and then stops.

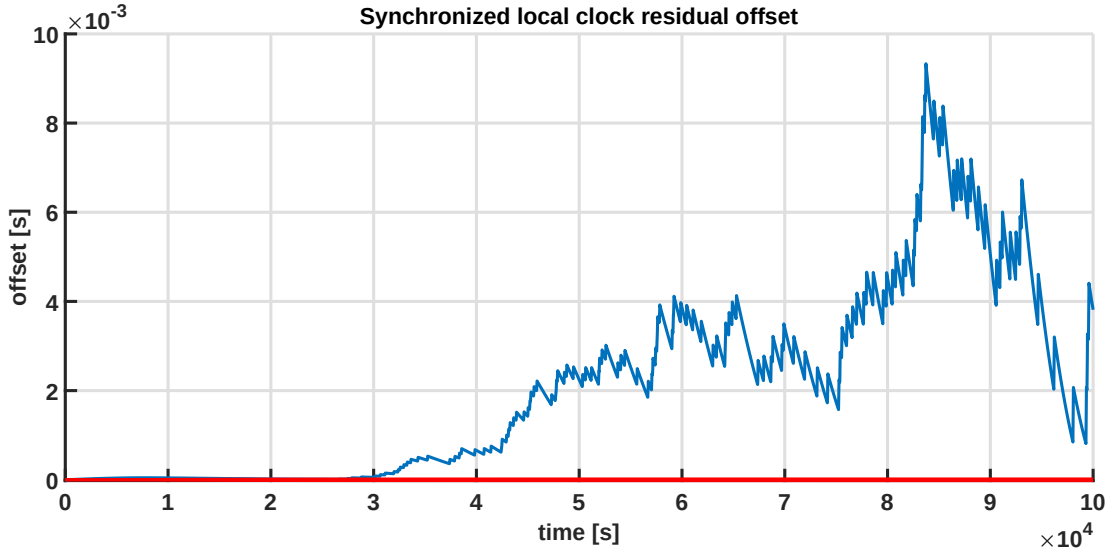

Figure 7.3: *Residual offset between the slave and the master clock shown in the blue line with the uncertainty limits evaluated by the possibilistic KF given in red lines when the clock is not defending against the attack.*

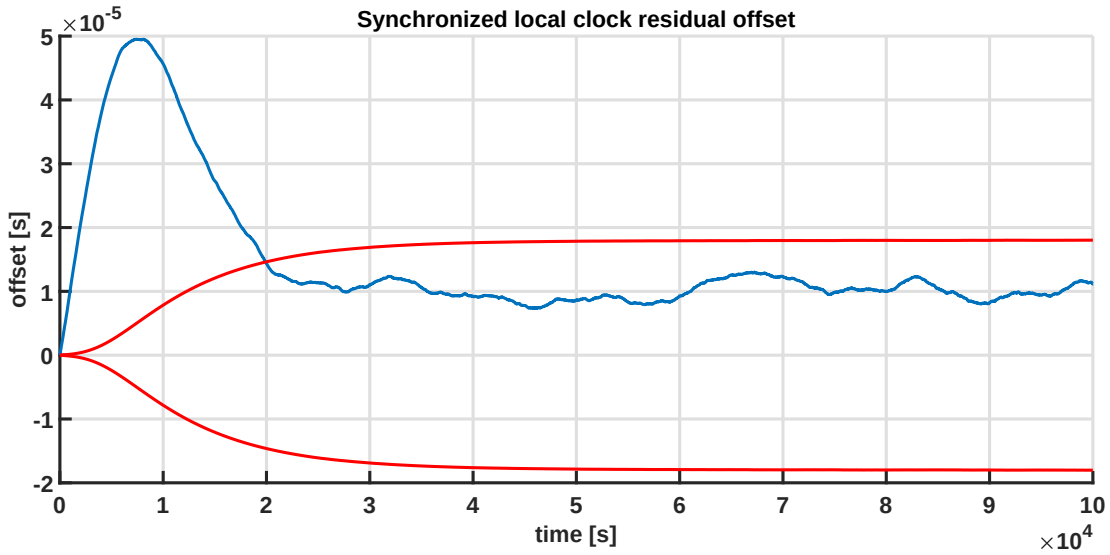

Figure 7.4: *Residual offset between the slave and the master clock shown in the blue line with the uncertainty limits evaluated by the possibilistic KF given in red lines when the defense strategy is employed.*

The results for situation I can be seen in Fig. 7.3. The residual offset between the slave and the master clock is shown in the blue line. The uncertainty limits evaluated by the possibilistic KF are given in red lines. It can be seen that the residual offset is quite high and goes to a maximum of about 9 ms from the attack and is completely outside the uncertainty limits evaluated by the possibilistic KF.

The results for situation II can be seen in Fig. 7.4. In this situation, invalid timestamps falling outside the uncertainty limits are, again, discarded. Again, the residual offset between the slave and the master clock is shown in the blue line. The uncertainty limits evaluated by the possibilistic KF are given in red lines. Again, it can be clearly seen that the residual offset between the slave and the master clock is well within the uncertainty limits (red lines) evaluated by the possibilistic KF and is almost the same as seen in Fig. 6.10. So, it can be clearly seen that the proposed defense strategy is quite effective to defend in the case of a malicious attack on the PTP network.

CHAPTER 8

Error compensation Kalman filter and Drone

8.1 Introduction

As explained in chapter 5, there have been numerous attempts to further the classcial KF algorithm to be able to consider and propagate systematic contributions to uncertainty [42, 43, 52, 53], still using the theory of probability. And as has already been explained, the theory of possibility provides a better mathematical frame to express and propagate systematic contributions to uncertainty.

Articles presenting KF algorithms based on the theory of possibility and fuzzy logic are available in the literature [40, 44]. And there are also possibilistic KFs that are based on RFVs as defined in 5 and [13, 20] so that uncertainty can be expressed and propagated in a way that is compatible with GUM. But all these KF algorithms only attempt to propagate the systematic contributions to uncertainty and none of them attempt to compensate or reduce them.

Starting from the modified possibilistic KF defined in Sect. 5.4, this chapter proposes an alternative version, which also allows to reduce the systematic contributions to uncertainty, thereby reducing the overall uncertainty associated to the system state predictions. While the modified possibilistic KF defined in Sect. 5.4 is useful when we are only interested in propagating the residual systematic uncertainty to evaluate the total uncertainty associated to the state predictions from both the random and systematic contributions, the KF defined in this chapter can be used to reduce the systematic uncertainty and thereby also reduce the overall uncertainty associated to the state predictions.

To facilitate an easy comparison between the proposed alternative possibilistic KF and the original one defined in Sect. 5.4, a similar simulated case study as in Sect. 5.2 is considered here, as briefly described in Sect. 8.2.

8.2 The case study

The considered case study is quite simple and is similar to the one described in Sect. 5.2. A vehicle is moving at a velocity $v_{\text{ref}}(t)$ with an acceleration $a_{\text{ref}}(t)$, as shown in Fig. 8.1.

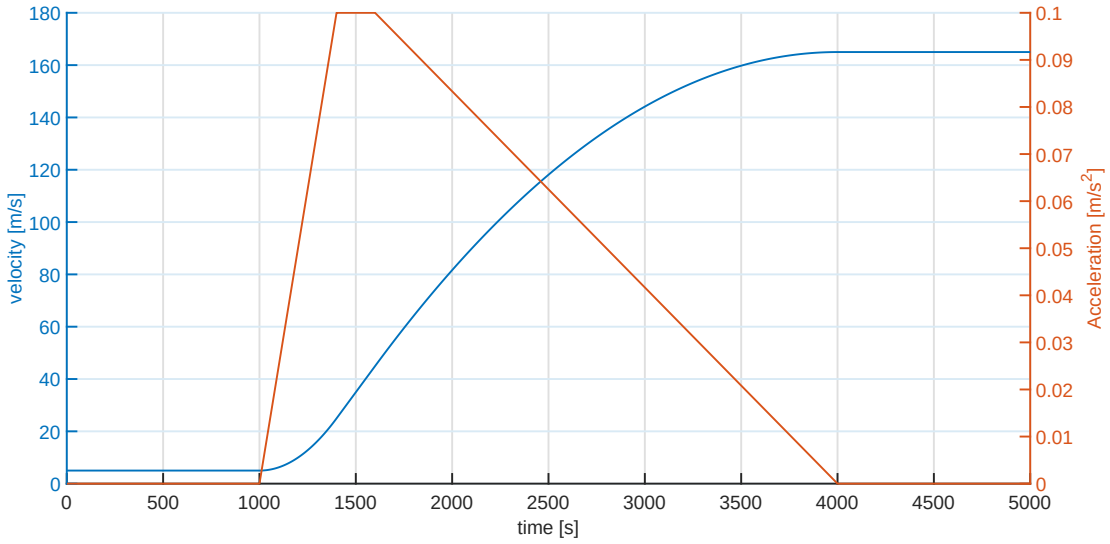

Figure 8.1: *Reference values of velocity (blue line) and acceleration (red line) over time.*

The state equations of the vehicle can be written as:

$$\begin{aligned} v_k &= v_{k-1} + \tau \cdot a_{k-1} + w_k^v \\ a_k &= a_{k-1} + w_k^a \end{aligned} \tag{8.1}$$

- v_k and a_k are velocity and acceleration of the vehicle at time k;
- w_k^v and w_k^a are the standard deviation of the noise in velocity and acceleration respectively at time k;
- τ is the time period within two successive measurements

It is assumed that the noises do not vary with time and are gaussian since the same considerations have been taken as in Sect. 5.2. So, $w_k^v = w^v$ and $w_k^a = w^a$ are the standard deviations of constant normal distributions with zero mean.

w^v is assumed to be 0.003 m/s. This value has been derived by considering the accuracy of a GPS which has been reported in the official GPS website [1], which is usually quite accurate compared to the speedometer of the vehicle. Whereas, w^a is assumed to be $0.0005\, m/s^2$. This has been assumed to be because of some noise in the circuit or due to the driver applying force on the accelerator.

The measured values of the velocity and the acceleration are supposed to have been obtained from the on board sensors of the vehicle. The accuracies of the onboard sensors are in general one or two magnitudes less accurate than a GPS based measurement. So, the following is considered:

- For the velocity, the random contribution is assumed to be normally distributed with a standard deviation of $\sigma_m^v = 0.16\,\mathrm{m/s}$. It has also been assumed that there is a residual systematic error in the measurement with an estimated value of $0.3\,\mathrm{m/s}$. But, this is unknown and only an interval of possible values is known: $e_{sys} = \pm 0.32\ \mathrm{m/s}$ has been assumed.

- For the acceleration, it has been assumed that there is no systematic error in the measurements and the random error is supposed to be normally distributed with a standard deviation of $\sigma_m^a = 0.005\ \mathrm{m/s^2}$.

8.3 The modified possibilistic Kalman filter

Although this has been explained in detail in sec. 5.4, the flowchart of the algorithm has been recalled in this chapter for an easy comparison with the algorithm for the alternative possibilisitc KF defined in this chapter.

In the possibilistic Kalman filter defined in sec. 5.4, all the states are RFVs.

The algorithm is as shown in Fig. 8.2 [20].

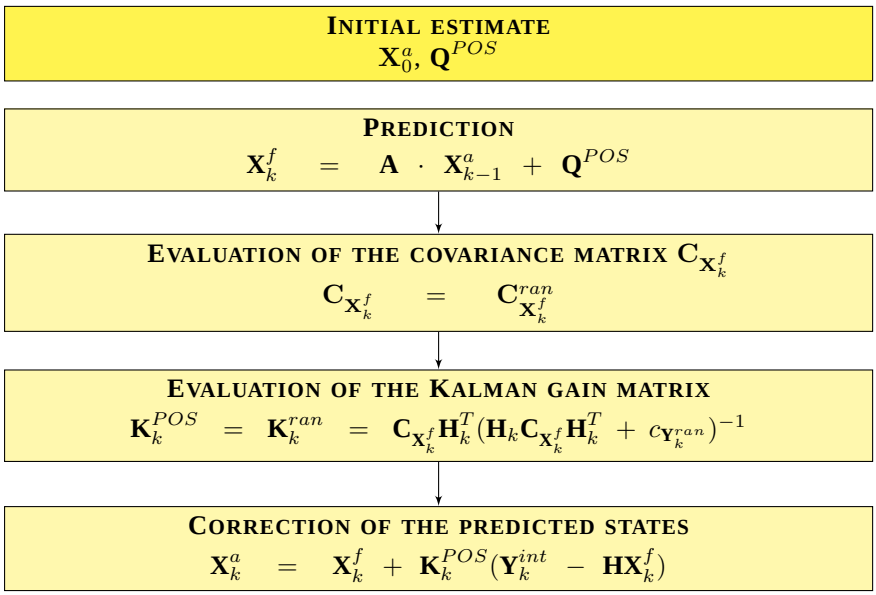

Figure 8.2: *The possibilistic Kalman filter algorithm [20]*

According to eqn. (8.1), $\mathbf{A}_k = \mathbf{A} = \begin{bmatrix} 1 & \tau \\ 0 & 1 \end{bmatrix}$ and $\mathbf{H}_k = \mathbf{H} = \begin{bmatrix} 1 & 0 \\ 0 & 1 \end{bmatrix}$.

Matrix $\mathbf{Q}^{POS}$ considers the model uncertainties and is a matrix of RFVs. According to the assumptions given in Sec. 8.2, we define $\mathbf{Q}^{POS}$ where:

- The element related to velocity is an RFV obtained by transforming the velocity noise variable into possibility domain. Since there is no systematic error in the noise and the random part is assumed to be gaussian, there is no internal PD in the RFV and the random PD is obtained by using the probability-possibility transformation on the zero mean normal pdf with standard deviation w^v in the possibility domain;

- Similarly, the element related to acceleration is also an RFV in which there is no internal PD and the random PD is obtained by using the probability-possibility transformation on a zero mean normal pdf with standard deviation w^a in the possibility domain;

As for the initial state vector $\mathbf{X}_0^a$, it is assumed that there are no systematic contributions to uncertainty. So, the RFV is obtained by just the random PD as follows:

- The initial velocity is an RFV consisting of just the random PD which is obtained by using the probability-possibility transformation on a normal pdf with mean equal to the first measured value for velocity (v_{m1}) and standard deviation w^v;
- Similarly, the initial acceleration is an RFV consisting of just the random PD obtained by using a probability-possibility transformation on a normal pdf with mean equal to the first measured value for acceleration (a_{m1}) and standard deviation w^a.

As for the measured values in each step k, matrix $\mathbf{Y}_k$ is the matrix of the RFVs of the velocity and acceleration measurements.

The RFV associated to the simulated measured velocity is centered on the simulated measured velocity at step k (v_{mk}) and

- The internal PD is a rectangular PD with width $\pm e_{sys}$ around v_{mk};
- the random PD is obtained by using the probability-possibility transformation on a zero mean normal pdf, with standard deviation σ_m^v.

On the other hand, the acceleration has no systematic error. So, the RFV associated to the simulated measured acceleration is centered on the simulated measured acceleration at step k (a_{mk}) and:

- the internal PD is nil;
- the random PD is obtained by using a probability-possibility transformation on a normal pdf, with mean a_k and standard deviation u_{ran}^a.

Matrix $\mathbf{C}_{\mathbf{X}_k^f}$ is the noise covariance matrix of the velocity and acceleration RFVs. But, as it is shown in the equations in Fig. 8.2, $\mathbf{C}_{\mathbf{X}_k^f} = \mathbf{C}_{\mathbf{X}_k^f}^{ran}$. So, the possibilistic variances and covariances are evaluated from only the random contributions to uncertainty in both the velocity and acceleration RFVs.

Similarly, $\mathbf{C}_{\mathbf{Y}_k} = \mathbf{C}_{\mathbf{Y}_k^{ran}}$ which means that the possibilistic variances and covariances of the noise covariance matrix associated to the measurements are evaluated from just the random uncertainty contributions in the velocity and accleration measurements.

The described Kalman filter has been applied to the case study described in Sec. 8.2. The results obtained from the simulations are presented in the following figures 8.3 and 8.4.

The predicted values of the velocity and acceleration from the Kalman filter are obtained by evaluating the mean values of the *a posteriori* RFVs in the matrix $\mathbf{X}_k^a$.

In both figures 8.3 and 8.4, the blue lines represent the differences in the predicted values given by the Kalman filter and the true values of the velocity and acceleration respectively.

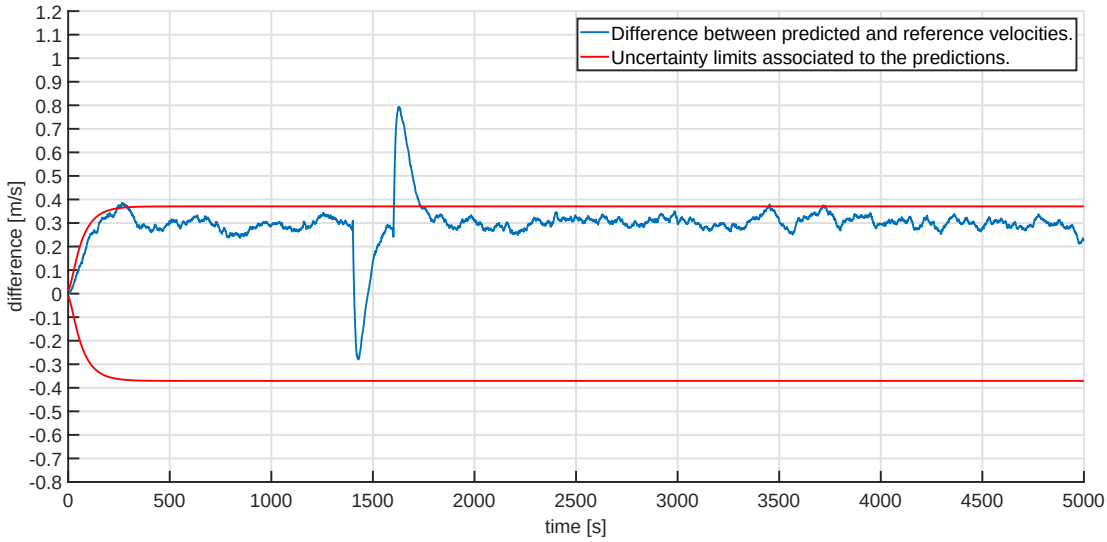

Figure 8.3: *Difference in the reference and predicted velocity values (blue line) provided by the possibilistic Kalman filter together with the predicted uncertainty interval (red lines).*

The uncertainty limits associated the state predictions (red lines) are the $\alpha-$cut at $\alpha = 0.01$ of the velocity and acceleration RFVs predicted by the Kalman filter. The $\alpha-$cut can be considered as the confidence interval at the confidence level 1-α [48]. For $\alpha = 0.01$, these intervals correspond to 99% confidence interval in the corresponding pdf.

8.4 The alternative possibilistic Kalman filter Algorithm

In this chapter, an alternative version of the Kalman filter algorithm recalled in the previous is presented, which attempts to reduce the residual systematic error. It can be clearly seen in the results in fig. 8.3 and 8.4, the possibilistic Kalman filter algorithm described in Sec. 8.3 propagates the systematic contributions to uncertainty and estimates the overall uncertainty and confidence intervals associated to the predictions very accurately in the presence of a systematic error. However, the systematic error is still present in the state predictions provided by the KF.

Since the systematic contributions to uncertainty are propagated accurately, this means that an interval of values is available within which the overall systematic error in the state predictions lies. Hence, it is proposed to use this knowledge to compensate for the systematic error and attempt to reduce the systematic error and thereby reduce the overall uncertainty in the state predictions. The new KF algorithm also called the alternative possibilistic KF algorithm is synthetically shown in fig. 8.5. With respect to the algorithm in sec. 8.3, all the steps except the last step are the same. The final step in the new algorithm corresponds to the “correction of the predicted states."

The idea of the algorithm is to use the internal membership of the state RFVs that have been predicted in each iteration to compensate for any possible systematic uncertainty in the measurement data and thereby the predicted states, since they follow the measurement data in the usual case.

To accomplish this, in the new algorithm, a new RFV $\mathbf{Y}_k^{comp}$ is defined which con-

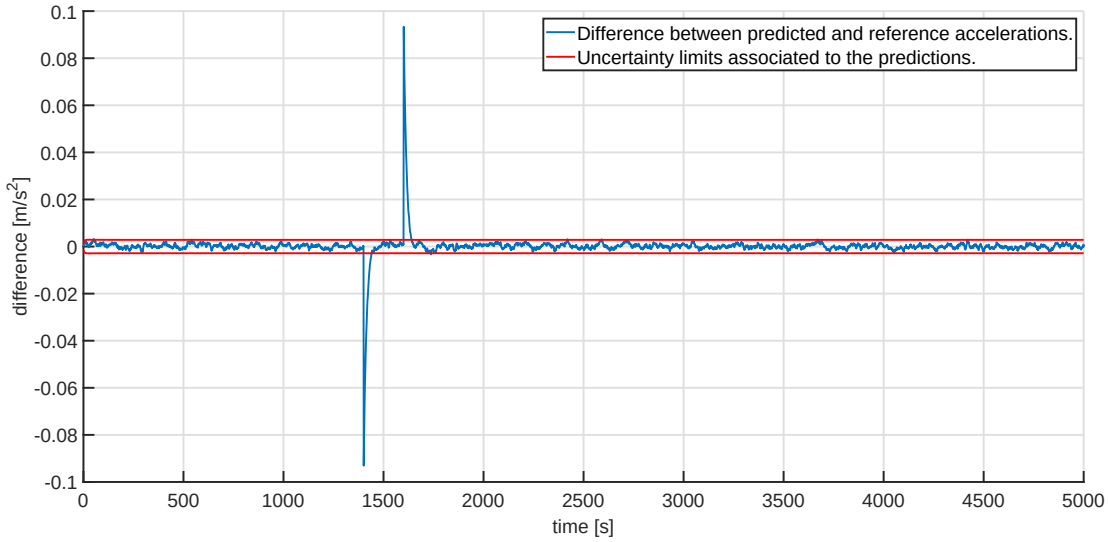

Figure 8.4: *Difference in the reference and predicted acceleration values (blue line) provided by the possibilistic Kalman filter together with the predicted uncertainty interval (red lines).*

tributes to reduce the overall systematic contributions to uncertainty. $\mathbf{Y}_k^{comp}$ is related to the RFVs of the state estimates obtained in the previous iteration $\mathbf{X}_{k-1}^a$. In particular, at each step k, $\mathbf{Y}_k^{comp}$ consists of just the internal membership function of $\mathbf{X}_{k-1}^a$ but centered at the positive uncertainty limit evaluated by the Kalman filter at the previous iteration (step $k-1$). Only the internal membership function is taken since this is the part that corresponds to the systematic contribution to uncertainty. Moreover, since the objective is to compensate for the maximum possible systematic error, it is proposed to have the $\mathbf{Y}_k^{comp}$ centered at the positive uncertainty limit.

$\mathbf{Y}_k^{int\_modified}$ is then obtained by adding or subtracting the RFV $\mathbf{Y}_k^{comp}$ from $\mathbf{Y}_k^{int}$, depending on if the systematic error is positive or negative:

$$\mathbf{Y}_k^{int\_modified} = \begin{cases} \mathbf{Y}_k^{int} + \mathbf{Y}_k^{comp} & \text{if systematic error} < 0 \\ \mathbf{Y}_k^{int} - \mathbf{Y}_k^{comp} & \text{if systematic error} > 0 \end{cases} \tag{8.2}$$

This is similar to a negative feedback loop in a regular system in which the output of the system is fed back to make a comparison with the reference value for the output so that the system stabilizes at the reference value. In this case, the uniform possibility distribution representing the overall systematic contribution to uncertainty within which the systematic error is supposed to lie in, predicted by the Kalman filter, is used as a feedback input to compensate for a systematic error in the predictions, so that any possible systematic error in the state prediction is at least partially compensated for. Since the systematic contribution to uncertainty in the RFVs associated to the state predictions is also reduced with every iteration, because of the compensation of the error, it means that the compensation applied in each step also keeps going down till the system stabilizes around a particular value, which is around half of the original systematic contribution to uncertainty.

To apply the algorithm, there is one intrinsic requirement. Some knowledge of the systematic error is required. It is a given that the magnitude of the systematic error is

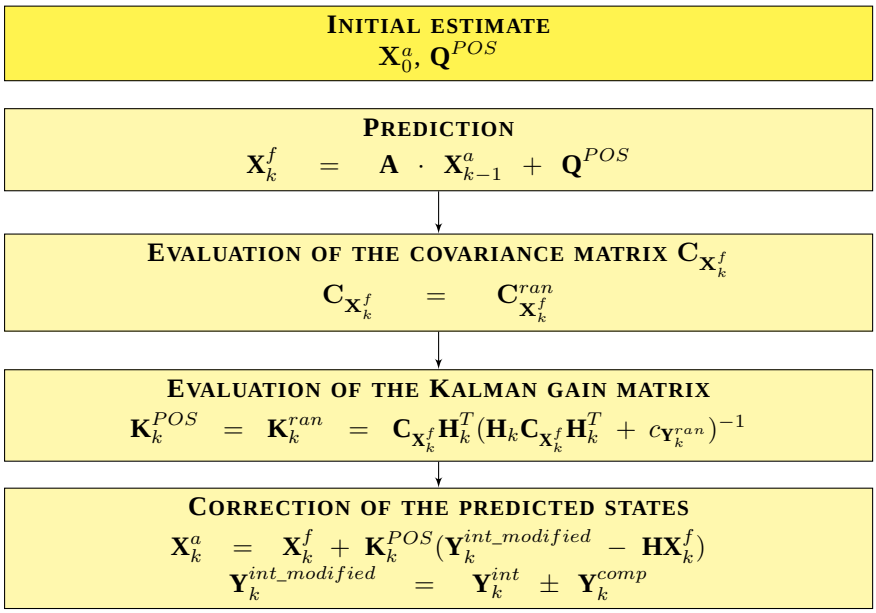

Figure 8.5: *The alternative possibilistic Kalman filter algorithm.*

unknown since, otherwise, it would simply be compensated for and eliminated. Instead, the direction or the sign of the systematic error must be known i.e., it should be known if the systematic error is positive or negative.

8.4.1 Simulation results

The same example described in the previous Sect. 8.3 is also considered to apply the alternative possibilistic KF, for an easy comparison of the obtained results. As recalled in Sect. 8.2, the velocity measurement has been assumed to have a systematic error of $+0.3m/s$, whose value is assumed to be unknown, but whose sign is assumed here to be known to the user. According to this assumption, the expression for $\mathbf{Y}_k^{int\_modified}$ is given by:

$$\mathbf{Y}_k^{int\_modified} = \mathbf{Y}_k^{int} - \mathbf{Y}_k^{comp} \tag{8.3}$$

The obtained results are shown in Fig. 8.6 and 8.7 for the velocity and the acceleration respectively. Again, the predicted values for the velocity and acceleration given by the Kalman filter are the mean values of the velocity and acceleration RFVs in matrix $\mathbf{X}_k^a$.

As in Fig. 8.3 and 8.4, in Fig. 8.6 and 8.7, the blue lines represent the differences in the predicted values given by the Kalman filter and the true values of the velocity and acceleration respectively.

The uncertainty limits associated the state predictions (red lines) are the $\alpha - cut$ at $\alpha = 0.01$ of the velocity and acceleration RFVs predicted by the Kalman filter.

It can be clearly seen, by comparing the results in Fig. 8.6 with those shown in Fig. 8.3, that the uncertainty limits have been significantly reduced along with the residual systematic error in the velocity estimate provided by the Kalman filter defined in this chapter. For easier reference, the important results have been presented in a tabular

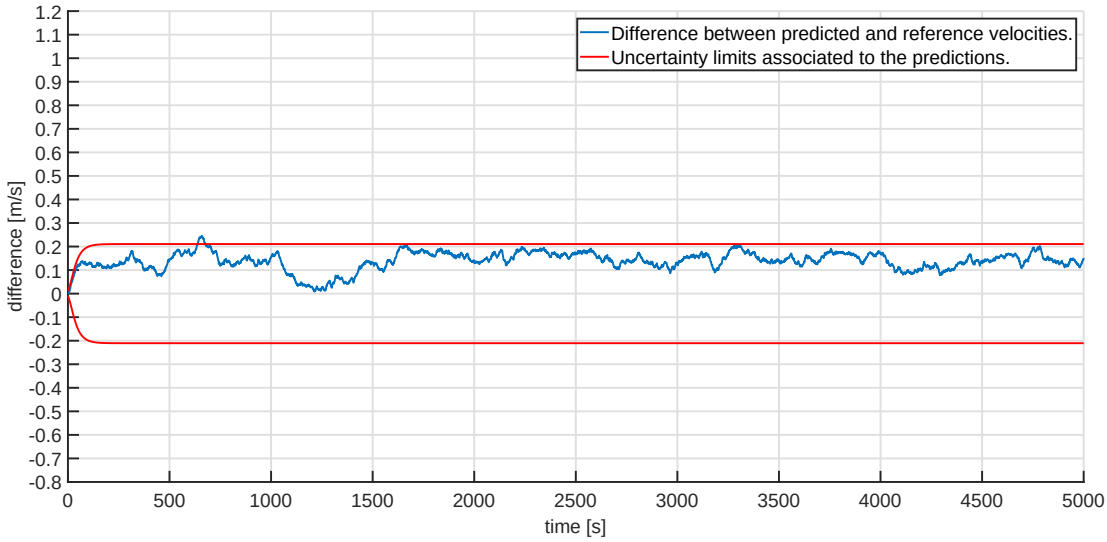

Figure 8.6: *Difference in the reference and predicted velocity values (blue line) provided by the possibilistic Kalman filter defined in this chapter, together with the predicted uncertainty interval (red lines).*

format in table 8.1.

KF	Modified Possibilistic	alternative Possibilistic
Mean Steady-state error	0.3024	0.1657
Uncertainty limits	± 0.3706	± 0.2106

Table 8.1: *Synthetic indexes for velocity estimates in Fig. 8.3 and 8.6.*

8.5 Further simulations to verify the extreme situations

As has been explained in the previous section, in the alternative possibilistic KF, the maximum possible value of the interval predicted by the KF, in which the systematic error should lie in, is used to compensate for the residual systematic error. This means that no matter what the actual systematic error is, it is always compensated by the maximum possible value since the uncertainty limit of the RFVs evaluated in each step (which is the value of the α-cut at $\alpha = 0.01$ of the RFV) is used to compensate for any possible systematic error.

This means that it could be possible that the residual systematic error is overcompensated, since the magnitude of this is unknown. But this scenario would not be detected by us, since the actual magnitude of the systematic error is not known to us, but only an interval of values in which it might be, represented by the uniform possibility distribution. The worst case scenario would be when there is no actual systematic error present and there has been a compensation of a non-existent systematic error.

In this specific situation, it would be very important that the systematic error that may still be present after the compensation lies inside the total uncertainty limits evaluated by the KF algorithm.

This means that even in the worst case scenario, where the actual systematic error is zero, the compensation should be low enough for the state predictions of the KF to still

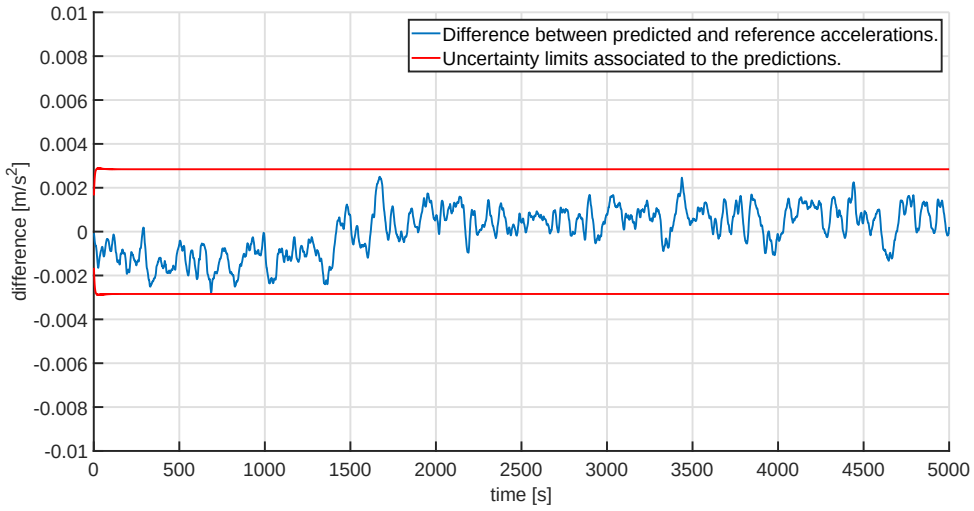

Figure 8.7: *Difference in the reference and predicted acceleration values (blue line) provided by the possibilistic Kalman filter defined in this chapter, together with the predicted uncertainty interval (red lines).*

lie inside the new uncertainty limits evaluated after the compensation.

To verify the effectiveness of the proposed algorithm in all possible situations, further simulations have been performed, considering the worst case scenario in which the alternative possibilistic KF algorithm has been applied, but the actual residual systematic error zero.

The same example described in the Sec. 8.2 is now considered except that the systematic error is considered to be zero (instead of $+0.3m/s$).

When the alternative possibilistic KF is applied to the considered scenario, the obtained results in Fig. 8.8 and 8.9 are obtained for velocity and acceleration respectively.

As expected, it can be seen in Fig. 8.8 that there is definitely an overcompensation of the systematic error in the velocity, since, basically, the algorithm actually introduces a systematic error in the prediction in the worst case scenario where the actual systematic error is zero, but it is still well-bound by the uncertainty limits newly evaluated by the KF.

This demonstrates that the proposed Kalman filter algorithm successfully decreases the overall uncertainty associated to the state predictions provided by the Kalman filter in all situations. In fact, the average uncertainty in Fig 8.8 is in any case smaller than the one in Fig. 8.3.

8.6 Experimental case study

An experimental validation of the proposed algorithm has been performed, considering the parrot AR drone, shown in Fig. 8.10. The parrot AR drone has been developed as a low cost drone by “parrot” company and is quite customizable. The code is open source and can be modified according to the necessity. It has a variety of sensors and the data can be obtained from them and processed as needed. For the present case study, the velocity and acceleration measurements have been considered.

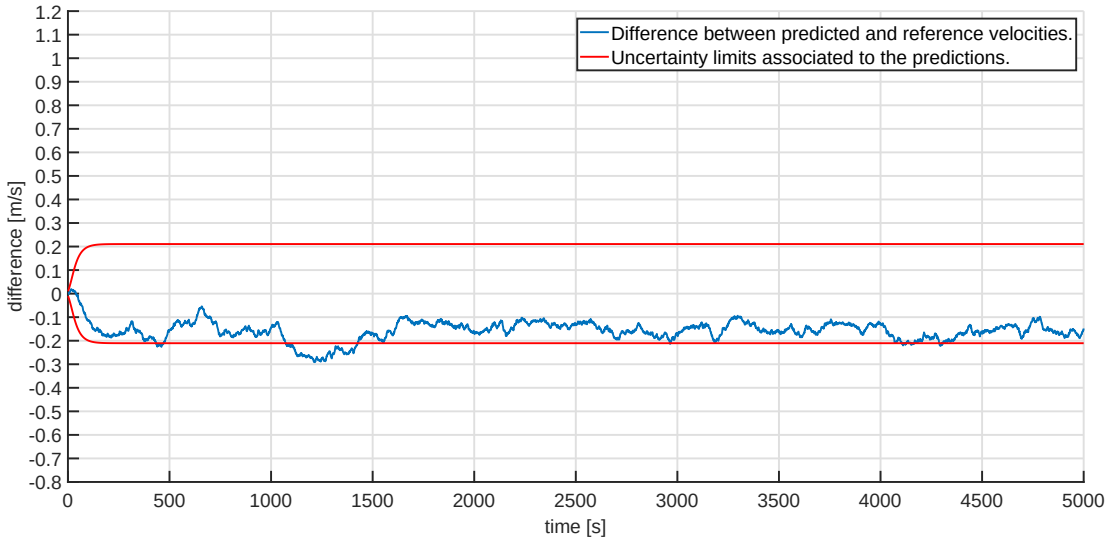

Figure 8.8: *Difference in the reference and predicted velocity values (blue line) provided by the possibilistic Kalman filter defined in this chapter, together with the predicted uncertainty interval (red lines) when residual systematic error is zero.*

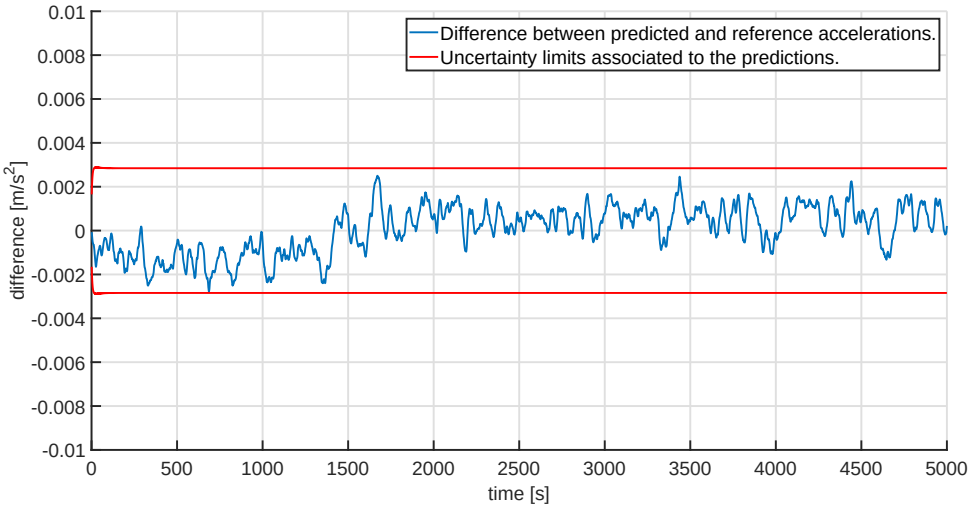

Figure 8.9: *Difference in the reference and predicted acceleration values (blue line) provided by the possibilistic Kalman filter defined in this chapter, together with the predicted uncertainty interval (red lines) when residual systematic error is zero.*

The drone that was used has been observed to have a negative systematic error in the velocity measurements obtained from the sensors present in the drone. So, the velocity is being underestimated by the sensors of the drone. It has also been observed that the systematic error is not constant for all runs. Each individual run had a systematic error that may be different from the other runs. So, only an interval of values can be estimated and the error can not just be compensated for.

By performing a large number of runs of the drone, the interval for the systematic error has been estimated and this was used to construct the internal membership function of the RFV for the measured velocity. The constructed RFV, assumed in this figure

Figure 8.10: *The parrot drone.*

to be centered at zero velocity, can be seen in Fig. 8.11.

The measured acceleration, on the other hand, doesn't have any systematic contributions to uncertainty. Hence, the RFV can be constructed by simply using a probability-possibility transformation on the probability distribution of the acceleration.

The drone was made to fly for a few seconds to cover a distance of approximately 4 m. The velocity and acceleration data from the sensors is obtained from the drone every 5 ms. The defined possibilistic KF described in Sec. 8.4 has been used to provide the filtered velocity and acceleration predictions with their respective uncertainties as well as compensate partially for the systematic error in the velocity measurements provided by the drone.

The velocity estimates provided by the Kalman filter have been integrated to get

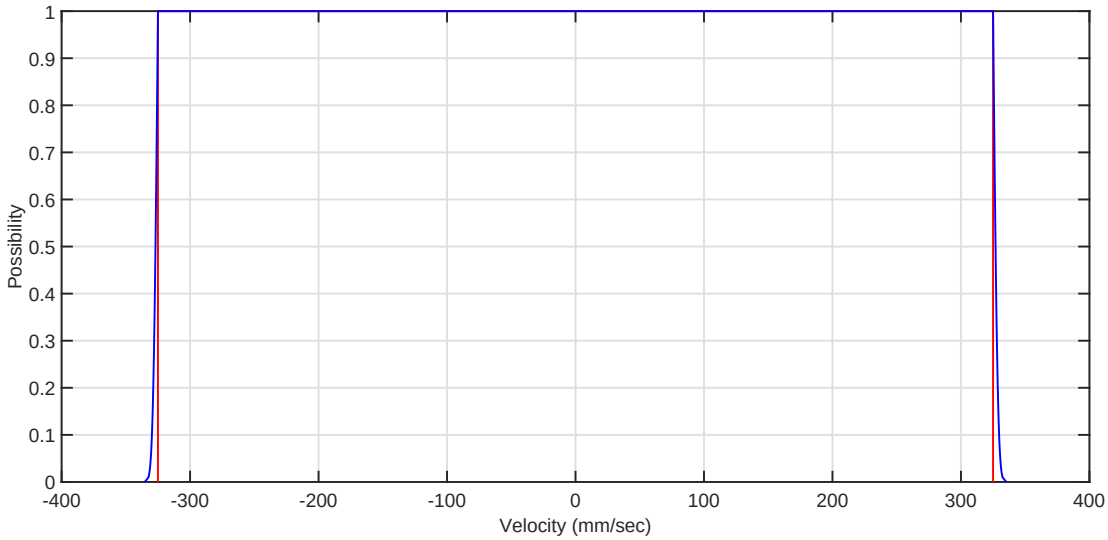

Figure 8.11: *RFV of the velocity constructed from the data. Blue line represents the external membership function and the red line represents the internal membership function.*

the estimated distance that the drone traveled. Similarly, the velocity measurements directly obtained by the drone have been integrated as well, to get the distance that the drone traveled according to the sensors present in the drone.

At the end of every run, the actual distance from the starting point has been measured. Several runs have been made and the distances estimated by the KF and those estimated according to the sensor data have been compared with the actual distance traveled by the drone.

To facilitate a comparision between the alternative KF defined in this chapter and the possibilistic KF defined in Sect. 8.3, the sensor data has been processed using both the KFs seperately.

The results using the possibilistic KF defined in Sect. 8.3 can be seen in Fig. 8.12. The green line represents the distances estimated according to the velocity measurements obtained directly from the sensors in the drone. The blue line represents the distance obtained from the velocity estimates of the defined possibilistic KF. The black line represents the actual distance traveled by the drone. Finally, the red lines represents the upper and lower bounds for the uncertainty.

It can be seen that the distances estimated by the possibilistic KF are quite close to the distances from the sensors. The blue line and the green line in Fig. 8.12 are almost the same and that is why only the green dots and the blue line can be seen in the figure. But, the real measurements lie inside the uncertainty limits of the distances provided by the possibilistic KF.

The results using the alternative KF defined in this chapter can be seen in the Fig. 8.13. Again, the green line represents the distances estimated according to the velocity measurements obtained directly from the sensors in the drone. The blue line represents the distance obtained from the velocity estimates of the defined possibilistic KF. The black line represents the actual distance traveled by the drone. Finally, the red lines represents the upper and lower bounds for the uncertainty.

It can be clearly seen that the distance obtained using the alternative KF defined in

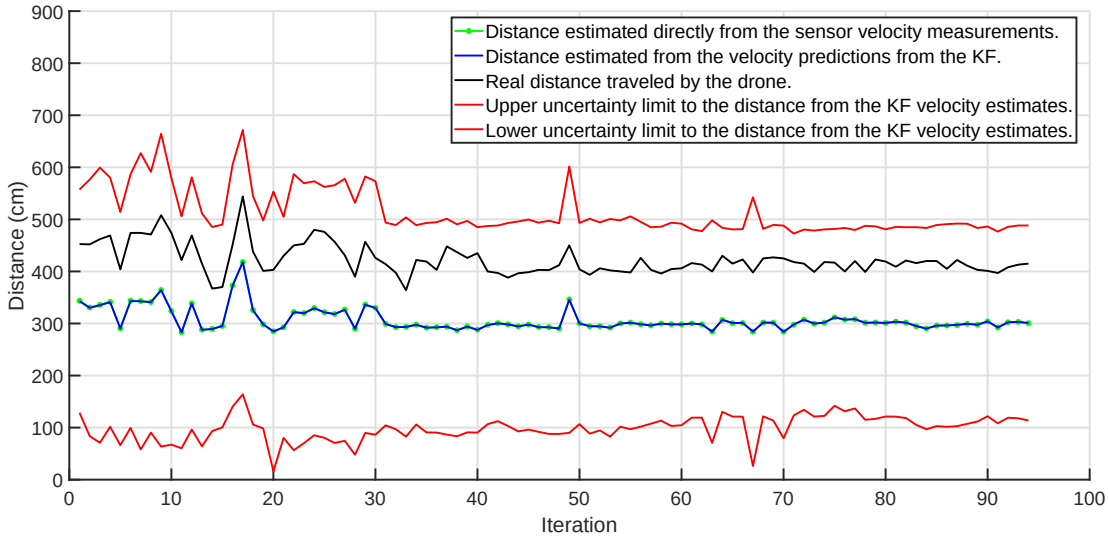

Figure 8.12: *Distances obtained from the velocity estimates of the possibilistic KF (blue line). The predicted uncertainty intervals (red lines). Actual distance traveled by the drone (black line) and distances estimated according to the velocity measurements obtained directly from the sensors in the drone (green line). Green line and blue line are almost the same.*

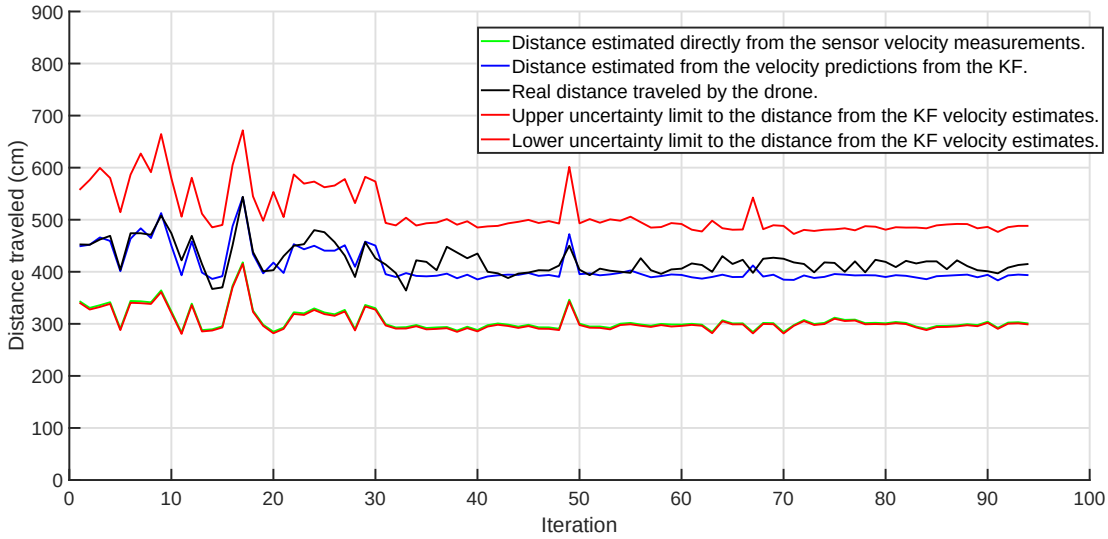

Figure 8.13: *Distances obtained from the velocity estimates of the defined alternative possibilistic KF (blue line). The predicted uncertainty intervals (red lines). Actual distance traveled by the drone (black line) and distances estimated according to the velocity measurements obtained directly from the sensors in the drone (green line)*

this chapter is much more accurate and closer to the real measurements than the distances obtained from the sensor measurements or those obtained from the possibilistic KF defined in [20].

Also, it can be easily seen that the width of the uncertainty limits associated to the distance (red lines) are smaller in Fig. 8.13 compared to that in Fig. 8.12.

This confirms that, by using the defined alternative possibilistic Kalman filter, the systematic error in the velocity has been compensated quite efficiently and the overall

uncertainty associated to the predictions is decreased as well.

CHAPTER 9

Bayes' theorem in Conformity Analysis.

9.1 Introduction

As explained in the chapter 1, a measurement result can not simply be expressed as a single numerical value along with it's unit. It should be accompanied by additional information such as its measurement uncertainty or confidence interval. When the uncertainty and the confidence interval is specified along with the measurement result, the pdf can be assumed or derived from some additional information about the measurand.

To recall a few more concepts that have been given in chapter 1, in the case, when the confidence interval can not be directly determined because the probability distribution of the measurand is not known, a Monte Carlo method is implemented and a probability density function (pdf), which represents the distribution of the values that can be reasonably attributed to the measurand is derived. Then, from this pdf, it is possible to retrieve [27, 28]

1. a measured value and a standard uncertainty, which are given, respectively, by the mean value and standard deviation of the pdf;

2. a confidence interval, about the measured value, that is an interval of possible measurement values along with the associated confidence level, or coverage probability.

Regardless to the way measurement uncertainty is evaluated, its correctness depends on the correctness of the available information, and how well it is processed to evaluate the different contributions to uncertainty and propagate them through the measurement process [19, 27, 28].

Usually, measurement results are employed as input elements in decision-making processes, such as conformity assessment. This is probably the most frequent use of

measurement results, especially in industrial applications, as well as in healthcare, environment protection and many other important applications.

In most situations, we also have access to preexisting sources of information about the measurand in addition to the measurement result. When we have this *a priori* information, usually it is benificial to use it so that we can make a more informed decision which in general is expected to result in a better decision. This is usually done by applying the Bayes' theorem to combine both the *a priori* information as well as the measurement result to derive a subjective probability distribution which can then be used in the decision making process.

When doing this though, ensuring that the available information is reliable is a critical key point. But what happens when this information is not reliable? This could happen when the measuring instrument deviates resulting in the measurement result being wrong or when the process deviates resulting in the *a priori* information being wrong. In this chapter, it is demonstrated what happens when the Bayes' theorem is applied in a blind manner without having reliable information.

In the next section, some concepts about conformity assessment have been recalled.

9.2 Conformity assessment

Conformity assessment is defined broadly as any activity whose goal is to judge if a particular quantity or product meets a certain standards and specified requirements.

As has been expressed earlier, a measurement result is expressed in terms of probability distribution function which gives a best estimate of the measurand along with the associated measurement uncertainty or a coverage interval which contains the true value of the measurand with a specified coverage probability. Due to the uncertainty in any measurement, it is inevitable that there is always a risk of making incorrect decisions about an item's conformity or non conformity.

The general terms and definitions related to conformity assessments are given in ISO/IEC 17000:2004 document. In any conformity assessment, the decision if a given product meets the specific requirement is dependent on the measurement of the relevant measurand. ISO 10576-1:2003 document stipulates the rules to check the conformity within specified limits and the coverage interval of the measurement is compared with a tolerance interval.

The JCGM guide 106 [29] extends the approach to conformity analysis to consider risks, such as producer's risk or consumer's risk in the case where conformity is incorrectly assessed, and provides some general guidelines to perform a conformity analysis depending on a measurement result.

Hence, an *acceptance interval* can be defined by specifying a set of acceptable values for a measurand in such a way that the risk of wrong decision of both conformity and non conformity can be balanced to minimize the cost due to either of the wrong decisions. An acceptance interval is the interval which enables us to make a binary conformity analysis about a quantity. So, if the value of the measurand lies inside the acceptance interval, the item is conforming and non conforming otherwise.

Some basic definitions to perform a conformity analysis are as follows [29]:

- A tolerance interval, on the other hand, is defined as an interval of permissible values for a property.

- Tolerance limit is the specified upper or lower bound of permissible values of a property.
- Tolerance is defined as the difference between the upper and lower tolerance limits.
- A decision rule is a documented rule that describes how measurement uncertainty will be accounted for with regard to accepting or rejecting an item, given a specified requirement and the result of a measurement.
- Specific consumer's risk is the probability that a particular accepted item is non-conforming.
- Specific producer's risk is the probability that a particular rejected item is conforming.
- The measurement capability index C_m is a parameter which characterizes the quality of measurement with respect to a requirement specified by a tolerance and is given by,

$$C_m = \frac{T_u - T_l}{4u_m}. \tag{9.1}$$

According to [29], a conformity analysis is done in three sequential steps:

- Measure the property of interest of the product.
- Compare the measurement result with the specified requirement.
- Decide on a subsequent action whether to reject or accept the product.

Once a measurement result is obtained, the decision on whether to reject or accept the product is done based on a previously established decision rule.

A coverage interval corresponds to the set of values such that the probability that the quantity lies inside the coverage interval is equal to a specified probability called the coverage probability.

If the true value of the measurand lies inside the tolerance limits, then the corresponding quantity is said to conform to the specified requirement.

If the probability distribution of the measurand is in fact, known, and it is assumed that it is represented by $g(\eta|\eta_m)$, then the statement of conformity is an inference with a certain probability of it being true. If the set of conforming values of the measurand Y are denoted by C, the conformance probability is given as shown below [29]:

$$p_c = Pr(Y \in C|\eta_m) = \int_c g(\eta|\eta_m)d\eta. \tag{9.2}$$

If an upper and lower tolerance levels (T_u and T_l respectively) are given , then the equation modifies to,

$$p_c = \int_{T_l}^{T_u} g(\eta|\eta_m)d\eta. \tag{9.3}$$

A measurement result can often be summarized by just a coverage interval with an associated coverage probability without a probability distribution function that is explicitly stated for the measurand. In such a case, [29] says that a statement of conformance probability can be made by comparing the coverage interval with the tolerance interval. If the entire coverage interval with the corresponding coverage probability p lies inside the tolerance limit, then the conformity probability is definitely more than p. If the entire coverage interval lies outside the tolerance limit, then it is definitely less than p. But, if part of the interval is inside the tolerance limit and part of it outside, no decision can be made about the conformance probability.

9.3 Discussion

From all the discussion about the conformity assessment, it can be seen that no decision can be taken without the knowledge of the measurement uncertainty value associated to the obtained measured value.

Therefore, in this respect, it could be thought that the GUM [27] provides the main and most important guidelines to be followed. However, the approach followed by the GUM to assign a pdf to a measured value is perfectly good when no *a-priori* information about the measurand is available, which is the case in most calibration labs. However, when *a priori* information is, in fact, available, the more recommended approach is the application of Bayes' theorem. It is in fact recommended by the [29] to use the Bayes' theorem whenever prior information is available about a particular quantity.

It follows that Bayes' theorem is expected to provide a better result than that provided by the commonly employed GUM approach. The aim of this chapter is to further discuss this statement and the robustness of the proposed approach with respect to the correctness of the *a priori* assumptions. Simulation and experimental results will be proposed and analyzed to this purpose.

The next section recalls Bayes' theorem and tries to highlight its advantages and disadvantages when it is applied in metrology.

9.4 Bayes' theorem in metrology

Let us consider a random variable X, mathematically represented by its probability density function $p_X(x)$, and a random variable Y, mathematically represented by its probability density function $p_Y(y)$, where x and y represent single realizations of X and Y respectively.

If the possible mutual dependence of X and Y is also known, it is possible to define the joint probability density function $p_{X,Y}(x, y)$ of the two variables X and Y.

In particular, it can be written:

$$p_{X,Y}(x, y) = p_X(x) \cdot p_{Y|X}(y|x) \tag{9.4}$$

where $p_{Y|X}(y|x)$ is the conditional probability of random variable Y, given X.

It is obvious that the conditional probability $p_{Y|X}(y|x)$ of event y given x depends on the particular value assumed by the random variable X. When the random variables X and Y are independent of each other, the conditional probability $p_{Y|X}(y|x)$ of event

y given x does not depend on the value x assumed by X. Therefore, it is:

$$p_{Y|X}(y|x) = p_Y(y) \tag{9.5}$$

Under this assumption, it follows:

$$p_{X,Y}(x, y) = p_X(x) \cdot p_Y(y) \tag{9.6}$$

Equation (9.4) can be also rewritten as:

$$p_{X,Y}(x, y) = p_{X|Y}(x|y) \cdot p_Y(y) \tag{9.7}$$

where $p_{X|Y}(x|y)$ is the conditional probability of random variable X, given Y. $p_{X|Y}(x|y)$ depends on the particular value assumed by random variable Y, except when X and Y are independent variables. In this case:

$$p_{X|Y}(x|y) = p_X(x) \tag{9.8}$$

and (9.7) becomes the same as (9.6).

In the more general situation of dependent variables, because of (9.4) and (9.7), it is:

$$p_{X,Y}(x, y) = p_X(x) \cdot p_{Y|X}(y|x) = p_{X|Y}(x|y) \cdot p_Y(y) \tag{9.9}$$

that can be rewritten as:

$$p_{X|Y}(x|y) = \frac{p_X(x) \cdot p_{Y|X}(y|x)}{p_Y(y)} \tag{9.10}$$

which is the formulation of Bayes' theorem.

From the mathematical point of view, it is also:

$$p_Y(y) = \int_x p_{X,Y}(x, y)dx = \int_x p_X(x) \cdot p_{Y|X}(y|x)dx \tag{9.11}$$

where $p_Y(y)$ is called the marginal probability distribution.

Thanks to (9.11), it follows that $p_{X|Y}(x|y)$ can be obtained by simply knowing $p_X(x)$ and $p_{Y|X}(y|x)$.

Eq. (9.10) is very important in metrology. Indeed, let us suppose that random variable X represents the measurand and random variable Y represents the measurement result. The obtained distribution of the measured values is $p_{Y|X}(y|x)$, since it is the distribution of the measured values, given the particular measurand's value.

However, the very aim of a measurement process is not that of knowing the distribution of the measured values ($p_{Y|X}(y|x)$), but knowing the distribution of values that can reasonably be attributed to the measurand, given the measured value. In mathematical terms, this means that the aim of a measurement process is that of evaluating $p_{X|Y}(x|y)$.

This can be obtained by applying Bayes' theorem (9.10). In fact, according to [29], Bayes' theorem can be effectively employed to obtained the desired distribution if reliable *a-priori* information ($p_X(x)$) is available about a measurand.

In particular, the following interpretation is given to the quantities in (9.10):

1. $p_X(x)$ is the pdf expressing the *a-priori* information about the measurand;

2. $p_{Y|X}(y|x)$ is the pdf representing the distribution of measured values provided by the measurement process;

3. $p_Y(y)$ is the marginal pdf, given by (9.11);

4. $p_{X|Y}(x|y)$ is the pdf associated to the measurand, which combines the *a-priori* information with the information provided by the distribution of measured values.

The main advantage in the use of Bayes' theorem in metrology is that it yields the pdf associated to the measurand (*posterior*), by combining two different kinds of information: the available information about the measurand itself (*prior*) and the information provided by the measured values.

However, all previous considerations have been derived under a purely mathematical perspective, that does not doubt about the correctness of all considered quantities. In other words, the implicit assumption behind Bayes' theorem is that there is full belief on both the *a-priori* knowledge and the distribution of measured values. This means full knowledge about the possible distribution of the measurand values and zero doubts about the correctness in the evaluation of the uncertainty associated to the measured value.

It can be readily perceived that this is not the situation in practical applications. Even if the measurand variability is known, because, for instance, the production process is known, it may always drift from the normal operating conditions. Similarly, the measurement process may deviate from its expected operating conditions, thus making the evaluated uncertainty incorrect. It is then important to understand the consequences of a lack of total trust on the *a-priori* knowledge or the measured values.

This chapter considers, with both simulations and experimental data, the effect of the application of Bayes' theorem in different possible situations:

1. when one can assign total belief on both the *a-priori* knowledge and the measured values;

2. when no total belief can be assigned to the *a-priori* knowledge $p_X(x)$; this means that a deviation might occur in the process model, or the process model does not represent exactly the manufacturing process;

3. when no total belief can be assigned to the assumed distribution of measured values; this means that the measured values might deviate from the expected distribution due, for instance, to a drift in the employed measurement instrument.

This chapter also considers the risk in taking a wrong decision (false acceptance or false rejection of a product) when the obtained measurement results are employed in conformity assessment [29]. A comparison is made, under different assumption, in the obtained risks values:

- when only the distribution of measured values is taken into account without applying the Bayes' theorem to estimate the measurand value;

- when Bayes' theorem is applied, that is when the *a posteriori* values are considered as the measurement result.

9.5 Simulations

A typical example of conformity assessment is considered to discuss the robustness of Bayes' approach: the resistance of the manufactured resistors is measured to check whether it is inside the tolerance limits or not. The *a-priori* information is represented by the expected dispersion of the resistance values of the manufactured resistors due to variations in the production process.

A nominal value $R_{\mathrm{nv}} = 15\ \Omega$ is assumed for the resistors, and the given production tolerance is $\pm 0.5\%$, that is $\pm 75\ \mathrm{m}\Omega$. The dispersion of values due to the production process is supposed to be represented by a normal probability distribution, where the $\pm 3\sigma$ coverage interval is assumed to be the same as the tolerance interval. Therefore, in the considered example, the *prior* distribution is given by:

$$p_X(x) = \mathcal{N}\left(R_{\mathrm{nv}}, \sigma_{\mathrm{nv}}^2\right) \tag{9.12}$$

where $R_{\mathrm{nv}} = 15\ \Omega$ and $\sigma_{\mathrm{nv}} = 25\ m\Omega$.

It is then assumed that the resistance is measured by a Fluke 8845A, 6.5 digit precision multimeter[1]. According to the manufacturer specifications, the following applies:

- the measured $15\ \Omega$ value falls in the $100\ \Omega$ range;
- in the $100\ \Omega$ range, an accuracy interval

  $$\pm 0.003\%\ \text{of reading} \pm 0.003\%\ \text{of range}$$

  is provided, which corresponds to:

  $$\pm R_{\mathrm{m}} \cdot 3 \cdot 10^{-5} \pm 3 \cdot 10^{-3}\ \Omega$$

  where R_{m} is the resistor measured value.

The distribution of the possible measured values is assumed to be a normal distribution, with mean value equal to the measured value R_{m} and standard deviation given by:

$$\sigma_{\mathrm{m}} = 0.001\%\ \text{of reading} \pm 1\mathrm{m}\Omega = \pm \mathrm{R_m} \cdot 1 \cdot 10^{-5} \pm 1 \cdot 10^{-3}\ \Omega$$

If, for instance, $R_{\mathrm{m}} = R_{\mathrm{nv}}$, then it is $\sigma_{\mathrm{m}} = 1.15\mathrm{m}\Omega$.

10000 values have been considered, in each simulation, for the measured values, and the three following cases have been considered.

9.5.1 Case I: no deviation in the instrument or the process

Case I considers the situation in which neither the instrument nor the process is deviating.

According to the assumptions given above in Sec. 9.5, an *prior* normal pdf with mean value R_{nv} and standard deviation σ_{nv} is associated to each resistor. Then, since the process is not deviating, the "simulated true values" R_{STV} of the 100000 resistors have been simulated by randomly generating 100000 values from this normal pdf.

On the other hand, since the instrument is not deviating, to simulate the measurement of each resistor (R_{m}), a random value is generated from a normal pdf centered on the

[1] The behavior of this instrument was simulated, because this same instrument was used in the experimental validation process.

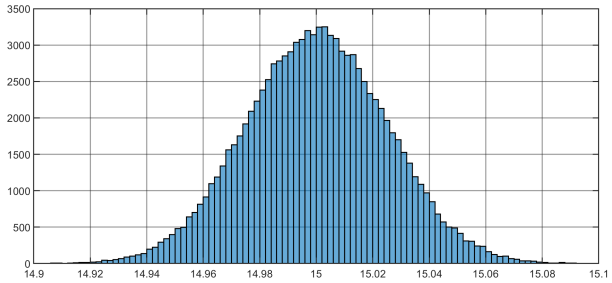

Figure 9.1: *Histogram associated to the obtained* 100000 *a posteriori values, in case I.*

corresponding "simulated true value" R_{STV} and with standard deviation σ_{m}. Hence, a normal pdf centered at R_{m} with the corresponding standard deviation σ_{m} is associated to every measured value.

Bayes' theorem is then applied, according to the measurement data and the *a priori* knowledge.

It is well-known that the mean value of the *posterior* pdf, according to the given measurement data y and the *a priori* knowledge is given by:

$$\mu_{\textit{posterior}} = \frac{\mu_{a\ priori} \cdot \sigma_y^2 + y \cdot \sigma_{a\ priori}^2}{\sigma_y^2 + \sigma_{a\ priori}^2} \tag{9.13}$$

Considering the proposed example, the quantities in (9.13) take the following values:

- $\mu_{a\ priori} = R_{\mathrm{nv}} = 15\ \Omega$;
- $\sigma_{a\ priori} = \sigma_{\mathrm{nv}} = 25\ \mathrm{m}\Omega$;
- $y = R_{\mathrm{m}}$;
- $\sigma_y = \sigma_{\mathrm{m}}$

Fig. 9.1 shows the histogram associated to the 100000 obtained *a posteriori* mean values $\mu_{\textit{posterior}}$, given by (9.13). These values represent the *a posteriori* values associated to the 100000 resistors ($R_{\textit{a posteriori}}$).

It can be readily checked that the obtained histogram approximates quite well a normal pdf, as expected since normal pdfs have been assumed. The mean and standard deviation associated to the 100000 obtained *a posteriori* means are evaluated and the normal pdf, drawn in blue line in Fig. 9.2, is obtained. This pdf is compared with the *a priori* pdf (red line in Fig. 9.2).

It can be seen that the two pdfs are in perfect agreement. This result was expected, since no deviation in the measuring instrument or the process is considered in this case I.

It is also possible to perform a risk analysis, according to $R_{\textit{a posteriori}}$. In fact, for every obtained value, it is possible to verify whether it falls inside the tolerance limit ($R_{\mathrm{nv}} \pm 75\ \mathrm{m}\Omega$) or not. If the value falls inside the limit, the resistor is within the tolerances and should be accepted; on the other hand, if the value falls outside the limit, the resistor is supposed to exceed the tolerances and should be rejected.

Of course, due to measurement uncertainty, the actual resistance value can differ from the measured one. Therefore, if this last value is considered in the comparison

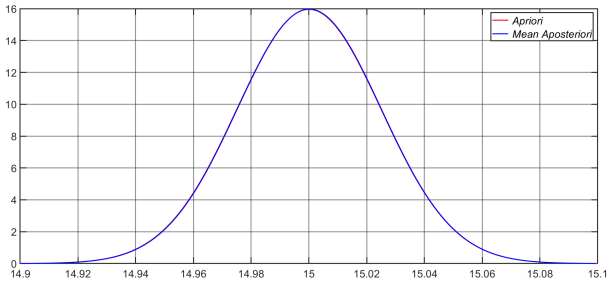

Figure 9.2: *A priori pdf associated to the resistors (red line) and a posteriori pdf (blue line), when case I is considered.*

with the tolerance limits, there is always a risk that a bad resistor is erroneously accepted, or that a good resistor is erroneously rejected. In order to state if a decision is correct or wrong, for every resistor, we also compared the corresponding "simulated true value" R_{STV} with the tolerance limit ($R_{\mathrm{nv}} \pm 75\ \mathrm{m}\Omega$) and verified if the two values ($R_{a\ posteriori}$ and R_{STV}) lead to the same decision. Of course, the correct decision is the one obtained when R_{STV}, which is the *true value* of the resistor, is considered.

The percentage risk of taking a wrong decision is defined as:

$$Risk_{\,\mathrm{total}} = \frac{\text{Total wrong decisions}}{\text{Total decisions}} \cdot 100 \tag{9.14}$$

When only false acceptances are considered, the following risk can be defined, which represents the risk that bad resistors are erroneously accepted:

$$Risk_{\,\mathrm{f.\ a.}} = \frac{\text{Total false acceptances}}{\text{Total decisions}} \cdot 100 \tag{9.15}$$

On the other hand, when only false rejections are considered, the following risk can be defined, which represents the risk that good resistors are erroneously rejected:

$$Risk_{\,\mathrm{f.\ r.}} = \frac{\text{Total false rejections}}{\text{Total decisions}} \cdot 100 \tag{9.16}$$

Of course, it is:

$$Risk_{\,\mathrm{total}} = Risk_{\,\mathrm{f.\ a.}} + Risk_{\,\mathrm{f.\ r.}}$$

Considering the values provided by Eq. (9.13) in this case I, the following percentage risk values have been obtained:

$$Risk_{\,\mathrm{total}} = 0.038\% \quad Risk_{\,\mathrm{f.\ a.}} = 0.02\% \quad Risk_{\,\mathrm{f.\ r.}} = 0.018\%$$

The total risk can be compared with the corresponding total risk value evaluated without applying the Bayes theorem, when the "measured values" R_m are taken into account and compared with the tolerance interval $R_{\mathrm{nv}} \pm 75\mathrm{m}\Omega$:

$$Risk_{\,\mathrm{total}} = 0.038\%$$

The obtained values are perfectly compatible, as expected since no deviation in the instrument or the process is supposed in this case I. Therefore, in this case I in which no deviation is present in the process or the instrument, the application of Bayes' theorem does not modify the results of the risk analysis.

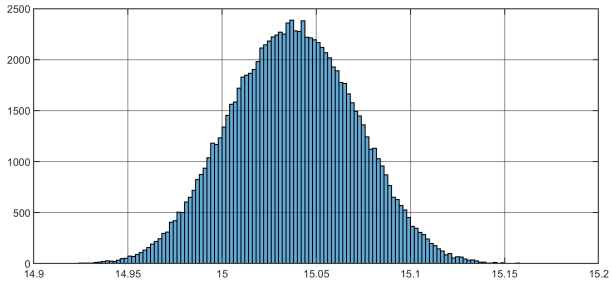

Figure 9.3: *Histogram associated to the obtained* 100000 *a posteriori values, in case II.*

9.5.2 Case II: deviation in the process

Case II considers the situation in which the process is deviating.

In this second case, to consider the process' deviation, the "simulated true values" cannot be extracted by the *a priori* pdf. Therefore, 100000 normal pdfs has been considered with:

- mean value
$$R_{\mathrm{nv}} + (0.75 \cdot k\ \mu\Omega)$$
where $k = 1...100000$;
- standard deviation σ_{nv}

In other words, the same shape and standard deviation of the *a priori* pdf are considered, but the mean value is not centered on the resistors' nominal value R_{nv}, but it is shifted by value $0.75 \cdot k\ \mu\Omega$. The value $0.75\ \mu\Omega$ has been chosen so that, at the end of the 100000 iterations, the process is deviated by exactly $75\ \mathrm{m}\Omega$ which is the tolerance limit (see Sect. 9.5).

Hence, the 100000 "simulated true values" R_{STV} are obtained by randomly extracting one value from each of the above pdfs.

On the other hand, since the instrument is not deviating, to simulate the measured value of each resistor (R_{m}), a random value is generated from a normal pdf centered on the corresponding "simulated true value" R_{STV} and with standard deviation σ_{m}. Hence, a normal pdf centered on R_{m} with the corresponding standard deviation σ_{m} is associated to every measured value.

Bayes' theorem is then applied, according to the measurement data and the *a priori* knowledge, as given by Eq. (9.13). In the application of this formula, with respect to previous case I, the *a priori* knowledge is always the same, but the measurement values R_{m} are different, as explained above. The histogram in Fig. 9.3 is obtained, associated to the obtained resistors' values $R_{\textit{a posteriori}}$.

Also in this case II, the histogram approximates quite well a normal distribution and the pdf in blue line in Fig. 9.4 represents the corresponding pdf. In this same figure, the *a priori* pdf is also reported (red line). It can be seen that the blue line is shifted in the direction in which the process is deviating. Moreover, it has a higher variance than the *a priori*.

As in case I, it is also possible to perform a risk analysis, according to the obtained values $R_{\textit{a posteriori}}$ (that is, when Bayes' theorem is applied) and according to the mea-

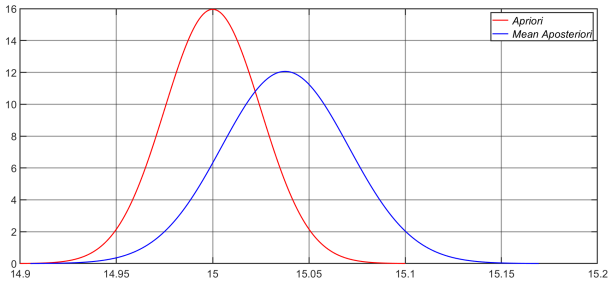

Figure 9.4: *A priori pdf associated to the resistors (red line) and a posteriori pdf (blue line), when case II is considered.*

sured values R_{m} (that is, without applying Bayes' theorem). The following values are obtained, as far as the total risk is concerned:

$$Risk_{\,\mathrm{total}} = 0.64\%$$

when $R_{a\ posteriori}$ is considered;

$$Risk_{\,\mathrm{total}} = 0.59\%$$

when R_{m} is considered.

It can be noted that the risk increases a little bit after the use of Bayes' theorem. Therefore, the application of Bayes' theorem, in this case, increases the risk of wrong decision.

It is worth noting that the amount of risk is strictly dependent on the accuracy of the instrument. The greater the accuracy of the instrument with respect to the *a priori*, the lesser the correction due to Bayes' theorem. Therefore, the lesser the difference in the risks with and without the application of Bayes' theorem. Therefore, with less accurate instruments, the risk of taking wrong decisions after the application of Bayes' theorem could become significant.

This is maybe a trivial conclusion, since very accurate instruments do not require, in principle, corrections. On the other hand, this conclusion must be taken into careful consideration if the correction obtained by the application of Bayes' theorem is used to counterbalance possible drifts in the measurement process. If this is the case, the belief in the stability of the manufacturing process must be higher than that in the stability of the measurement process not to have unpleasant surprises.

9.5.3 Case III: Deviation in the instrument

Case III considers the situation in which the instrument is deviating.

In order to simulate the true values of the resistors, since the process is not deviating, the same considerations as in case I apply. Therefore, 100000 extractions are taken from the *a priori* pdf. These are the "simulated true values" R_{STV}.

On the other hand, the measurements R_{m} must consider that the instrument is deviating. Therefore, 100000 normal pdfs has been considered with:

- mean value

$$R_{\mathrm{STV}} + (0.75 \cdot k\ \mu\Omega)$$

  where $k = 1...100000$;

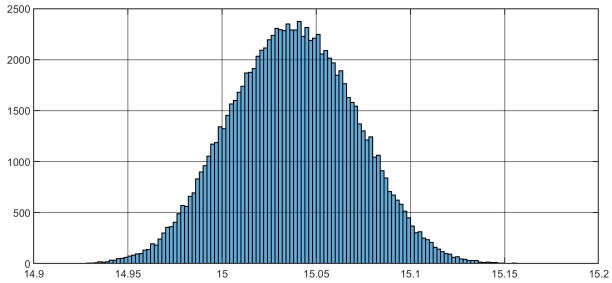

Figure 9.5: *Histogram associated to the obtained* 100000 *a posteriori values, in case III.*

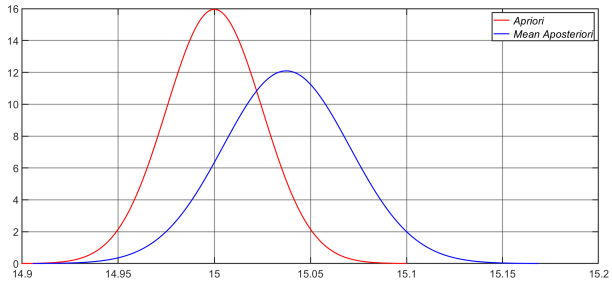

Figure 9.6: *A priori pdf associated to the resistors (red line) and a posteriori pdf (blue line), when case III is considered.*

- standard deviation σ_{m}

In other words, all pdfs have the same shape and standard deviation, but their mean value drifts. The value $0.75\ \mu\Omega$ has been chosen so that, for the last 100000^{th} resistor, the measued value is deviated by exactly $75\ \mathrm{m}\Omega$, which is the resistor tolerance limit (see Sect. 9.5).

Hence, the 100000 measurement results R_{m} are obtained by randomly extracting one value from each of the above pdfs. Then, for every measured value, a normal pdf with mean value R_{m} and standard deviation σ_{m} is assumed.

Bayes' theorem is then applied, according to the measurement data and the *a priori* knowledge, as given by Eq. (9.13). As already stated above, the *a priori* knowledge is always the same, but the measurement values R_{m} are different. The histogram in Fig. 9.5 is obtained, associated to the obtained resistors' values $R_{a\ posteriori}$.

Also in this case III, the histogram approximates quite well a normal distribution and the pdf in blue line in Fig. 9.6 represents the corresponding pdf. In the same figure, the *a priori* pdf is also reported (red line). It can be seen that the blue line is shifted in the direction in which the instrument is deviating. Moreover, it has a higher variance than the *a priori*.

As in the previous cases, a risk analysis has been performed, and the risks of wrong decisions, obtained when the measurements R_{m} and when the *a posteriori* values $R_{a\ posteriori}$ are considered, are compared with each other. In particular:

$$Risk_{\,\mathrm{total}} = 13.14\%$$

when $R_{a\ posteriori}$ are considered;

$$Risk_{\,\mathrm{total}} = 13.26\%$$

when R_{m} are considered.

The difference between the obtained values for the total risk is small, even in this case III. However it can be noted that, in this case, the application of Bayes' theorem yields better results.

Once again, it can be underlined that the risk depends on the accuracy of the instrument. The greater the accuracy of the instrument with respect to the *a priori* information, the lesser the correction due to Bayes's theorem and, consequently, the lesser the difference in the risks with and without the application of Bayes' theorem.

Of course, this makes sense because if the uncertainty associated to the measurement result is very low, it means that the measurement result is trusted much more than the *a priori* information. So, if the instrument deviates, the *a priori* information is still not trusted enough to correct the measurement result. So, in this situation, the more accurate the *a priori* information is with respect to the instrument, the more is the correction applied thereby leading to a better decision after the application of the Bayes' theorem.

It is also interesting to observe that:

$$Risk_{\,\mathrm{total}} = 13.14\% \text{ and } \mathrm{Risk}_{\,\mathrm{f\,r}} = 13.02\%$$

thus meaning that, among all the wrong decisions, most of them correspond to false rejection, because of the wrong measurements due to the instrument's deviation.

9.6 Experimental results

In order to verify whether the simulation results are experimentally confirmed, so that the method based on Bayes' theorem can be applied in practice, 80 resistors have been used with resistance value, given by the manufacturer specifications: $15 \pm 0.15\ \Omega$.

First of all, the values of the resistors have been measured with a reference multimeter: Fluke 8508A with 8.5 digits.

The obtained measurements have been considered the conventionally true values of the resistors. The mean of all conventionally true values has been found to be $14.94\ \Omega$. This value is indeed within the manufacturer tolerance interval but, ideally, it was supposed to be $15\ \Omega$. So, according to the three case studies described above, we are in the case in which "the process is deviating".

Moreover, for the sake of experiment, we also made a different assumption. Since the measured true values of the resistors were all inside the tolerance interval given by the manufacturer, in order to simulate some outliers, we assumed a stricter manufacturer specification: $15 \pm 0.075\ \Omega$. Also under this different assumption, the mean of the true values ($14.94\ \Omega$) falls within the tolerance interval.

Therefore, it is supposed that the *a priori* knowledge is represented by a normal pdf with mean value $15\ \Omega$ and standard deviation $25\ \mathrm{m}\Omega$.

At this point, we measured the resistance values of the 80 resistors with the Fluke 8845 multimeter. The obtained values are the resistors' measured values. Taking into account these measured values and the a priori knowledge, Bayes' theorem has been applied to get the *a posteriori* mean values according to (9.13), where:

- y is the measured value of the specific resistor;

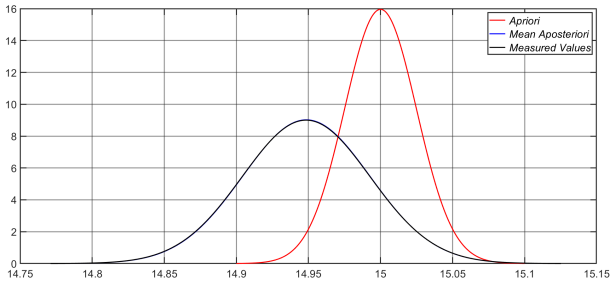

Figure 9.7: *A priori pdf (red line) and a posteriori pdf (blue line) in the first experimental study, where the process is deviating.*

- σ_y is the uncertainty associated to the resistor's measured value and, according to the Fluke 8845 precision multimeter specifications, it is calculated as:

$$\sigma_y = \frac{1}{3} \cdot \frac{0.003 \cdot y + 0.003 \cdot 100}{100} \tag{9.17}$$

  where it is assumed that the total error of the instrument, given by the manufacturer's accuracy specifications, corresponds to the $\pm 3\sigma$ interval;

- $\mu_{a\ priori} = 15\ \Omega$, that is the nominal value given by the manufacturer;

- $\sigma_{a\ priori} = 25\ \mathrm{m}\Omega$, as explained above.

The distribution of the *a posteriori* mean values is shown in Fig. 9.7 in blu line, while the red line shows, for a comparison, the distribution of the *a priori* knowledge.

The obtained *a posteriori* mean values have been stored and compared with the tolerance interval $15\ \pm 0.075\ \Omega$ in order to state weather the resistor is compliant with the specifications or not. This is what happens in the industrial world (in a resistor manufacturing company, in this case), where a decision needs to be made (accept or reject) whether the product is compliant or not with the specifications.

A risk analysis has been also made according to (10.3), by considering, firstly, the measured values and, subsequently, the *a posteriori* values. The following results have been obtained:

$$Risk_{\,\mathrm{total}} = 1.27\%$$

when the *a posteriori* means are considered;

$$Risk_{\,\mathrm{total}} = 0\%$$

when the measured values are considered.

This means that the application of Bayes' theorem worsens the results of the risk analysis, in this case. It is worthwhile to observe that the entire 1.27% risk is entirely due to false acceptances. So, actually, consumer risk has been increased because of the application of Bayes' theorem.

After this first experimental validation, which consider the case of a "deviation in the process", a "deviation in the instrument" has been simulated, by adding an increasing offset to the resistors.

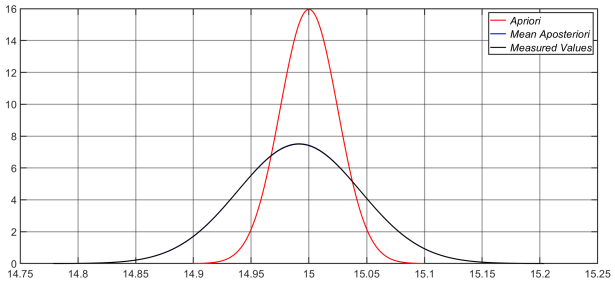

Figure 9.8: *A priori pdf (red line) and a posteriori pdf (blue line) in the second experimental study, where the instrument is deviating.*

In particular, we increased the offset by $5\ \mathrm{m}\Omega$ every 5 resistors starting with an offset of $5\ \mathrm{m}\Omega$ for the first 5 resistors. According to this assumption, a final offset of about $80\ \mathrm{m}\Omega$ is added at the end of the measurement procedure, which is a little above $0.075\ \Omega$, the 3σ interval of the considered *a priori* pdf.

The offset has been added to the resistors' measured values taken with the Fluke 8845A multimeter, as stated above, and the obtained values have been considered as the new measured values. These values have been used in Bayes' formula (9.13) to obtain the new *a posteriori* mean values.

The distribution of the obtained *a posteriori* values is shown in Fig. 9.8 in blue line, while the red line represents the pdf associated to the *a priori* knowledge and the black line represents the actual pdf, according to the resistors' true values.

A risk analysis has been done, according to both the new measured values and the *a posteriori* values. The following results are obtained:

$$Risk_{\,\mathrm{total}} = 26.58\%$$

when the *a posteriori* means are considered;

$$Risk_{\,\mathrm{total}} = 26.58\%$$

when the measured values are considered.

This result (equal total risk) should not be surprising: indeed, in this case, the employed instrument is quite accurate and the variance of the pdf expressing the distribution of the possible measured values is significantly lower than that of the *prior* pdf. Therefore, the correction provided by the application of the Bayes' theorem is negligible and does not go in favor of a risk reduction.

Moreover, if the partial risks $Risk_{\,\mathrm{f.\,a.}}$ and $Risk_{\,\mathrm{f.\,r.}}$ are analyzed, we get:

$$Risk_{\,\mathrm{f.\,a.}} = 22.78\% \ \text{ and } \ \mathrm{Risk}_{\,\mathrm{f.\,r.}} = 3.8\%$$

when the *a posteriori* mean values are considered; and

$$Risk_{\,\mathrm{f.\,a.}} = 22.78\% \ \text{ and } \ \mathrm{Risk}_{\,\mathrm{f.\,r.}} = 3.8\%$$

when the measured values are considered. So, also the partial risks do not differ. It is important to underline that, out of the total 26.58%, 22.78% of the risk is due to false acceptances, while only 3.8% is due to false rejection. This happens because the instrument is deviating in the opposite direction with respect to the process' deviation.

So, the bias caused by the process deviation is compensated by the bias caused by the instrument deviation. Therefore, in this case Bayes' theorem does not improve the measurement result and does not reduce the risk of wrong decision.

9.7 Conclusion

It should be noted that the application of the Bayes' theorem should not be used under the conditions assumed in this chapter. At least, when there is a suspicion of a bias either in the instrument or the process, the results of the Bayes' theorem should not be used.

But, how can we be sure that the information is correct? Usually, in the industry, the measuring instruments are calibrated at regular intervals. The calibration results simply specify the state of the instrument at the instant of calibration. So what is the guarantee that the instrument is behaving entirely correctly till the next calibration? For these reasons, a bias might remain undetected, sometimes even for long durations, thus producing incorrect results and causing problems.

For example, if the equipment used to evaluate the carbon emissions in an automobile deviates in an automobile industry and this is not detected, the entire manufacturing plant needs to be stopped to check the production process or even the design of the automobile itself may need to be re-investigated. These situations cost a lot of money to the company.

Therefore, the aim of the analysis done in this chapter is not to prove that the Bayes' theorem introduces errors in the presence of bias which is expected given that the requirements for the correct application of the Bayes' theorem are not satisfied. Rather, the aim is to show the significance of this error.

So, if somehow a possible deviation could be taken into account, a better result could be obtained. This is the aim of the next chapter.

CHAPTER 10

Conformity analysis in an industry using RFV based Bayes theorem

10.1 Introduction

As expressed in the previous chapter, JCGM 106:2012 document [29], encompassed in the ISO/IEC guide 99-4:2012 [26], is the main document when conformity assessment is considered. This guide provides guidance and procedures for assessing conformity of an item with specified requirements.

When also *a priori* information about the measurand is available, Bayes' theorem can be applied and, in such a case, its application is generally recommended in metrology [29], since it is expected to provide a better result than simply considering the measurement results and the associated uncertainties. In other words, it is expected that, thanks to the application of Bayes' theorem, there is a reduction in the risk of taking wrong decisions ("false acceptances" or "false rejections").

It has been shown in the previous chapter that it is not always the case. There are cases in practical scenarios when there are undetected deviations in the process or measurement such that the probability distribution assigned to them is inaccurate. In those cases, depending on the scenario, blindly applying the Bayes' theorem could even prove detrimental to our original goal of decreasing the risk of wrong decisions.

Especially, in industrial applications, situations occur quite often in which either the production process or the instrument suffer undetected deviations, thus adding an unknown systematic contribution to uncertainty. While the GUM [27] requires that all systematic effects are recognized and compensated for, and several tools, such as control charts, Process Capability Analysis (PCA) and Measurement System Analysis (MSA) can be used to detect systematic effects, they are not always applied in the common industrial practice either because of their cost or the time required to implement

them. Nevertheless, the contribution of such unknown, uncompensated systematic effects shall be taken into account to evaluate measurement uncertainty and use it to model the input variables to Bayes' theorem.

Since a deviation is, by its very nature, a systematic contribution, it can be modeled inside the theory of possibility [9, 18, 51], in terms of Random-Fuzzy Variables (RFVs) [17, 18] and Bayes' theorem can be reformulated inside this new framework.

There are articles available in the literature aimed at reformulating the classical Bayes' theorem using theory of possibility called the generalized Bayes' theorem [10, 37]. In [45], the authors consider the cases of imprecise probabilities in risk assessment and how to treat them using theory of possibility and possibilistic Bayes' theorem. But, the mathematics used is more complex and is, in fact, suitable for applications highly sensitive to risk. In industrial conformity analysis, often, a simple point value is used to make the decision of conformity and a more computationally efficient way is needed to save money and time for the industry. This chapter aims at providing such a solution.

A modified Bayes' theorem, based on the representation of the measurement results and the metrological *a priori* knowledge in terms of RFVs (Chapter 3), is considered in this chapter, with the aim to improve the results obtained by the application of the classical Bayes' theorem in the previous chapter and prove that it is more easily applicable than the ones based on a purely probabilistic approach [5, 21, 25] in an industrial context since, as it will be shown in the following, it requires only algebraic operations.

10.2 RFVs and the proposed modified Bayes' theorem

It has been shown in the chapter 9 that the application of Bayes' theorem could be detrimental as expected when it is applied incorrectly in the presence of deviations. So, if somehow the deviation in the process or the instrument can be taken into consideration while applying the Bayes' theorem, we should be able to get better results.

It is proposed in this chapter to represent both the *a priori* information and the measurement results in terms of RFVs and then apply a similar equation as (9.13), where the afore-mentioned possibilistic mean values and variances of RFVs [4] are considered instead of the probabilistic mean and variance

Just to recap what has already been discussed in chapter 3, an RFV can be defined also in terms of its α-cuts. While an RFV is described by an infinite number of α-cuts, α being a real variable, operatively, it can be represented by a finite discrete number of α-cuts. If N α-cuts α_i, with $i = 1...N$, are considered, mean value and variance of RFV $\mathbf{X}$ are defined as [4]:

$$M(\mathbf{X}) = \frac{1}{N} \cdot \sum_{i=1}^{N} \alpha_i \left(x_2^{\alpha_i} - x_1^{\alpha_i} \right)$$

$$Var(\mathbf{X}) = \frac{1}{2 \cdot N} \cdot \sum_{i=1}^{N} \alpha_i \left(x_2^{\alpha_i} - x_1^{\alpha_i} \right)^2$$

where $\alpha_i = \frac{1}{N-1} \cdot (i-1)$.

Hence the aposteriori mean and variance according to the modified Bayes' theorem are given by:

$$M_{\text{a posteriori}} = \frac{M(\mathbf{Y}_{\text{a priori}}) \cdot Var(\mathbf{Y}_{\text{m}}) + M(\mathbf{Y}_{\text{m}}) \cdot Var(\mathbf{Y}_{\text{a priori}})}{Var(\mathbf{Y}_{\text{a priori}}) + Var(\mathbf{y}_{\text{m}})} \tag{10.1}$$

where $\mathbf{Y}_{\text{apriori}}$ and $\mathbf{Y}_{\text{m}}$ are, respectively, the RFVs corresponding to the *a priori* knowledge and the measurement results, whose shapes are strictly related to the available metrological information.

In section 10.3.1, three case studies will be considered, with different metrological information. According to that, the RFVs in Eq. (10.1) will take different shapes and values.

10.3 Simulated case studies

As a case study, this chapter considers the same example, as has been discussed in chapter 9 in Sect. 9.5, where a typical industrial process where a property of one item is measured, to decide if the item is compliant or not with the specifications, in order to accept or reject it. The only difference from the example in Sect. 9.5 is that the measuring instrument is different in this chapter from that used in chapter 9.

For the sake of completeness, the same data and assumptions considered in Sect. 9.5 has been briefly summarized.

Resistors with nominal value $R_{\text{nv}} = 15\ \Omega$ are considered, with a tolerance of $\pm 0.5\ \%$. We suppose that the tolerance interval corresponds to the $\pm 3\sigma$ coverage interval of a normal probability distribution which represents the dispersion of values due to the production process. Therefore, according to the above assumptions, the tolerance interval is $\pm 75\ \text{m}\Omega$ and the *a priori* distribution is given by:

$$p_X(x) = \mathcal{N}\left(R_{\text{nv}}, \sigma_{\text{nv}}^2\right) \tag{10.2}$$

where $R_{\text{nv}} = 15\ \Omega$ and $\sigma_{\text{nv}} = 25\ m\Omega$.

The resistance values are measured with an Agilent 5.5 Digit $34450A$ Multimeter. According to the manufacturer specifications, the following applies:

- the measured $15\ \Omega$ value falls in the $100\ \Omega$ range;
- in the $100\ \Omega$ range, an accuracy interval

  $$\pm 0.05\ \%\ \text{of reading} \pm 0.008\ \%\ \text{of range}$$

  is provided in the data sheet, which corresponds to:

  $$\pm\left(R_{\text{m}} \cdot 5 \cdot 10^{-4} + 8 \cdot 10^{-3}\right)\ \Omega$$

  where R_{m} is the resistor measured value.

Since the aim of this work is to compare the effectiveness of the modified Bayes' theorem with that of the classical Bayes' theorem, we suppose that the above interval is the $\pm 3\sigma$ coverage interval of a normal probability distribution which now represents the possible measured values of the resistor, so that a closed form solution for the *a posteriori* information can be derived when using the classical Bayes' theorem. We can hence evaluate a standard deviation:

$$\sigma_{\text{m}} = \frac{1}{3}\left(0.05\ \%\ \text{of reading} + 8\right)\ \text{m}\Omega$$

which represents the standard measurement uncertainty associated to the measured resistance. It can be noted that σ_{m} depends on the measured value R_{m}.

Three different possible situations are considered here.

1. **Case I: No deviation in either the instrument or the production process**
   In the first simulated case, we assume total belief on both the *a-priori* knowledge and the measured values. In other words, it is assumed that there are no deviations in neither the process nor the instrument.

2. **Case II: deviation in the production process**
   In the second simulated case, we assume that no total belief can be assigned to the *a priori* knowledge. This means that a deviation might occur in the production, or the production model does not represent exactly the production process.

3. **Case III: deviation in the instrument**
   In the third simulated case, we assume that no total belief can be assigned to the distribution of the measured values. This means that the measured values might deviate from the expected distribution due, for instance, to an undetected drift in the employed measurement instrument. This particular situation might occur, especially in industrial environment, even when accurate instruments are employed if the instrument itself suffers a drift that may result in instrument's operations outside the expected accuracy range and that may remain undetected till the next calibration. This situation is quite critical since, if the measured values are not corrected by the application of Bayes' theorem, the subsequent conformity assessment might be largely incorrect.

Under this respect, to prove that the proposed method works for any systematic contribution inside a pre-defined range of values, different process or instrument constant deviations selected at random are considered.

This chapter also considers the risk in taking a wrong decision (false acceptance or false rejection of a product) in conformity assessment [29]. The considered decision rule is to accept resistors whose values fall in the range $R_{\mathrm{nv}} \pm 75\ \mathrm{m}\Omega$, that is, fall inside the tolerance interval.

The percentage risk of taking a wrong decision is defined as:

$$Risk_{\,\mathrm{T}} = \frac{\text{Total wrong decisions}}{\text{Total decisions}} \cdot 100 \tag{10.3}$$

which is the sum of the risk of false acceptances:

$$Risk_{\,\mathrm{f.\ a.}} = \frac{\text{Total false acceptances}}{\text{Total decisions}} \cdot 100 \tag{10.4}$$

and the risk of false rejections:

$$Risk_{\,\mathrm{f.\ r.}} = \frac{\text{Total false rejections}}{\text{Total decisions}} \cdot 100 \tag{10.5}$$

A comparison of the obtained risk values is made, when evaluated according to three different situations:

- when there is no *a priori* information and hence, measurment data is directly used in conformity assessment;
- when classical Bayes' theorem is applied as shown in Sect. 9.4, and the obtained distribution of the *a posteriori* values is considered in conformity assessment;

- when the modified Bayes' theorem proposed in this chapter is applied, and the obtained possibility distribution of the *a posteriori* values is considered in conformity assessment.

10.3.1 Modified Bayes' theorem simulation results

Case I

In this case, the same considerations as those reported in Sect. 9.5.1 apply, after having represented the *a priori* information and the measurement results in terms of RFVs. In particular, the blue lines in Fig. 10.1 represent the *a priori* RFV $\mathbf{R}_{\mathrm{nv}}$, and its random PD is obtained by applying the probability-possibility transformation, in Sect. 2.3.2, to pdf $\mathcal{N}(R_{\mathrm{nv}}, \sigma^2_{\mathrm{nv}})$. On the other hand, the green lines represent the RFV $\mathbf{R}_{\mathrm{m}}$ of one of the measurements ($\mathbf{R}_m$ = 15.04Ω). Its random PD is obtained by applying the probability-possibility transformation [48] to pdf $\mathcal{N}(R_{\mathrm{m}}, \sigma^2_{\mathrm{m}})$, where R_{m} and σ_{m} are the same simulated values as in Sec. 9.5.1.

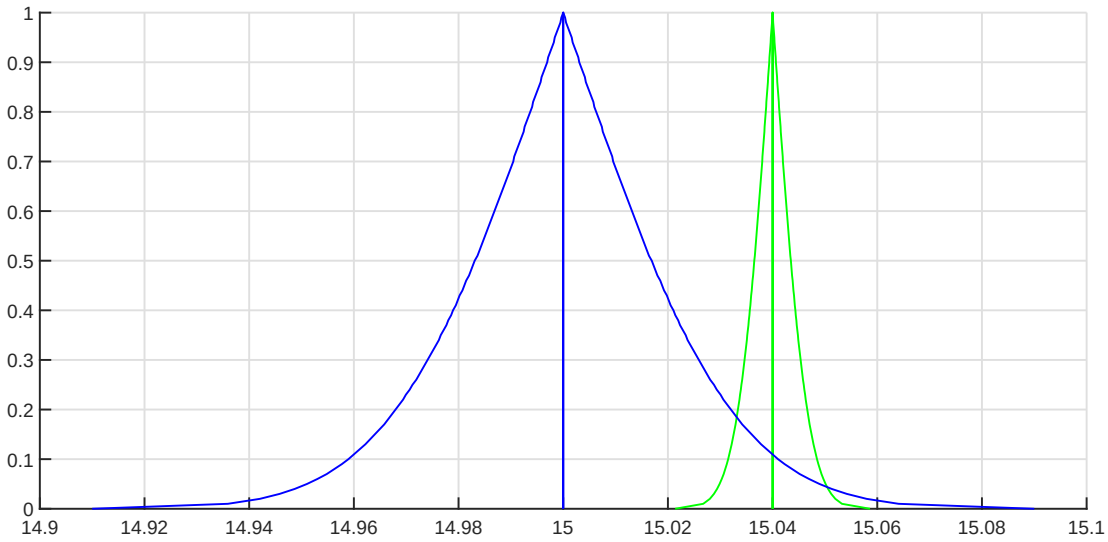

Figure 10.1: *A priori RFV is represented by blue and RFV associated to one measured value represented in green, in case I.*

Eq. (10.1) is applied to all RFVs representing the simulated measured values and the distribution of the possibilistic means of the 1000 *a posteriori* RFVs is represented by the green pdf in Fig. 10.2 (completely overlapped to the blue pdf since the same information as that used in sect. 9.5.1 has been processed here).

Conformity assessment is also considered, by considering the results from (10.1), and the risk's values given in the last row of Table 10.1 are obtained, thus showing the perfect agreement of the modified Bayes' theorem and the classical Bayes' theorem in this case. The results in the first two rows of the table are those in the situation when there is no *a priori* information and hence, measurement data is directly used in conformity assessment and in the situation when the classical Bayes' theorem has been applied to obtain the *a posteriori* value which has then been considered in conformity assessment. These results have been reported for the sake of comparison.

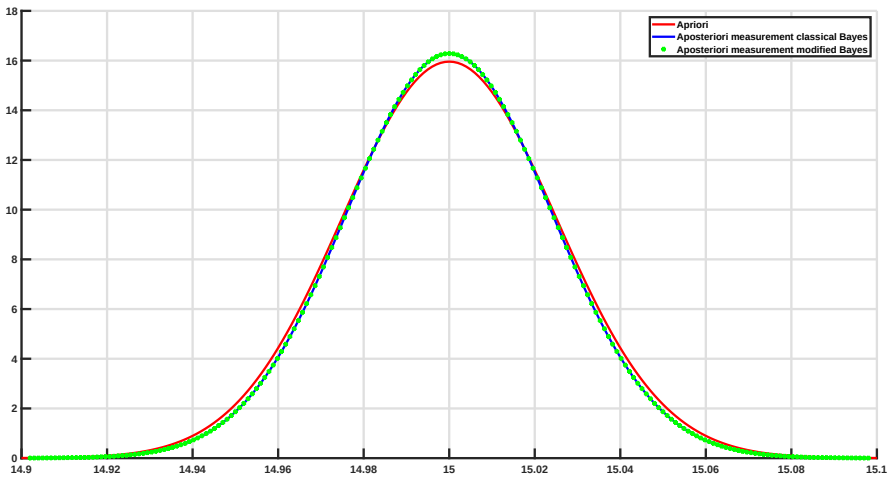

Figure 10.2: *Case I: a priori pdf associated to the resistors (red line); pdf of the a posteriori mean values when the classical Bayes approach is followed (blue line); pdf of the a posteriori mean values when the modified Bayes approach is followed (green line).*

Table 10.1: *Evaluated risks in case I.*

	$\mathbf{Risk}_{\mathrm{T}}$	$\mathbf{Risk}_{\mathrm{f.\,a.}}$	$\mathbf{Risk}_{\mathrm{f.\,r.}}$
No *a priori*	0.5 %	0.1 %	0.4 %
classical Bayes'theorem	0.4 %	0.2 %	0.2 %
modified Bayes'theorem	0.4 %	0.2 %	0.2 %

Case II

In case II, we suppose that the process is deviating, and we simulate the deviation of the process as explained in Sec. 9.5.2 . We can take into account this deviation in the *a priori RFV*, by considering the presence of a systematic contribution. Under this assumption, the *a priori* RFV $\mathbf{R}_{\mathrm{nv}}$ (blue lines) and the RFV $\mathbf{R}_{\mathrm{m}}$ associated to one measured value (green lines, $R_{\mathrm{m}} = 15.04$ in the figure) are the ones shown in Fig. 10.3. The random PDs in both RFVs are built in the same way as in case I, while the internal PD of $\mathbf{R}_{\mathrm{nv}}$ is built by considering a rectangular PD over interval $\pm 3\sigma_{\mathrm{nv}}$.

Eq. (10.1) is applied to all RFVs representing the simulated measured values and the distribution of the obtained $1,000$ $M_{\mathrm{a\ posteriori}}$ values is represented by the green pdf in Fig. 10.4. Conformity assessment is also considered, by considering the results from (10.1), and the risk's values given in the last row of Table 10.2 are obtained. Again, the results in the first two rows of the table are those in the situation when there is no *a priori* information and hence, measurement data is directly used in conformity assessment and in the situation when the classical Bayes' theore has been applied to obtain the *a posteriori* value which has then been considered in conformity assessment. These results have been reported for the sake of comparison.

These values show a small reduction of the total risk, with respect to the other two considered methods (first and second rows in the same Table). In particular, it can be stated that the modified Bayes' theorem provides better results than the classical one and it can be applied also when there is a deviation in the process, without worsening

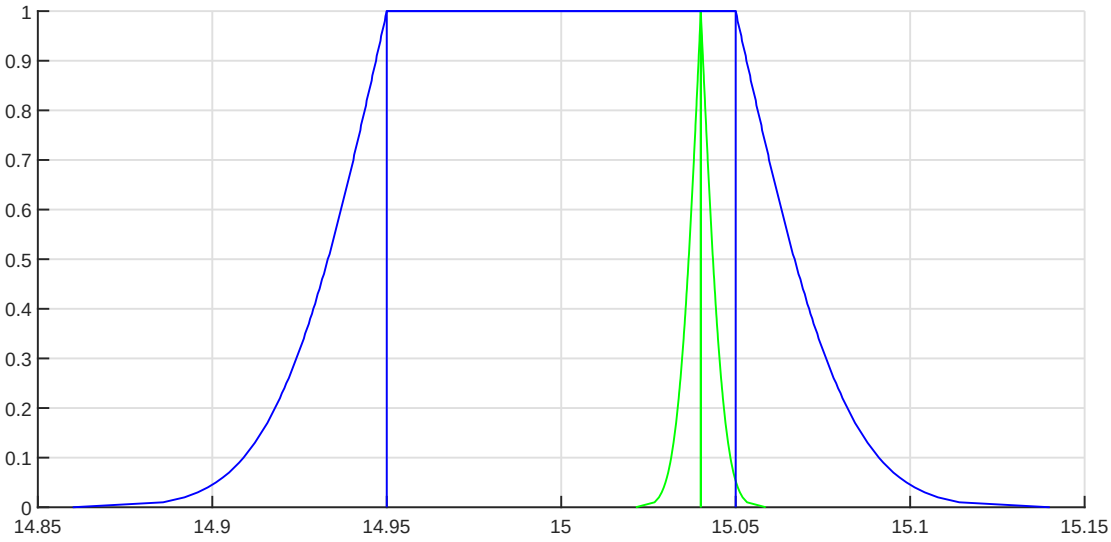

Figure 10.3: *A priori RFV is represented by blue and RFV associated to one measured value represented in green, in case II.*

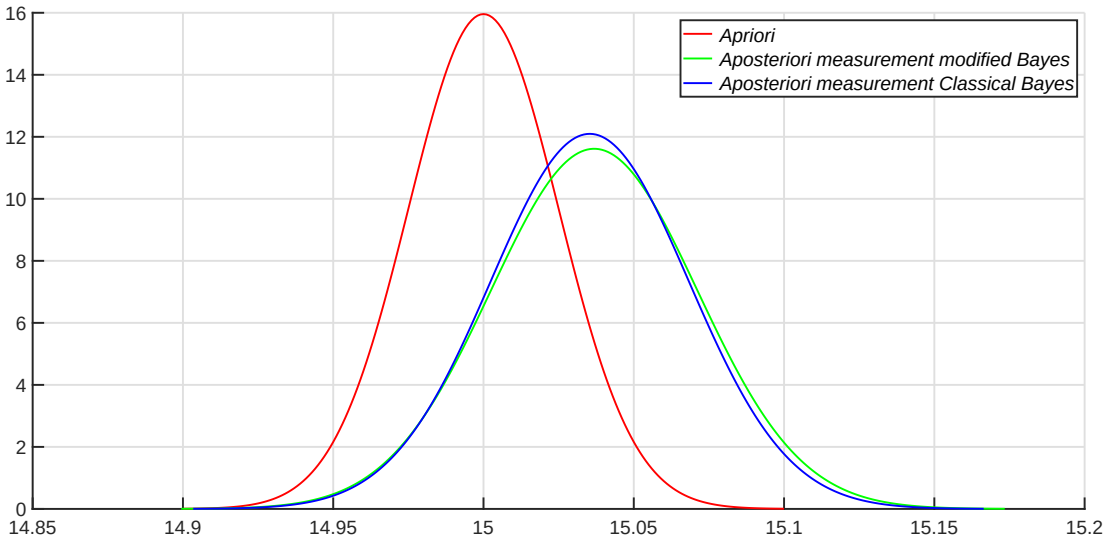

Figure 10.4: *Case II: a priori pdf associated to the resistors (red line); pdf of the a posteriori mean values when the classical Bayes approach is followed (blue line); pdf of the a posteriori mean values when the modified Bayes approach is followed (green line).*

the risk values.

When the process is deviating and the classical Bayes' theorem has been applied, the *a priori* information is being used to "correct" the measurement result. Since the *a priori* information is incorrect, this would result in an incorrect "correction" in the measurement result thereby causing an increase in risk. But, since the instrument has a very low uncertainty compared to that of the *a priori* information, the amount of correction is very low. So, the increase in risk of wrong conformity analysis is very low.

In the modified Bayes' theorem, the uncertainty of the *a priori* information is further

increased because of the internal membership function. So, the "correction" in the measurement result is lower than that in the classical Bayes' theorem. So, the risk of wrong conformity analysis is slightly decreased than that of the classical Bayes' theorem.

Table 10.2: *Evaluated risks in case II.*

	$\mathbf{Risk}_{\mathrm{T}}$	$\mathbf{Risk}_{\mathrm{f.\,a.}}$	$\mathbf{Risk}_{\mathrm{f.\,r.}}$
No *a priori*	2.8 %	1.3 %	1.5 %
classical Bayes'theorem	3.0 %	2.4 %	0.6 %
modified Bayes'theorem	2.8 %	1.3 %	1.5 %

Case III

In case III, we suppose that the instrument is deviating, and may operate outside its accuracy range due to a large undetected systematic deviation that may remain undetected till the next calibration. Under such condition, the measured values become much less reliable than the *a priori* knowledge about the process, and the application of Bayes' theorem is expected to assign full credibility to the *a priori* information, provided that the range of the possible instrument deviation is correctly estimated[1].

Therefore, to take into account also extreme situations, the deviation of the instrument is simulated as explained in Sec. 9.5.3 . We can take into account this deviation in the RFV associated to each measured value, by considering the presence of a systematic contribution. Under this assumption, the *a priori* RFV $\mathbf{R}_{\mathrm{nv}}$ (blue lines) and the RFV $\mathbf{R}_{\mathrm{m}}$ associated to one measured value (green lines, $R_{\mathrm{m}} = 15.04$ in the figure) are the ones shown in Fig. 10.5. The random PDs in both RFVs are built in the same way as in case I, while the internal PD of $\mathbf{R}_{\mathrm{m}}$ is built by considering a rectangular PD over interval $\pm 3\sigma_{\mathrm{nv}}$.

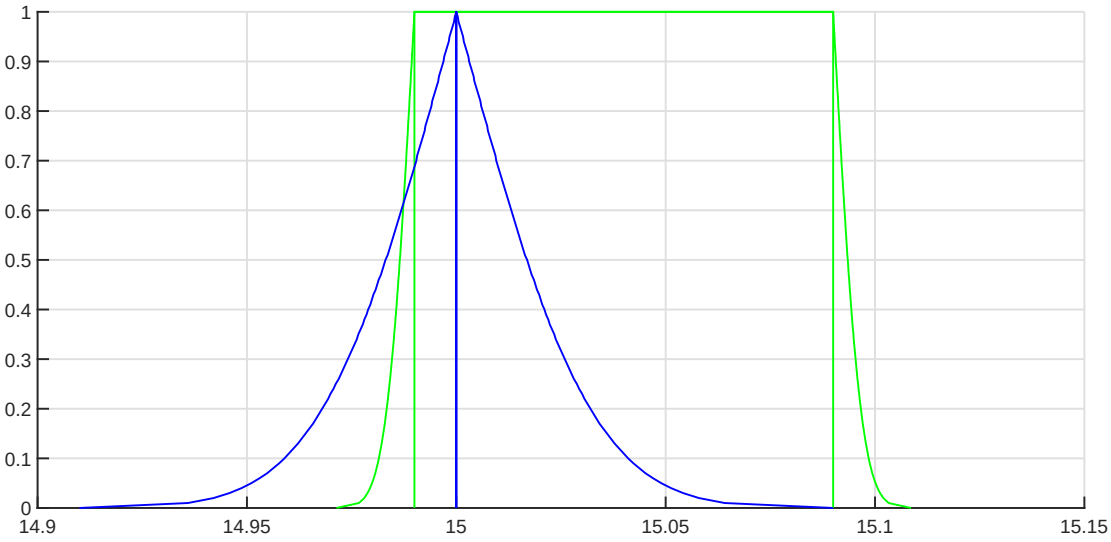

Figure 10.5: *A priori RFV is represented by blue and RFV associated to one measured value represented in green, in case III.*

[1]This can be done by analysing the history of all previous calibration results.

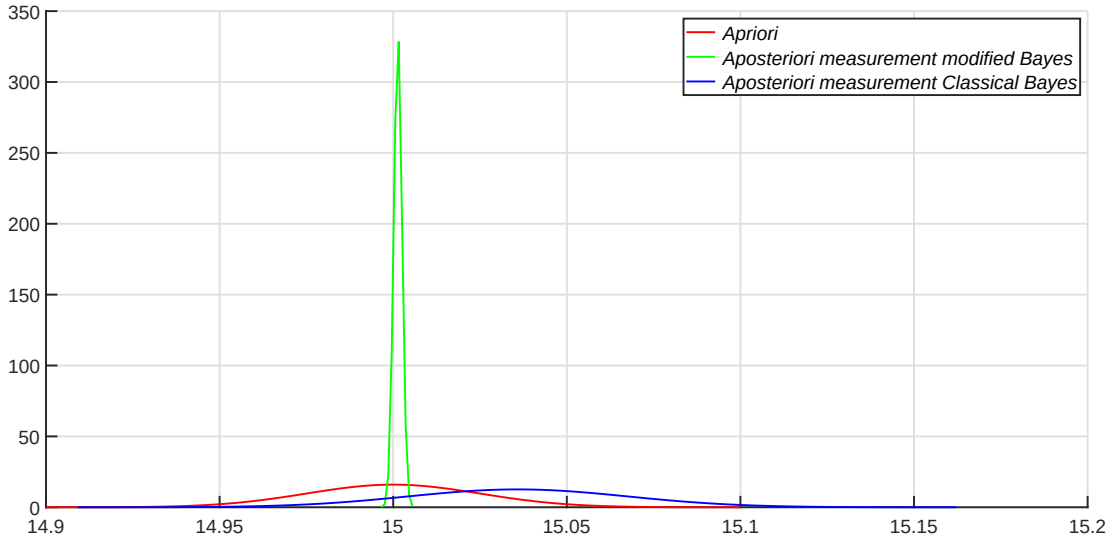

Figure 10.6: *Case III: a priori pdf associated to the resistors (red line); pdf of the a posteriori mean values when the classical Bayes approach is followed (blue line); pdf of the a posteriori mean values when the modified Bayes approach is followed (green line).*

Eq. (10.1) is applied to all RFVs representing the simulated measured values and the distribution of the obtained $M_{\text{a posteriori}}$ values is represented by the green pdf in Fig. 10.6. It can be seen, in this figure, that the distribution of the possibilistic means of the *a posteriori* RFVs is significantly narrower than the distribution of the *a posteriori* mean values obtained from the classical Bayes' theorem. This is due to the fact that the possible instrument's undetected systematic deviation is correctly modeled by the RFV representation and, consequently, a significantly larger correction is applied on the measured values provided by the instrument. This implies that RFVs are providing a better model of the available information compared to a probability distribution function. This does also explain why the false rejection risk is even lower than the one shown in Table 10.1. It is worth noting that, should the instrument operate under these critical conditions, the provided measurement results would be useless without the applied correction and the risk of false rejection would be very high. The application of Bayes' theorem, by considering the available *a priori* information, corrects the measured values so that this risk is reduced. It is also worth noting that this reduction is not due to acceptance of all resistors, but only to the fact that those outside tolerance are correctly identified and discarded. Moreover, the fact that a large deviation is modeled by the RFV representing the measured values does not mean that the measured values are indeed useless, as it might be incorrectly thought, since the same results are obtained when much smaller deviations are considered, as proved by the additional simulation results provided in next Section 10.4.

Conformity assessment is also considered, by considering the results from (10.1), and the risk's values given in the last row of Table 10.3 are obtained. Again, the results in the first two rows of the table are those in the situation when there is no *a priori* information and hence, measurement data is directly used in conformity assessment and in the situation when the classical Bayes' theore has been applied to obtain the *a posteriori* value which has then been considered in conformity assessment. These

results have been reported for the sake of comparison.

The obtained results show a great reduction of the risk values (the total risk is decreased by two orders of magnitude), thus also showing the great advantage in the use of the proposed modified approach.

Table 10.3: *Evaluated risks in case III.*

	$\mathbf{Risk}_{\mathrm{T}}$	$\mathbf{Risk}_{\mathrm{f.\,a.}}$	$\mathbf{Risk}_{\mathrm{f.\,r.}}$
No *a priori*	13.5 %	0.1 %	13.4 %
classical Bayes'theorem	11.4 %	0.1 %	11.3 %
modified Bayes'theorem	0.3 %	0.3 %	0.0 %

10.4 Additional simulations

In order to verify the validity of the proposed approach, many different other simulations have been run.

In the examples considered above (case II and case III), the RFV representing the possible *deviations* (process or instrument) is built by taking an internal PD of width $\pm 3\sigma_{\mathrm{nv}}$.

Other simulations have been run, by considering, in the RFV representing *deviation*, an internal PD of width ranging from $\pm\sigma_{\mathrm{nv}}$ to $\pm 5\sigma_{\mathrm{nv}}$, that is lower and greater than the considered deviation ($3\sigma_{\mathrm{nv}}$). The results obtained under this assumption are shown in Table 10.4, and show that the proposed modified approach works in a satisfactory way even if the deviation is underestimated or overestimated, provided that the possibility that a deviation exist is taken into account. The slight differences in the provided results are due to numerical noise in the simulation..

Table 10.4: *Evaluated risk for different widths of the internal part of the RFV representing the possible deviation of the process or the instrument when the modified Bayes' theorem is applied*

Internal PD width	Production Process Deviating			Instrument Deviating		
	$\mathbf{Risk}_{\mathrm{T}}$	$\mathbf{Risk}_{\mathrm{f.\,a.}}$	$\mathbf{Risk}_{\mathrm{f.\,r.}}$	$\mathbf{Risk}_{\mathrm{T}}$	$\mathbf{Risk}_{\mathrm{f.\,a.}}$	$\mathbf{Risk}_{\mathrm{f.\,r.}}$
$1 \cdot \sigma$	2.7 %	1.4 %	1.3 %	0.3 %	0.3 %	0.0 %
$1.5 \cdot \sigma$	2.8 %	1.4 %	1.4 %	0.3 %	0.3 %	0.0 %
$2 \cdot \sigma$	2.8 %	1.3 %	1.5 %	0.3 %	0.3 %	0.0 %
$2.5 \cdot \sigma$	2.8 %	1.3 %	1.5 %	0.3 %	0.3 %	0.0 %
$3 \cdot \sigma$	2.7 %	1.2 %	1.5 %	0.3 %	0.3 %	0.0 %
$3.5 \cdot \sigma$	2.7 %	1.2 %	1.5 %	0.3 %	0.3 %	0.0 %
$4 \cdot \sigma$	2.8 %	1.3 %	1.5 %	0.3 %	0.3 %	0.0 %
$4.5 \cdot \sigma$	2.7 %	1.2 %	1.5 %	0.3 %	0.3 %	0.0 %
$5 \cdot \sigma$	2.8 %	1.3 %	1.5 %	0.3 %	0.3 %	0.0 %

This shows that, applying the modified Bayes' theorem (based on the possibility distributions) and considering also the systematic contributions in the RFVs of either the production process or the instrument improves the results and reduces the risks' values, even if the amount of the deviation is not exactly known and hence somehow roughly estimated. Even if such a statement may appear as counterintuitive, especially when the deviation is underestimated, it is absolutely plausible, given the fact that the considered deviation is the same as the required tolerance. Therefore, even when a smaller

correction than the actual deviation is considered by the modified Bayes' theorem, it is enough to reduce the risk of wrong decision due to the instrument deviation and reduce it when the production process is deviating.

10.5 Evaluating the possibility of deviation

The main limitation in the industrial application of the classical Bayes' theorem is that, since, if either the process or the instrument deviate with respect to the situation represented by the employed distributions, the *a posteriori* information might be misleading. On the other hand, even if we want to use the modified Bayes' theorem presented in this chapter, to construct the RFVs, it is necessary to know the possibility of deviation in the *a priori* information or the instrument.

In principle, while it is possible to detect deviations in the instrument behavior by calibrating it, though with a possible delay with respect to occurrence time, deviations in the process might be difficult - if not impossible - to detect unless additional information is available.

In the present day where there is Internet of Things (IOT) and Big data, we have access to a huge amount of data from a large number of sources. In an industrial scenario, this means that we have access to data from hundreds or thousands of sensors placed throughout the industry. If any of that data is somehow correlated to the measurand, that would mean that this data could be used to make a correlation between the measurand and the additional data,in other words, more educated guesses about the measurand could be made using this data.

So, theoretically speaking, if we have access to the right sort of data, it is not impossible to verify our measurement results with this additional information so that any possible deviation in either the instrument or the process could be detected. In the age of big data, this sort of data is probably available to the metrologist, since it offers the opportunity to access data, different from those directly related to the process or the measurement results, but, still, correlated to the measurand. By analyzing those data, it is possible to have a clearer idea if either the process, represented by the *a priori* distribution, or the instrument is deviating.

In principle, once evidence is collected about the presence of a possible deviation, but it is not possible to apply a correction, it is possible to adapt the *a priori* information or the measurement result to recount for it.

10.6 Experimental case study

To verify the modified Bayes' theorem based on the RFVs as well as to demonstrate how the use of other measurement data could be used to evaluate the possibility of a deviation as proposed in Sect. 10.5, a simple experiment has been considered: A simple electric circuit is built as shown in Fig. refcircuit, which simulates a power system supplying an industry; the voltage and the current on the load side are being monitored. The voltage needs to be within certain limits and this is the *a priori distribution*.

The voltage source V_S is the grid voltage. The source resistance has been taken to be $2\ \Omega$. The load side resistance is a variable resistor and is varied from $104\ \Omega$ to the maximum value which is $600\ \Omega$. The minimum value $104\ \Omega$ that can be set on the variable resistance is evaluated so as to not exceed the 2 A current rating of the

elements used in the circuit.

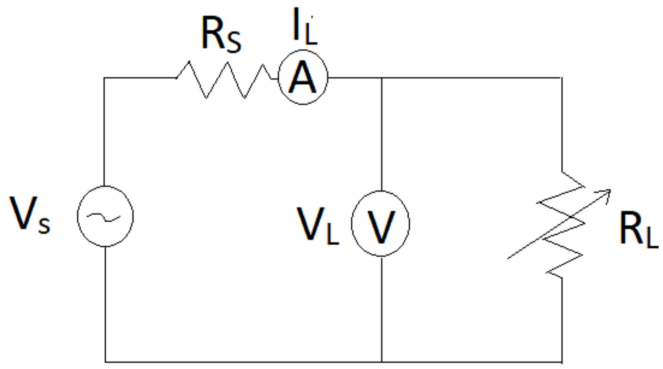

Figure 10.7: *Electrical circuit used for the experiment.*

The $a\ priori$ information about the the supply voltage during normal operation needs to be known to perform the conformity analysis as well as to be used in the classical and modified Bayes' theorems.

To collect information about the possible variability of the supply voltage (V_L) during normal operations, data have been gathered for a few days using the NI 9215 DAQ board without changing any parameter in the circuit so that the source was loaded with a constant current of 1 A and did not contribute to voltage variability. 2000 data have been collected and the distribution attributed to these measured voltage values has been assumed as the *a priori* distribution. The histogram of the collected data is shown in Fig. 10.8 and the same Fig. 10.8 shows that their distribution can be very well approximated by a normal distribution with mean value $V_{ap} = 220$ V and standard deviation $\sigma_v = 1.14$ V. The uncertainty of the experimental setup is negligible compared to this and hence has not been included.

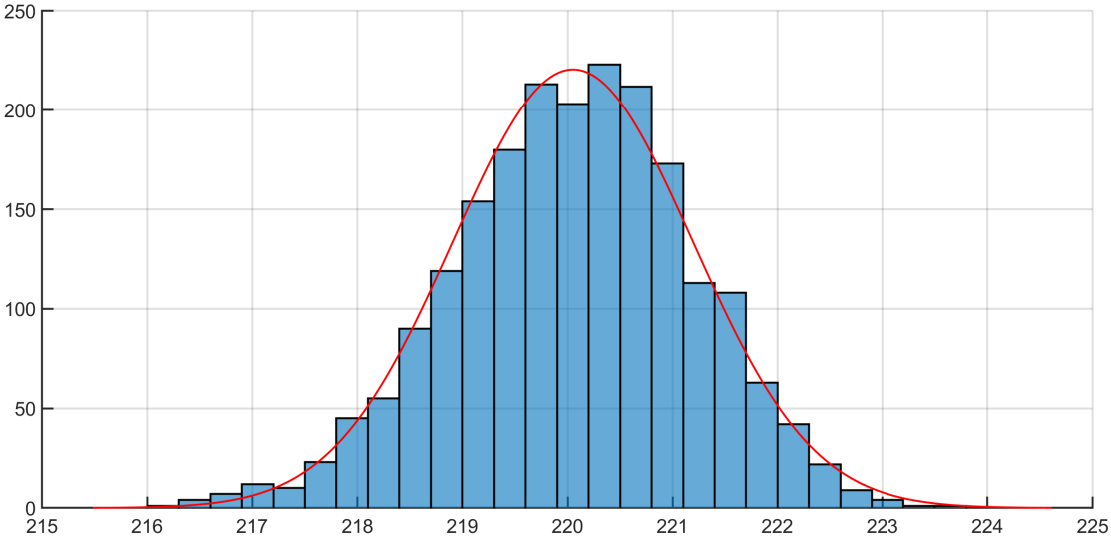

Figure 10.8: *Distribution of the supply voltage values.*

So, the *a priori* distribution is hence given by

$$p_X(x) = \mathcal{N}\left(V_{ap}, \sigma_v^2\right) \tag{10.6}$$

where $V_{ap} = 220$ V and $\sigma_v = 1.14$ V.

This *a priori* distribution can be used to perform the conformity analysis on the measured values of the supply voltage.

Since the current and voltage on the load are correlated, it is possible to perform a regression and obtain a relation between these two quantities. This is used while monitoring the supply voltage on the load side. Hence, when the voltage is measured, it is possible to look at the corresponding current and have an idea if a deviation occurred in either the instrument or the *a priori* distribution of the voltage.

To do this, the current on the load side has been measured by using a $1\ \Omega$ shunt and measuring the voltage across the shunt using an NI 9215 DAQ board.

As already stated, a regression analysis has been performed, keeping the source voltage constant, to obtain a relationship between the load voltage and the load current which could be used to asses whether variations in the measured load voltage should be attributed to variations in the load (process variations) or instrument drifts. The relationship between the voltage and current in this particular case has been found to be as below:

$$V_{est} = 230.08 - 12.36 \cdot I_m \tag{10.7}$$

where V_{est} is the estimated voltage given I_m which is the measured value of the load current. The regression line is shown in Fig. 10.9, together with the acquired data, and it can be readily recognized that the regression equation is not a perfect fit for all measured values. So, the estimated values of voltage obtained from the regression equation may have a high residual error with respect to the actual value and cannot be used to compensate for the deviation but only to assess whether a deviation has likely occurred either in the process or the instrument.

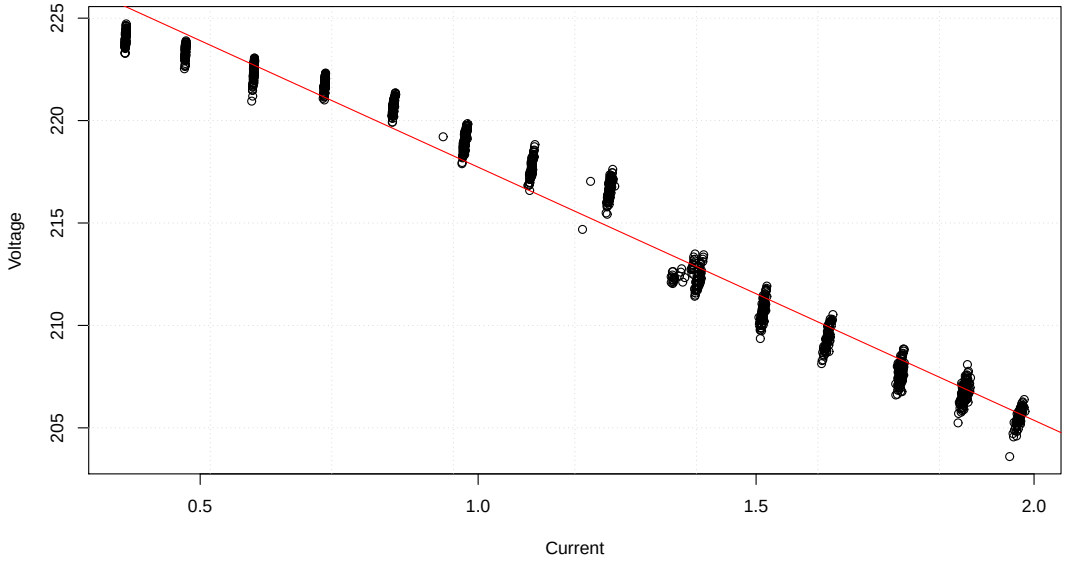

Figure 10.9: *Regression plot.*

Reference values for the supply voltage V_L RMS value are obtained by means of a specifically designed measurement setup, based on a resitive voltage divider, an NI 9215 DAQ board and a developed VI in LabView to evaluate the RMS value from the acquired samples. The standard uncertainty of this setup is estimated to be 6.8 mV. The values measured by this setup were used as "true values" of the supply voltage.

On the other hand, an Agilent 34450A 5.5 digit multimeter has been used to generate the actual measured values of the supply voltage V_L to be used in the conformity analysis.

According to the manufacturer specifications for measurement of AC voltages, the following applies for the 34450A multimeter:

- the measured 220 V and 50 Hz voltage falls in the 750 V and 45 Hz – 10 kHz range;
- in the 750 V range, an accuracy interval

  $$\pm 0.2\ \%\ \text{of reading} \pm 0.1\ \%\ \text{of range}$$

  is provided in the data sheet, which corresponds to:

  $$\pm \left(V_m \cdot 2 \cdot 10^{-3} + 750 \cdot 10^{-3} \right)\ \text{V}$$

  where V_m is the measured voltage value.

To estimate how the measured value distribute inside this accuracy interval, a constant voltage with rms value $V = 220$ V was generated and sent to the multimeter input. 2000 measured values have been collected, and the histogram in Fig. 10.10 has been generated. It can be readily checked that the obtained histogram can be pretty well

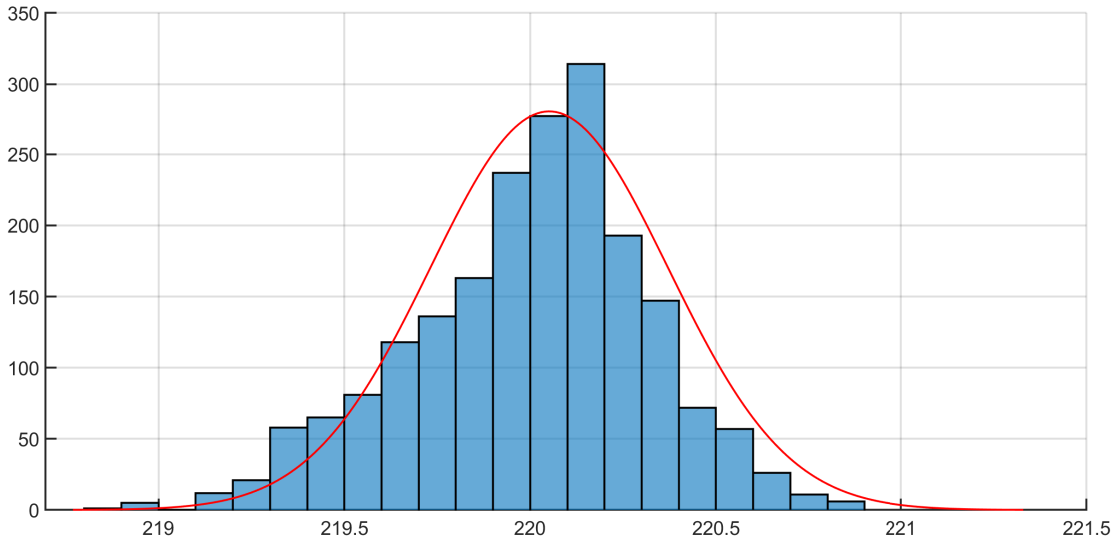

Figure 10.10: *Distribution of the voltage values measured by the multimeter under a constant ac input voltage.*

interpolated by a normal distribution $\mathcal{N}(220, \sigma_m^2)$. Therefore, the pdf corresponding to the measurement can be represented by $\mathcal{N}(V_m, \sigma_m^2)$.

Only the two cases where either the instrument or the process deviates have been considered as it has already been established through simulations that when there is no deviation in either the instrument or the *a priori* distribution, both the classical and the modified Bayes' theorem provide correct results.

10.6.1 Conformity analysis

The considered experimental set-up is aimed at modeling the case of a customer whose contract with the utility grants strict tolerance limits for the admissible variation of the supply voltage at the coupling point.

In the considered example, a tolerance interval of $\pm 3\sigma_v$ limit ($\sigma_v = 1.14$ V) was set for the supply voltage V_L about its rated value of 220 V. Consequently, a conformity analysis on the measured values is performed, to asses whether the voltage supplying the load (V_L) remains inside these limits

To perform the conformity analysis on the voltage measurements using the modified Bayes' theorem, the following steps have been considered:

- **Determine if there is a deviation in the instrument or the supply voltage**
  To estimate whether a deviation occurred in the source (here assimilated to the *process* of the previous examples) or in the instrument, for any measured voltage value, equation (10.7) is used to compute the estimated voltage (V_{est}) corresponding to the measured current value I_m. This value is compared with the corresponding measured voltage value V_m. If the two values are compatible, then it means that the source that is likely deviating. If the values are not compatible, it means that the instrument is likely deviating.

- **Estimate the deviation and construct the appropriate RFV for the process and instrument.**

Supply voltage deviation: When the supply voltage is deviating, we can estimate the contribution of such a deviation to uncertainty in the definition of the *a priori* distribution as the difference between the mean of the *a priori* distribution (V_{ap}) and the estimated voltage (V_{est}) using equation (10.7). This deviation is considered as the width of a uniform PD centered at V_{ap}, which represents the internal membership function of the RFV corresponding to the *a priori* distribution.

Instrument deviation: When the instrument deviates, it is possible to estimate the contribution of such a deviation to uncertainty in the measured voltage as the difference between the estimated voltage (V_{est}) using equation (10.7) and the measured value (V_m). This deviation is again considered as the width of the uniform PD, centered at V_m, which represents the internal membership function of the RFV used to represent the measurement.

- **Apply the modified Bayes' theorem as explained in section 10.2**.

10.6.2 Case I: Deviation in the Supply voltage

To simulate a deviation in the *a priori* distribution, the value of the variable resistor R_L has been varied from the maximum value to the minimum. This changes the value of the current and since the source side resistance is constant, the voltage drop on the source side changes which results in a change in the load side voltage.

The voltage measurements obtained using the NI 9215 DAQ are considered to be the true values and the decision made using these data is considered as the correct decision. Then, the decisions are again evaluated using the measurements obtained from Agilent 34450A multimeter in three scenarios:

- Without applying Bayes' theorem, that is directly using the measurements to make a conformity decision.
- Using the classical Bayes' theorem as explained in section 9.4 on the measurement data and using the *a posteriori* value to make a decision.
- Using the modified Bayes' theorem as explained in section 10.2 on the measurement data and using the *a posteriori* value to make a decision.

To use the modified Bayes' theorem, the RFVs representing the *a priori* distribution and the measurement are built as follows:

- *a priori:* The internal membership function representing the systematic contributions to uncertainty is evaluated as explained in section 10.6.1 and the PD representing the random contributions to uncertainty is obtained by making a probability-possibility transformation of $\mathcal{N}(V_{ap}, \sigma_{\mathrm{v}}^2)$. The RFV is then obtained as explained in section 10.2.
- *Measurement:* Since the deviation is only present in the source, the RFV representing the measurement result consists of only the random contribution to uncertainty. This is obtained by making a probability-possibility transformation of $\mathcal{N}(V_m, \sigma_m^2)$.

The RFVs for the *a priori* and the measurement can be seen in Fig. 10.11

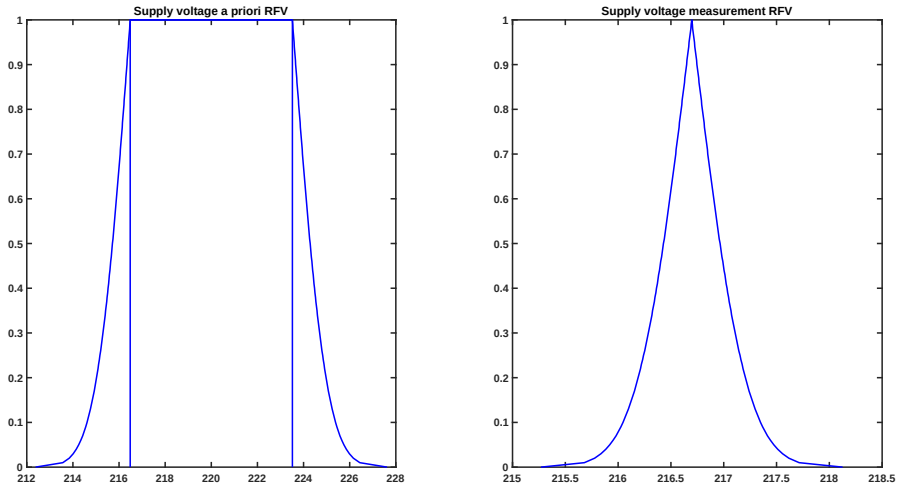

Figure 10.11: *RFVs for the a priori and the measurement of the supply voltage.*

Risk analysis has been performed just as in section 10.3 and the results are given in Table 10.5.

Table 10.5: *Evaluated risks when the process deviates.*

	$\mathbf{Risk}_{\mathrm{T}}$	$\mathbf{Risk}_{\mathrm{f.\,a.}}$	$\mathbf{Risk}_{\mathrm{f.\,r.}}$
No *a priori*	4.3 %	2.5 %	1.8 %
classical Bayes'theorem	6.6 %	6.2 %	0.4 %
modified Bayes'theorem	4.2 %	2.5 %	1.7 %

It can be clearly seen that the classical Bayes' theorem actually provides worse results whereas the modified Bayes' theorem provides slightly better results compared to the case where the measurement results are directly used to make a decision.

10.6.3 Case II: Deviation in the instrument

To simulate a deviation in the instrument, the current has been kept constant at 1 A and voltage has been measured using the Agilent 34450A, but some error has been added to the actual measured values. The error has been increased in each step such that the deviation in the final measurement would be exactly $3.5V$, which is equal to $3\sigma_v$.

Just like the previous case, the voltage measurements obtained using the NI 9215 DAQ are considered to be the true values and the decision made using these data is considered as the correct decision. Then, the decisions are again evaluated using the measurements obtained from Agilent 34450A multimeter in the three scenarios:

- Without applying Bayes' theorem, that is directly using the measurements to make a conformity decision.
- Using the classical Bayes' theorem as explained in section 9.4 on the measurement data and using the *a posteriori* value to make a decision.
- Using the modified Bayes' theorem as explained in section 10.2 on the measurement data and using the *a posteriori* value to make a decision.

To use the modified Bayes' theorem, the RFVs representing the *a priori* distribution and the measurement result are constructed as follows:

- *a priori:* Since the deviation is only present in the instrument, the RFV representing the *a priori* information consists of only the random contribution to uncertainty. This is obtained by making a probability-possibility transformation of $\mathcal{N}(V_{ap}, \sigma_v^2)$.
- *Measurement:* The internal membership function representing the systematic contributions to uncertainty is evaluated as explained in section 10.6.1 and the PD representing the random contributions to uncertainty is obtained by making a probability-possibility transformation of $\mathcal{N}(V_m, \sigma_{\mathrm{m}}^2)$. The RFV is then obtained by combining the two contributions as explained in section 10.2.

The RFVs for the *a priori* and the measurement can be seen in Fig. 10.12

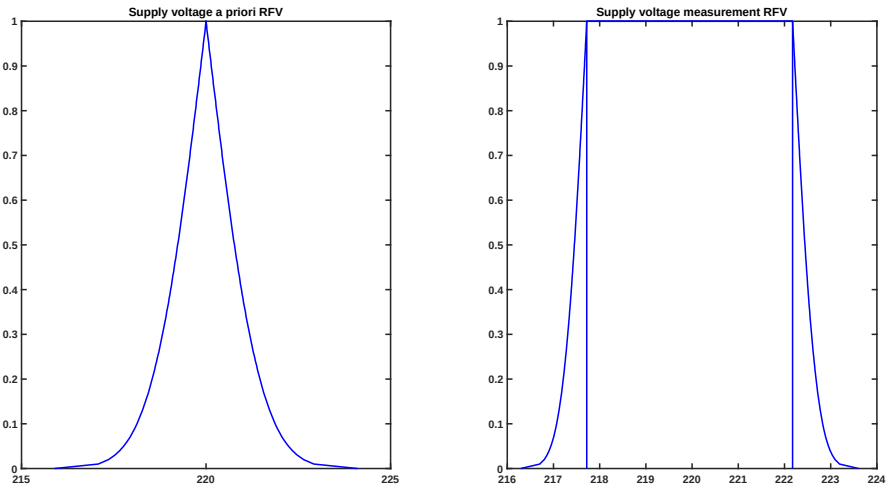

Figure 10.12: *RFVs for the a priori and the measurement of the supply voltage.*

Risk analysis has been performed just as in section 10.3 and the results are given in Table 10.6.

Table 10.6: *Evaluated risks when the instrument deviates.*

	$\mathbf{Risk}_{\mathrm{T}}$	$\mathbf{Risk}_{\mathrm{f.\,a.}}$	$\mathbf{Risk}_{\mathrm{f.\,r.}}$
No *a priori*	10.4 %	0.1 %	10.3 %
classical Bayes'theorem	5.5 %	0.0 %	5.5 %
modified Bayes'theorem	0.1 %	0.1 %	0.0 %

In this case, it can be seen that the results provided by the classical Bayes' theorem decrease the risk compared to the first case where the measurement results are directly used to make the decision. On the other hand, the modified Bayes' theorem still significantly decreases the risk compared to both the other cases.

CHAPTER 11

Conclusion and future research

11.1 Conclusion

In this work, it has been successfully demonstrated that the use of RFVs provides significant advantages in the areas of Kalman filtering and conformity analysis with respect to the corresponding algorithms based on the theory of probability, when there are systematic contributions to uncertainty.

There have been KF algorithms proposed in the literature, which make use of the theory of possibility to deal with systematic contributions to uncertainty. But these KF algorithms consider uncertainty in a fuzzy way. So, they are not compatible with the guidelines presented in the GUM. So, the uncertainty associated to the state predictions provided by these KFs are also not compatible with the GUM. RFVs, on the other hand, represent also the systematic contributions to uncertainty in a GUM-compatible way. Hence, an RFV based KF is more suitable when propagating systematic contributions to uncertainty.

Since a KF algorithm based on RFVs which can provide reliable state estimates while estimating uncertainty accurately has still been missing in the literature, a possibilistic RFV based KF algorithm was proposed in this thesis. The advantages of this possibilistic KF are accurate state and uncertainty limits estimates, with a high percentage of the predicted state estimates inside the evaluated uncertainty limits.

The applications of possibilistic KFs have been mainly in the areas of navigation systems and control systems. But, in time synchronization networks like PTP or NTP networks, there have been applications of only the probabilistic KF algorithms mainly to filter the random noise in the time offset calculations in the slave clock to provide a more accurate time synchronization. Possibilistic KFs have never been used in this area. In this thesis, the developed possibilistic KF algorithm has been used in a PTP network to not only propagate the systematic contributions to uncertainty in the network but also

to define a defense strategy to improve the security of the network against malicious attacks which has never been done before. It has been shown how the slave provides a reliable time even under attack when the proposed strategy is used.

There have never been any possibilistic KFs that try to reduce the systematic contributions to uncertainty. The proposed possibilistic KF has been developed further to provide a partial reduction in the systematic contribution to uncertainty thereby also reducing the overall uncertainty and it has been successfully applied in simulations as well as in a drone to estimate the distance traveled by the drone. It has been shown that the error in the estimated distance by the drone is significantly reduced by applying the proposed algorithm.

The proposed possibilistic KF algorithm could be used in the navigation systems in vehicles or robots and in control systems where there is a possibility of systematic error.

Another area of research covered by this thesis is related to metrology. There have been research articles that demonstrated the advantages of using RFVs to represent the measurement results when there are systematic contributions to uncertainty. However, up to now, RFVs have never been exploited in conformity analysis.

In this thesis, an RFV based conformity analysis has been presented along with a strategy to use other available information to make decisions which significantly improved the results decreasing the risk of wrong decisions especially when the measuring instrument deviates thereby having a systematic error in the measurement. The use of this method could provide significant advantages in industries, since this would decrease the risk for industries to stop their manufacturing processes because of the instrument deviation, thus saving a lot of time and effort.

11.2 Future Research

This thesis represents only a step in the application of the possibility theory and RFVs in metrology. Several interesting and important points in metrology would largely benefit of an RFV approach, such as the representation of bimodal or multimodal distributions in possibility and the deconvolution of probability distributions, but are still largely unsolved.

In particular, the second problem is very interesting in metrology and the mathematical tools proposed in this thesis might help finding a solution. If there is a large number of experimental data, if there is a way to perform the deconvolution of two distributions accurately, it would be possible to define a more accurate *a priori* information for a process removing the uncertainty of the measuring instrument.

This is especially useful when calibration is performed for instruments with an accuracy that is comparable with that of the calibration process itself. In this case, the uncertainty in calibration can not be neglected. So, if a deconvolution could be made, it would be possible to define a more accurate *a priori* for the instrument.

Currently, the problem is that the mathematics using probability is very easy to develop when the two pdfs are both normal distributions. When this is not the case, the mathematics would become much more computationally intensive. So, the use of PDs and RFVs could once again prove useful here.

JCGM guide 106 specifies the instructions and methodology to perform conformity

analysis. In particular, it discusses the calculations of the probabilities of conformity, acceptance intervals, consumer and producer risks etc. The entire document is based on the theory of probability. It would make an interesting study to see how the theory of possibility and RFVs could be used instead to redefine the methods to perform conformity analysis. This is also intended for the future.

As it has been demonstrated in chapters 6 and 7, the use of the possibilistic KF would make it possible to defend against malicious attacks in PTP networks. This is useful in various applications such as phasor measurement units (PMUs), intelligent circuit breakers in power systems etc. There are International standards defined for the communication and time synchronization in such devices in power systems.

IEC61850 is the standard that specifies the requirements and methods for communication between intelligent devices in a power system. In particular, IEC/IEEE 61850-9-3:2016 specifies the precision time protocol profile that is to be used in such devices.

There have been various research articles in the literature that investigate the effect of malicious attacks on PMUs and circuit breakers in power systems. But, none of them proposes a defense strategy against such attacks. So, the application of the proposed defense strategy would be quite useful. So this is also intended for the future.

Another interesting application would be in speedometers and odometers of vehicles. The regulations for speedometers in vehicles state that the speedometer in the car is supposed to be designed in such a way that it never shows a value that is lower than the actual speed of the vehicle and it is allowed to show a value up to 10% more than the actual speed of the vehicle.

This means that the speedometer of the car is allowed to have any systematic error in its reading between 0% and 10%. So, this means that it is safe to assume that there is a positive systematic error somewhere between 0% and 10%.

Therefore, the algorithm used in chapter 8 would be quite useful here. So, this is another case that could be investigated in the future.

Furthermore, further research can be also planned in devising control strategies for navigation of drones and robots using the possibilistic Kalman filter

Bibliography

[1] https://www.gps.gov/systems/gps/performance/accuracy/.

[2] C. Alsina, M. J. Frank, and B. Schweizer. *Associative Functions: Triangular Norms and Copulas*. World Scientific, 2006.

[3] Claudi Alsina, Berthold Schweizer, and Maurice J Frank. *Associative functions: triangular norms and copulas*. World Scientific Publishing Company, 2006.

[4] C. Carlsson and R. Fullér. On possibilistic mean value and variance of fuzzy numbers. *Fuzzy sets and systems*, 122(2):315–326, September 2001.

[5] Richard T Cox. Probability, frequency and reasonable expectation. *American journal of physics*, 14(1):1–13, 1946.

[6] A. P. Dempster. Upper and lower probabilities induced by a multivalued mapping. *Ann. Math. Statist.*, 38(2):325–339, 1967.

[7] J. Dombi. Towards a general class of operators for fuzzy systems. *IEEE Trans. Fuzzy Syst.*, 16(2):477–484, 2008.

[8] D. Dubois, L. Foulloy, G. Mauris, and H. Prade. Probability-possibility transformations, triangular fuzzy sets, and probabilistic inequalities. *Reliable Computing. Kluwer Academic Publishers*, 10:273–297, 2004.

[9] D. Dubois and H. Prade. Bayesian conditioning in possibility theory. *Fuzzy Sets and Systems*, 92(2):223–240, 1997.

[10] Didier Dubois and Henri Prade. Bayesian conditioning in possibility theory. *Fuzzy Sets and Systems*, 92(2):223–240, 1997. Fuzzy Measures and Integrals.

[11] R. Faragher. Understanding the basis of the kalman filter via a simple and intuitive derivation. *IEEE Signal Processing Magazine*, 29(5):128–132, September 2012.

[12] P. Ferrari, G. Giorgi, C. Narduzzi, S. Rinaldi, and M. Rizzi. Timestamp validation strategy for wireless sensor networks based on ieee 802.15.4 css. *IEEE Transaction on Instrumentation and Measurements*, 63(11):2512–2521, June 2014.

[13] A. Ferrero, R. Ferrero, S. Salicone, and W. Jiang. The kalman filter uncertainty concept in the possibility domain. *IEEE Trans. Instrum. Meas.*, pages 1–13, 2019.

[14] A. Ferrero, M. Prioli, and S. Salicone. Joint random-fuzzy variables: A tool for propagating uncertainty through nonlinear measurement functions. *IEEE Trans. Instrum. Meas.*, 65(5):1015–1021, May 2016.

[15] A. Ferrero, M. Prioli, S. Salicone, and B. Vantaggi. 2D probability-possibility transformations. In *SMPS 2012*, Konstanz, Germany, October 4 - 6, 2012.

[16] A. Ferrero, M. Prioli, S. Salicone, and B. Vantaggi. A 2-D metrology-sound probability-possibility transformation. *IEEE Trans. Instrum. Meas.*, pages 1–9, 2013.

[17] A. Ferrero and S. Salicone. The random-fuzzy variables: a new approach for the expression of uncertainty in measurement. *IEEE Trans. Instrum. Meas.*, 53(5):1370–1377, 2004.

[18] A. Ferrero and S. Salicone. Uncertainty: Only one mathematical approach to its evaluation and expression? *IEEE Trans. Instrum. Meas.*, 61(8):2167–2178, 2012.

[19] A. Ferrero and S. Salicone. A comparison between the probabilistic and possibilistic approaches: The importance of a correct metrological information. *IEEE Trans. Instrum. Meas.*, 67(3):607–620, March 2018.

[20] Alessandro Ferrero, Harsha Vardhana Jetti, and Simona Salicone. The possibilistic kalman filter: Definition and comparison with the available methods. *IEEE Transactions on Instrumentation and Measurement*, 70:1–11, 2020.

[21] Andrew Gelman, John B Carlin, Hal S Stern, David B Dunson, Aki Vehtari, and Donald B Rubin. *Bayesian data analysis*. CRC press, 2013.

[22] G. Giorgi. An event-based kalman filter for clock synchronization. *IEEE Transaction on Instrumentation and Measurements*, 64(2):449–457, August 2014.

[23] G. Giorgi and C. Narduzzi. Performance analysis of kalman-filter based clock synchronization in ieee 1588 networks. *IEEE Transaction on Instrumentation and Measurements*, 60(8):2902–2909, June 2011.

[24] G. Giorgi and C. Narduzzi. Precision packet-based frequency transfer based on oversampling. *IEEE Transaction on Instrumentation and Measurements*, 66(7):1856–1863, March 2017.

[25] Michael Goldstein and David Wooff. *Bayes linear statistics: Theory and methods*, volume 716. John Wiley & Sons, 2007.

[26] ISO/TMBG Technical Management Board - groups. *ISO/IEC GUIDE 98-4:2012. Uncertainty of measurement â Part 4: Role of measurement uncertainty in conformity assessment*, 2012.

[27] JCGM 100:2008. *Evaluation of Measurement Data – Guide to the Expression of Uncertainty in Measurement, (GUM 1995 with minor corrections)*. Joint Committee for Guides in Metrology, 2008.

[28] JCGM 101:2008. *Evaluation of measurement data – Supplement 1 to the Guide to the expression of uncertainty in measurement – Propagation of distributions using a Monte Carlo method*. Joint Committee for Guides in Metrology, 2008.

[29] JCGM 106:2012. *Evaluation of measurement data – The role of measurement uncertainty in conformity assesment*. Joint Committee for Guides in Metrology, 2012.

[30] JCGM 200:2012. *International Vocabulary of Metrology – Basic and General Concepts and Associated Terms (VIM 2008 with minor corrections)*. Joint Committee for Guides in Metrology, 2012.

[31] A. Kaufmann and M. M. Gupta. *Introduction to fuzzy arithmetic: theory and applications*. Van Nostrand Reinhold Co., New York, NY, USA, 1985.

[32] E. P. Klement, R. Mesiar, and E. Pap. *Triangular Norms*. Kluwer, Dordrecht, Netherlands, 2000.

[33] Erich Peter Klement, Radko Mesiar, and Endre Pap. Triangular norms. position paper I: basic analytical and algebraic properties. *Fuzzy Sets and Systems*, 143(1):5 – 26, 2004.

[34] Erich Peter Klement, Radko Mesiar, and Endre Pap. Triangular norms. position paper II: general constructions and parameterized families. *Fuzzy Sets and Systems*, 145(3):411 – 438, 2004.

[35] G. J. Klir and B. Yuan. *Fuzzy sets and fuzzy logic. Theory and applications*. Prentice Hall PTR, Englewood Cliffs, NJ, USA, 1995.

[36] George J. Klir and James F. Geer. Information-preserving probability-possibility transformations:. In R. Lowen and M. Roubens, editors, *Fuzzy Logic*, volume 12 of *Theory and Decision Library*, pages 417–428. Springer Netherlands, 1993.

[37] StÃ©phane Lapointe and Bernard BobÃ©e. Revision of possibility distributions: A bayesian inference pattern. *Fuzzy Sets and Systems*, 116(2):119–140, 2000.

[38] S. Lee. An enhanced ieee 1588 time synchronization algorithm for asymmetric communication link using block burst transmission. *IEEE Communications Letters*, 12(9):687–689, Sep. 2008.

[39] M. LÃ©vesque and D. Tipper. Improving the ptp synchronization accuracy under asymmetric delay conditions. In *2015 IEEE International Symposium on Precision Clock Synchronization for Measurement, Control, and Communication (ISPCS)*, pages 88–93, Oct 2015.

[40] F. Matìa, A. Jiménez, B. M. Al-Hadithi, D. Rodrìguez-Losada, and R. Galán. The fuzzy kalman filter: State estimation using possibilistic techniques. *Fuzzy Sets and Systems*, 157(16):2145 – 2170, 2006.

[41] T. Murakami and Y. Horiuchi. Improvement of synchronization accuracy in ieee 1588 using a queuing estimation method. In *2009 International Symposium on Precision Clock Synchronization for Measurement, Control and Communication*, pages 1–5, Oct 2009.

[42] B. Noack, V. Klumpp, and U. D. Hanebeck. State estimation with sets of densities considering stochastic and systematic errors. In 12^{th} *International Conference on Information Fusion*, Seattle, WA, USA, July 6-9, 2009.

[43] Roman Y Novoselov, Shawn M Herman, Sabino M Gadaleta, and Aubrey B Poore. Mitigating the effects of residual biases with schmidt-kalman filtering. In *2005 7th International Conference on Information Fusion*, volume 1, pages 8–pp. IEEE, 2005.

[44] M. Oussalah and J. De Schutter. Possibilistic kalman filtering for radar 2d tracking. *Information Sciences*, 130(1):85 – 107, 2000.

[45] Nicola Pedroni, Enrico Zio, Alberto Pasanisi, and Mathieu Couplet. A critical discussion and practical recommendations on some issues relevant to the nonprobabilistic treatment of uncertainty in engineering risk assessment. *Risk Analysis*, 37(7):1315–1340, 2017.

[46] M. A. Rahman, T. Kunz, and H. Schwartz. Delay asymmetry correction model for master-slave synchronization protocols. In *2014 IEEE 28th International Conference on Advanced Information Networking and Applications*, pages 1–8, May 2014.

[47] S. Salicone. *Measurement Uncertainty: an approach via the mathematical theory of evidence*. Springer series in reliability engineering. Springer, New York, NY, USA, 2007.

[48] S. Salicone and M. Prioli. *Measurement Uncertainty within the Theory of Evidence*. Springer series in Measurement Science and Technology. Springer, New York, NY, USA, 2018.

[49] S. Schriegel, H. Trsek, and J. Jasperneite. Enhancement for a clock synchronization protocol in heterogeneous networks. In *2009 International Symposium on Precision Clock Synchronization for Measurement, Control and Communication*, pages 1–5, Oct 2009.

[50] G. Shafer. *A Mathematical Theory of Evidence*. Princeton Univ. Press, Princeton, NJ, USA, 1976.

[51] P. Walley. *Statistical Reasoning with Imprecise Probabilities*. Chapman and Hall, London, UK, 1991.

[52] W. Wei, S. Gao, Y. Zhong, C. Gu, and A. Subic. Random weighting estimation for systematic error of observation model in dynamic vehicle navigation. *International Journal of Control, Automation and Systems*, 14(2):514–523, April 2016.

[53] Y. Yang, N. Rees, and T. Chuter. Reduction of encoder measurement errors in ukirt telescope control system using a kalman filter. *IEEE Transactions on Control Systems Technology*, 10(1):149–157, Jan 2002.

[54] LA Zadeh. Zadeh, fuzzy sets. *Inform Control*, 8:338–353, 1965.

[55] C. Zucca and P. Tavella. The clock model and its relationship with the allan and related variances. *IEEE Transactions on Ultrasonics, Ferroelectrics, and Frequency Control*, 52(2):289–296, 2005.